5-2013

Nature and Degree of Aqueous Alteration of Outer Main Belt Asteroids and CM and CI Carbonaceous Chondrites

Driss Takir
dtakir@utk.edu

To the Graduate Council:

I am submitting herewith a dissertation written by Driss Takir entitled "Nature and Degree of Aqueous Alteration of Outer Main Belt Asteroids and CM and CI Carbonaceous Chondrites." I have examined the final electronic copy of this dissertation for form and content and recommend that it be accepted in partial fulfillment of the requirements for the degree of Doctor of Philosophy, with a major in Geology.

Harry Y. McSween Jr., Joshua P. Emery, Major Professor

We have read this dissertation and recommend its acceptance:

Jeffery E. Moersch, Michael W. Guidry

Accepted for the Council:
Dixie L. Thompson

Vice Provost and Dean of the Graduate School

(Original signatures are on file with official student records.)

Nature and Degree of Aqueous Alteration of Outer Main Belt Asteroids and CM and CI Carbonaceous Chondrites

A Dissertation Presented for the
Doctor of Philosophy Degree
The University of Tennessee, Knoxville

Driss Takir
May 2013

Dedication

In memory of my father

Acknowledgements

This dissertation would not been completed without the guidance of my advisors, Dr. Joshua P Emery and Dr. Harry Y McSween Jr. I feel lucky to have worked on fascinating and exciting projects with leading experts in planetary sciences. Josh and Hap both taught me what a professional scientist should be. I would especially like to thank them for their generous financial support during my time at the University of Tennessee that allowed me to attend conferences and do research in various places in the US and around the world. I also wish to thank Dr. Jeffery E Moersch and Dr. Michael W Guidry (my committee members) for their helpful comments improving this dissertation, Roger Clark (USGS) and Karl Hibbitts (APL) for allowing me to use their laboratories to measure meteorite spectra, NASA IRTF staff for their excellent assistance with asteroid observations, and Earth & Planetary Sciences department staff, students, and faculty for their support and encouragement. I also owe a great deal of gratitude to my family, especially my mother and my wife. This dissertation would not been possible without their moral support through the years.

Abstract

CM (Mighei-like) and CI (Ivuna-like) carbonaceous chondrites are primitive meteorites that consist of some of the most pristine matter known in the Solar System. They are thought to be genetically related to outer Main Belt asteroids (C-, D-, G-, F-, T-, and B-types) that span the $2.5 < a < 4.0$ AU region. They are also thought to be the source that might have delivered water and organics to terrestrial planets during their accretion. The goal of this dissertation is to develop reliable 3-μm [micron] spectral indicators that can place constraints on the degree and location of aqueous alteration in the outer Main Belt region, and on the nature of phyllosilicate mineralogy on the surface of these asteroids. To that end, we have undertaken combined petrologic, geochemical, and spectroscopic analyses of CM and CI chondrites and outer Main Belt asteroids. Using the SpeX spectrograph/imager at NASA Infrared Telescope Facility (IRTF), we measured near-infrared (NIR: 0.7-4.0 μm) spectra of 40 outer Main Belt asteroids that allowed the identification of four 3-μm spectral groups, each of which presumably reflects a distinct surface mineralogy. We also measured spectra of 9 CM chondrites (in addition to the CI chondrite Ivuna) in the laboratory under asteroid-like conditions. These measurements revealed three spectral groups of CM chondrites, all of which are distinct from the spectrum of Ivuna on the basis of the 3-μm band center and shape of spectra, showing that distinct parent body aqueous alteration environments experienced by different carbonaceous chondrites can be distinguished using reflectance spectroscopy. All CM and CI chondrites in the present study are found to be similar to the group of asteroids that are located in the $2.5 < a < 3.3$ AU region and exhibit a sharp 3-μm feature, attributed to OH-stretching in hydrated minerals. However, no meteorite match was found for asteroids with a rounded 3-μm feature that are located farther from the Sun ($3.0 < a < 4.0$ AU), or for groups with distinctive spectra like 1 Ceres or 52 Europa.

Table of Contents

List of Tables

Chapter 1

Chapter 2

Chapter 3

List of Figures

Chapter 1

Chapter 2

Introduction

CM and CI carbonaceous chondrites exhibit evidence for past occurrence of liquid water in the form of hydrated phases (e.g., McSween 1979; Zolensky and McSween 1988; Brearley 2006). These chondrites are widely thought to be related genetically to outer Main Belt asteroids (e.g., C-, D-, G-, K-, F-, and B-types) (e.g., Gaffey et al. 1993). Here, we define hydrated phases as minerals that include structurally bound OH (hydroxyl) or H_2O, which possess chemical bonds with other elements in the mineral (e.g., serpentine: $[Mg_3Si_2O_5(OH)_4]$) (Rivkin et al. 2002). However, there are some minerals that were formed by contact with liquid water, but they do not possess OH or H_2O molecules (Jewitt et al. 2007).

The objectives of this doctoral dissertation are: (1) to investigate hydrated minerals (any mineral that contains H_2O or OH) on outer Main Belt asteroids spanning the $2.5 < a < 4.0$ AU region, (2) to develop reliable 3-μm spectral indicators of mineralogy on the basis of petrological, geochemical, and spectral analyses of CM and CI chondrites, and (3) to apply these 3-μm spectral indicators to outer Main Belt asteroids in order to provide more details on the alteration state and phyllosilicate mineralogy of these asteroids. Addressing these objectives is important in order to place crucial constraints on how and where aqueous alteration occurred, and provide a unique glimpse into the effects of asteroidal processing on early solar system materials. Of particular interest is the question of the abundance of water in the early solar system and its significant role in the evolution of the mineralogy and cosmochemistry of a number of diverse solar system bodies. Understanding the behavior of water during the earliest phases of the solar system is an important component in the broader investigation of the role and behavior of biologically important material through geologic time.

As a multifaceted investigation, this doctoral dissertation has special significance in integrating asteroid and meteorite studies, which are important to develop robust criteria for evaluating asteroidal vs. preaccretionary environments for aqueous alteration.

Chapter 1 of this dissertation examines near-infrared (NIR) spectra of 28 outer Main Belt asteroids located in the $2.5 < a < 4.0$ AU region. The asteroids were observed using NASA IRTF and SpeX spectrograph/ Imager and its two modes, prism and long wavelength cross-dispersed.

Chapter 2 describes the petrological, geochemical, and spectral indicators of mineralogy that relate to the degree of aqueous alteration in nine CM and one CI (Ivuna) carbonaceous chondrites. The meteorites were analyzed using an electron microprobe, an optical microscope, and various spectrometers. Meteorite spectra were measured under dry and vacuum conditions, for subsequent comparison with reflectance spectra of asteroids.

Chapter 3 examines the linkage between CM and CI carbonaceous chondrites and outer Main Belt asteroids spanning the $2.5 < a < 4.0$ AU region. We also apply the 3-μm spectral indicators in CM and CI chondrites to outer Main Belt in order to constrain the nature and location of aqueous alteration, and to provide more details on the alteration state and phyllosilicate mineralogy on the surface of these asteroids.

REFERENCES

Brearley, A.J. (2006) The action of water. In *Meteorites and the Early Solar System II* (eds. Dante Lauretta, H.Y. McSween Jr), Arizona University Press, pp. 587-624.

Gaffey S. J., McFadden L. A., Nash D., and Pieters C. M. (1993b) Ultraviolet, visible, and near-infrared reflectance spectroscopy: Laboratory spectra of geologic materials. In *Remote Geochemical Analysis: Elemental and Mineralogical Composition* (C. M. Pieters and P. J. Englert, eds.), pp. 43–77. Cambridge Univ., Cambridge.

Jewitt, D., Chizmadia, L., Grimm, R., Prialnik, D. (2007) Water in the Small Bodies of the Solar System. In Protostars and Planets V, p863-878 Univ.of Arizona Press, Tucson.

McSween H.Y. Jr. 1979. Alteration in CM carbonaceous chondrites inferred from modal and chemical variations in matrix. *Geochimica et Cosmochimica Acta* 43:1761-1170.

Rivkin, A. S.; Howell, E. S.; Vilas, F.; Lebofsky, L. A., (2002) Hydrated Minerals on Asteroids: The Astronomical Record. *In Asteroids III,* (eds. W. F. Bottke Jr., A. Cellino, P.

Zolensky M.E. and McSween H.Y.Jr.1988. Aqueous alteration. In *Meteorites and the Early Solar System,* edited by F. Kerridge and M. Mattews. Tucson: University of Arizona, pp. 114-143.

Chapter 1

Outer Main Belt asteroids: Identification and Distribution of Four 3-μm Spectral Groups

This chapter is a reformatted version of a paper, by the same name, published in Icarus in 2012.

Takir D. and Emery J.P. (2012) Outer Main Belt asteroids: Identification and distribution of four 3-um spectral groups. *Icarus* **219**:641-654.

Abstract

This paper examines the distribution and the abundance of hydrated minerals (any mineral that contains H_2O or OH) on outer Main Belt asteroids spanning the $2.5 < a < 4.0$ AU region. The hypothesis we are testing is whether planetesimals that accreted closer to the Sun experienced a higher degree of aqueous alteration. We would expect then to see a gradual decline of the abundance of hydrated minerals among the outer Main Belt asteroids with increasing heliocentric distance ($2.5 < a < 4.0$ AU). We measured spectra (0.8-2.5 μm and 1.9-4.1 μm) of 28 outer Main Belt asteroids using the SpeX spectrograph/imager at the NASA Infrared Telescope Facility (IRTF). We identified four groups on the basis of the shape and the band center of the 3-μm feature. The first group, which we call ‘‘sharp’’, exhibits a sharp 3-μm feature, attributed to hydrated minerals (phyllosilicates). Most asteroids in this group are located in the $2.5 < a < 3.3$ AU region. The second group, which we call ‘‘Ceres-like’’, consists of 10 Hygiea and 324 Bamberga. Like asteroid Ceres, these asteroids exhibit a 3-μm feature with a band center of 3.05 ± 0.01 μm that is superimposed on a broader absorption feature from ~2.8 to 3.7 μm. The third group, which we call ‘‘Europa-like’’, includes 52 Europa, 31 Euphrosyne, and 451 Patientia. Objects in this group exhibit a 3-μm feature with a band center of 3.15 ± 0.01 μm. Both the Ceres-like and Europa-like groups are concentrated in the $2.5 < a < 3.3$ AU region. The fourth group, which we call ‘‘rounded’’, is concentrated in the $3.4 < a < 4.0$ AU region.

Asteroids in this group are characterized by a rounded 3-μm feature, attributed to H_2O ice. A similar rounded 3-μm feature was also identified in 24 Themis and 65 Cybele. Unlike the sharp group, the rounded group did not experience aqueous alteration. Of the asteroids observed in this study, 140 Siwa, a P-type, is the only one that does not exhibit a 3-μm feature. These results are important to constrain the nature and the degree of aqueous alteration in outer Main Belt asteroids.

1.0 INTRODUCTION

Water in some form has been discovered throughout the outer Solar System (Rivkin et al. 2002). It has been detected on Kuiper Belt Objects (KBOs) (Brown et al. 1997), on the icy Galilean moons of Jupiter (Calvin and Clark 1991; McCord et al. 1999), on the planets as vapor and polar ice (e.g., Encrenaz et al., 1999; Bibring et al., 2004), and on comets (Campins et al. 1983; Mumma et al. 1986; Weaver et al. 1986) and asteroids as ice (Rivkin and Emery 2010; Campins et al. 2010; Licandro et al. 2011). Water has also been discovered bound in minerals on some asteroids and Mars (e.g., Lebofsky 1980; Mustard et al. 2008). Water, which was a major planet-building element in the protoplanetary disk, condensed beyond a certain distance from the proto-Sun called the snow-line (Lunine 2006). Although the location of the snow-line before and during planet formation is uncertain, some evidence suggests it may have fallen within the asteroid belt (Lunine 2006). Even if the snow-line itself was located outside the asteroid belt, gas drag may have allowed the subsequent migration of water ice grains inwards, resulting in the existence of water in planetesimals throughout much of the asteroid belt (Cyr et al. 1998). More recent models of nebular kinetics suggest that the snow-line itself may have migrated as the nebula evolved, sweeping across the entire asteroid belt (e.g., Dodson-Robinson et al. 2009). Additionally, recent dynamical models (e.g., Walsh et al. 2011) suggest that perhaps a sizable fraction of Main Belt asteroids originated between or beyond the giant planets, where water ice would have been stable.

The study of meteorites has revealed that water was widely available in the asteroid belt during the earliest history of the Solar System (Brearley 2006). Aqueous alteration is a widespread process that has affected primitive Solar System materials and chondritic meteorites (Brearley 2006). Carbonaceous chondrites in particular, including CM (Mighei-like) and CI

(Ivuna-like), exhibit evidence of fluid-assisted alteration to varying degrees (McSween 1979; Bunch and Chang 1980; Tomeoka and Buseck 1985; Zolensky and McSween 1988).

C-, D-, G-, F-, and B-asteroids are likely related genetically to carbonaceous chondrites (Gaffey et al. 1993a; Pieters and McFadden 1994; Hiroi et al. 2001; Kanno et al. 2003). Telescopic observations of these asteroids have revealed that hydrous minerals are present on their surfaces (Vilas and Gaffey 1989; Vilas et al. 1993, 1994; Jones et al. 1990). Hydrated minerals exhibit a variety of spectral features. For asteroid science, absorptions in the visible (0.4–0.93 μm) and near-infrared (2.4–3.6 μm) regions are particularly diagnostic (Gaffey et al. 1993b). The latter is the so-called 3-μm band (Rivkin et al. 2002). Absorption features near 3-μm have been discovered in a number of C-asteroids (Lebofsky 1980; Jones et al. 1990; Rivkin et al. 2002, 2006). Jones et al. (1990) found a weak correlation that suggested that the fraction of hydrated asteroids, mostly of the C-class and subclasses, decreased with increasing heliocentric distance, supporting a scenario in which these asteroids were originally composed of mixtures of anhydrous minerals and ice that were later melted by heat released by decay of short-lived radionuclides, forming hydrated minerals (Grimm and McSween 1993).

With telescopic observations of outer Main Belt asteroids, many questions such as how, where, and when this aqueous alteration occurred can be constrained, offering a unique glimpse at the effects of processing on early Solar System materials. Telescopic observations can also constrain the question of the abundance and the distribution of water in the early Solar System and its significant role in the evolution of a number of diverse Solar System bodies, including asteroids. Investigating the behavior of water during the earliest phases of Solar Systems is vital to understand how water was delivered to terrestrial planets, including Earth, during accretion.

This study examines hydrated minerals (any mineral that contains H_2O or OH) on outer Main Belt asteroids spanning the 2.5 < a < 4.0 AU region. Our targets have diameters ranging from ~100 to ~400 km and include different spectral classes (C, P, D, G, and T) and dynamical families/groups (Hygiea, Themis, Cybele, and Hilda). If planetesimals that accreted closer to the Sun experienced a higher degree of aqueous alteration, we would expect to see a gradual decline of the abundance of hydrated minerals among the outer Main Belt asteroids with increasing heliocentric distance across the 2.5 < a < 4.0 AU region.

2.0 METHODOLOGY

2.1. Observational Techniques

To investigate the 3-μm band in the outer Main Belt region, we collected reflectance spectra of 28 asteroids, using the prism (0.8-2.5-μm) and the long wavelength cross dispersed (LXD: 1.9-4.2-μm) modes of the SpeX spectrograph/imager at the NASA Infrared Telescope Facility (IRTF). Our targets were observed over the course of six periods, April 2009, August 2009 and January 2010, April 2010, August 2010, (April, May, June) 2011, and (August, September) 2011. SpeX has two detectors: a 1024 x 1024 InSb array for the spectrograph and a 512 x 512 InSb array that images the slit (Rayner et al. 2003, 2004). This investigation also includes previously published visible spectra (~0.4-0.93-μm) as well as near-infrared spectra (NIR: ~0.4-2.5-μm), to help provide a deeper understanding of the phyllosilicates, anhydrous silicates, and the opaque/carbonaceous components of the surfaces of these asteroids (see Table A1).

The LXD mode of SpeX and an 0.8 x 15 arcsec slit with an image scale of 0.15 arcsec/pixel were used to obtain K-band (1.95-2.5 μm) and L-band (2.85-4.1 μm) data

simultaneously. The LXD mode covers the wavelength range 1.9-4.1 μm with a resolving power ($R = \lambda/\Delta\lambda$) of ~1000. In LXD mode, the full wavelength range is covered in six orders, which are recorded simultaneously on the detector and stacked on the chip to get relatively broad wavelength coverage at moderate resolution (Rayner et al. 2003). We extracted these orders separately and spliced them together in the reduction process. The primary focus of these observations was on the L-band because it includes the 3-μm feature, attributed to hydrated minerals and/or H_2O ice. The telescope time was 5-6 h per each target with a moderate seeing of 0.7", resulting in signal-to-noise (S/N) of 30-50. Spectra of G-dwarfs with solar-like B-V and V-K colors were obtained for each asteroid to remove telluric water vapor absorption features and to correct for the solar spectrum. The selected G-dwarfs, located as close to the asteroid as possible, were observed with a frequency sufficient to ensure the airmass was similar to that of the object (±0.05) in order to have better atmospheric correction. On average, 8-10 asteroid and star sets were taken. We used a calibration box, which is attached to SpeX and contains argon lamp, for wavelength calibration. We also obtained the flat field frames by illuminating an integrating sphere in the calibration box. Telluric absorption lines were used for wavelength calibration in the 2.8-4.1 μm region because the argon lines are too faint in this wavelength range (see Table A2).

We observed 19 asteroids in the prism mode. On average, 1-2 sets were obtained for each asteroid. Ten prism spectra were obtained from the MIT-UH-IRTF Joint Campaign for NEO Reconnaissance database. The prism mode, which is designed for faint objects, covers the wavelength range 0.8-2.5-μm and has an 0.8 x 15 arcsec slit with a resolving power ($R = \lambda/\Delta\lambda$) of ~100 (Rayner et al. 2003). The same observation technique used for the LXD mode was used for the prism mode. For all observations, the slit was aligned with the parallactic angle. Unlike the

LXD mode, the entire 0.8-2.5-μm region in the prism mode is dispersed by a single prism onto one quadrant of the 1024 x 1024 array (see Table A3).

Visible spectra were obtained from the second phase of the Small Main Belt Asteroid Spectroscopic Survey (SMASSII) (Bus and Binzel 2002). During the SMASSII survey, visible-wavelength charge-coupled device (CCD) spectra (~0.4–0.93 μm) of 1447 Main Belt asteroids were measured. For a deeper and more comprehensive analysis, we spliced SMASS II visible spectra with the prism data.

2.2. Data Reduction

Standard NIR reduction techniques were used in order to reduce both prism and LXD spectra. The data were reduced using the IDL (Interactive Data Language)-based spectral reduction tool Spextool (v3.4) (Cushing 2004) in combination with some custom IDL routines (Emery and Brown 2003). The reduction techniques include subtracting the asteroid/star spectrum at beam position A from spectrum at beam B of the telescope in order to remove the background sky (mostly OH line emission through most of the wavelength range and thermal emission from the sky and telescope longward of ~2.3 μm). Residual background remaining after this subtraction was removed by subtracting the median background (outside of data aperture) for each channel. Asteroid and standard star spectra were extracted by summing the flux at each channel within a user defined aperture (8 pixels wide here). In Spextool and the prism routine of Emery and Brown (2003), asteroid spectra were shifted to sub-pixel accuracy to align with the calibration star spectra and then were divided by appropriate calibration star spectra at the same airmass (±0.05) to remove telluric water vapor absorption features. On some nights when weather conditions were poor, telluric absorptions were not completely corrected. Finally, both prism and LXD spectra were smoothed and binned to lower spectral resolution in order to

improve the S/N. Wavelength calibration was accomplished at λ < 2.5 μm by mapping measured emission lines from the argon calibration lamp to their known wavelengths and at λ > 2.5 μm using telluric absorption lines.

2.3. Thermal Excess Removal in the 3-μm Region

The measured LXD spectra of asteroids exhibit a steep increase of apparent reflectance longward of ~3.6 μm, attributed to thermal radiation from the asteroids' surfaces (Figure A1). The amount of thermal excess and the wavelength at which it becomes apparent depend on surface temperature, which is a function of solar distance and several surface properties, such as albedo, roughness, and thermal inertia. The thermal excess was removed using the methodology described in Rivkin et al. (2005) and Reddy et al. (2009). Rivkin et al. (2005) defined the thermal excess (γ_λ) as a measure of the thermal flux found at these wavelengths by

$$\gamma_\lambda = \frac{R_\lambda + T_\lambda}{R_\lambda} - 1, \qquad (1)$$

where R_λ represents the reflected flux at a wavelength λ, T_λ represents the thermal flux at a given wavelength, and the quantity $R_\lambda + T_\lambda$ represents the measured relative spectrum. The task here is to fit the measured thermal excess with a model thermal excess as a way of constraining the model thermal flux. This model thermal flux is then subtracted from the measured relative spectrum. Several similar techniques have been used by other authors to remove the thermal excess for asteroids (Howell et al. 1994; Abell 2003; Rivkin et al. 2005). For all targets, thermal excess in the region of the 3-μm band (λ < ~3.3 μm) is not significant; however, it can be substantial at longer wavelengths and can affect the slope beyond ~3.6 μm (Figures A1 and A 2).

The Near-Earth Asteroid Thermal Model (NEATM; Harris 1998), which is a variation of the Standard Thermal Model (STM) of Lebofsky et al. (1986), was used to calculate the thermal

flux in the 3-μm region. Inputs that include heliocentric and geocentric distances, geometric albedo, and phase angle at time of observation were obtained from the Jet Propulsion Laboratory Horizon online ephemeris generator[1]. The default value for the slope parameter *G* of 0.15 was used for all objects (Bowell et al. 1989). This model uses the beaming parameter (η) to adjust the surface temperature to match the measured thermal flux (e.g., Harris and Lagerros 2002). The model temperature decreases with increasing η. Beaming parameters $\eta > 1$ likely indicate a relatively high thermal inertia, whereas $\eta < 1$ likely correspond to low thermal inertia and significant macroscopic surface roughness (Figure A2). Spectral emissivity is assumed to be constant, and both bolometric and spectral emissivities are assumed to be 0.9. The reflectance in the 3-μm region is modeled by a linear extrapolation of the K-band reflectance, where the thermal excess is not significant for the surface temperatures experienced by Main Belt asteroids.

2.4. The 3-μm and 0.7-μm Band Depth and Uncertainty

The band depth, D_λ, at a given wavelength λ is calculated relative to the continuum (the linear regression line across the K-band):

$$D_\lambda = \frac{R_c - R_\lambda}{R_c}, \quad (2)$$

where R_λ is the reflectance at a given wavelength λ, and R_c is the reflectance of the continuum at the same wavelength as R_λ. The linear regression equation across the K-band is defined as:

$$y = m * x + b, \quad (3)$$

where *m* is the slope and *b* is the intercept defined as (Montgomery and Peck 1992):

[1] http://ssd.jpl.nasa.gov/horizons.cgi

$$m = \frac{S_{xy}}{S_{xx}} \quad and \quad b = \bar{y} - m * \bar{x}, \qquad (4)$$

with

$$S_{xx} = \sum_{i=1}^{i=N} (x_i - \overline{x})^2 \text{ and } S_{xy} = \sum_{i=1}^{i=N} y_i * (x_i - \overline{x})$$

(N is the number of data points and $\overline{x}$ and $\overline{y}$ are the mean of the set of x and y data points).

If $R_1 = R_c - R_\lambda$, then the uncertainty in R_1 is:

$$\delta R_1 = \sqrt{(\delta R_c)^2 + (\delta R_\lambda)^2}, \qquad (5) \text{ (Taylor 1982)}$$

δR_c and δR_λ can be computed using the uncertainty at each wavelength, calculated during the data reduction process.

Thus, the uncertainty in D_λ is:

$$\delta D_\lambda = D_\lambda * \sqrt{(\frac{\delta R_1}{R_1})^2 + (\frac{\delta R_c}{R_c})^2} \quad . \quad (6) \text{ (Taylor 1982)}$$

If $D_\lambda > 2\ \delta D_\lambda$, then the asteroid's spectrum exhibits an absorption feature at a given wavelength λ (i.e., the criterion is a 2σ detection). We chose a representative wavelength, 3.00 μm, for the nominal band-depth calculation (Figure A3). Hence, an asteroid's spectrum was found to possess a 3-μm band if $D_{3.00} > 2\ \delta D_{3.00}$ (Table A4, column 5). The same technique was used to calculate the band-depth at 0.7 μm in visible wavelength spectra. The 3.00 μm and the 0.7 μm band-depths for each asteroid are reported in Table A4.

2.5. The Identification of Four 3-μm Spectral Groups

Initial inspection of the LXD spectra revealed an apparent variation in band shape as well as depth. Using visual inspection, we qualitatively identified four 3-μm spectral groups: 1) a group with a sharp 3-μm feature (reflectance decreases with decreasing wavelength into the 2.5 –

2.85 μm spectral region obscured by Earth's atmosphere), 2) a group with a rounded 3-μm feature (reflectance increases with decreasing wavelength shortward of about 3.07 μm), 3) a group with a Ceres-like feature (relatively narrow feature centered at 3.05 μm superposed on a much wider absorption), and 4) a group with a Europa-like feature (longer wavelength band minimum and steeper rise on the long-wavelength edge of the absorption). Quantitative criteria were also developed for classification of the 3-μm band shapes.

To characterize the sharp and rounded 3-μm features, we removed the continuum and fit a trendline to LXD spectra across the 2.85-3.25-μm region. We used a chi-squared test to determine whether the best fit was a linear regression or a higher-order polynomial (Figure A4, A5, and A6). Then we calculated the reflectance at 2.90 μm, $R_{2.90}$, and at 3.05 μm, $R_{3.05}$. To distinguish between the groups with sharp and rounded 3-μm features, we calculated the ratio $R_{2.90} / R_{3.05}$. An asteroid was grouped with the sharp 3-μm group when the best fit was a linear regression and the ratio was less than 1. The asteroid was grouped with the rounded 3-μm group when the best fit is a polynomial and the ratio was greater than 1 (Table A4, column 8). The group with the Ceres-like feature is characterized by a 3-μm band center around 3.05 μm, while the group with the Europa-like feature is characterized by a 3-μm band center around 3.15 μm (Table A4, column 4).

3.0 RESULTS

For target selection, the Main Belt was divided into four heliocentric (semi-major axis) bins: $2.5 < a < 2.9$ AU, $2.9 < a < 3.3$ AU, $3.3 < a < 3.6$ AU, and $3.6 < a < 4.0$ AU. We attempted to select a similar number of targets from each heliocentric bin. The two more distant bins are currently slightly underrepresented because there are fewer bright targets at those distances.

Applying the methodology described in section 2.5, we classified the observed asteroids into four spectral groups: sharp 3-μm, rounded 3-μm, Ceres-like, and Europa-like. Asteroids that exhibit sharp 3-μm, Ceres-like, and Europa-like features tend to fall in the first and the second heliocentric bins. Asteroids that exhibit the rounded 3-μm features fall in the third and fourth bins, which include two main groups, the Cybeles near 3.5 AU and the Hildas in the 3:2 resonance with Jupiter at ~ 4.0 AU.

3.1. The Sharp 3-μm Group

This group includes 15 asteroids that possess a sharp 3-μm feature. Some objects in this group exhibit a 0.7-μm feature with a generally convex NIR (0.85-2.5 μm) spectrum that forms a shape similar to a hockey stick (Figure A7). Asteroid 140 Siwa is the only asteroid that does not show any feature above the noise level in the 3-μm region (Figure A8).

3.2. The Ceres-like Group

This group includes two asteroids: 10 Hygiea and 324 Bamberga with diameters of 407.1 and 229.4-km respectively (Tedesco et al. 2002). These two asteroids exhibit a 3-μm feature that has a chevron shape with a band center at 3.05 ± 0.01 μm. At shorter wavelengths, 10 Hygiea exhibits a broad feature around 1-μm with a concave-up NIR (0.85-2.45 μm) spectrum. 324 Bamberga, on the other hand, is featureless in the 1-μm region (Figure A9).

3.3. The Europa-like Group

This group includes three asteroids: 52 Europa, 31 Euphrosyne, and 451 Patientia with diameters of 302.5, 256, and 225 km respectively (Tedesco et al. 2002). The three asteroids exhibit a 3-μm feature with a band center at 3.15 ± 0.01 μm. Both 52 Europa and 31 Euphrosyne exhibit a broad feature around 1-μm with concave-up NIR (0.85-2.45 μm) spectrum, similarly to 10 Hygiea. 31 Euphrosyne, however, is featureless in the 1-μm region (Figure A10).

3.4. The Rounded 3-μm Group

This group includes seven asteroids: 190 Ismene, 153 Hilda, 361 Bononia, 107 Camilla, 76 Freia, 790 Pretoria, and 401 Ottilia. These asteroids show a rounded 3-μm feature. 107 Camilla and 76 Freia have a concave-up NIR (0.85-2.45-μm) spectrum. 153 Hilda, 790 Pretoria, and 190 Ismene have a linear NIR spectrum, and 361 Bononia and 401 Ottilia have a convex-up NIR spectrum. No asteroid in this group exhibits a 0.7-μm feature (Figure A11).

4.0 DISCUSSION

Our observations include 28 asteroids with different classes (C, P, D, G, and T), diameters (~99-400-km), and families/groups (Hygiea, Themis, Cybele, and Hilda). On the basis of the 3-μm band shape and center criteria described in section 2.5, we classified these asteroids into four spectral groups:

4.1 The Sharp Group

The shape of the sharp 3-μm feature that distinguishes this group is most consistent with the presence of hydrated silicates on their surfaces (Lebofsky 1980; Jones et al. 1990; Rivkin et al. 2002). Phyllosilicates (or "clay minerals") are formed in environments where anhydrous rock and liquid water are in contact, and vary from serpentine with two OH groups per Si to clays (e.g., talc) with one OH per Si (Rivkin 2002). The most common phyllosilicates found in meteorites are serpentine-group, smectite-group, and chlorite-group minerals (Rubin 1996). The hydrated minerals on asteroids were likely produced from an original mixture of anhydrous silicates and melted ice by aqueous alteration processes similar to those suggested for hydrated phases in the CM and CI meteorites (e.g., McSween 1979; Grimm and McSween 1989).

Asteroids that do not possess such a 3-μm feature indicate a lack of abundant hydrated silicates on their surfaces (Gaffey 1993a).

Except for 121 Hermione and 334 Chicago, all asteroids with sharp 3-μm features are concentrated in the two heliocentric bins between 2.5 and 3.3 AU. Jones et al. (1990) found that two-thirds of the C-, G-, T-, F-, and B-type asteroids in the outer Main Belt region show hydrated silicate absorptions, indicating that the C asteroids underwent a widespread heating and aqueous alteration episode.

Figure A12 illustrates a possible weak correlation between the heliocentric distance and the band depth at 3-μm for asteroids across the $2.5 < a < 3.3$ AU region that exhibit the sharp OH 3-μm feature. This trend suggests hydrated silicates possibly decline in abundance with the heliocentric distance in agreement with the finding of Jones et al. (1990). If we exclude asteroids 48 Doris, 130 Elektra, and 121 Hermione from the plot, we would have a better correlation. The latter two asteroids are binaries. It is intriguing to consider that some mechanism (e.g., collisions) associated with binary formation may also be responsible for the deeper 3-μm absorption band. However, if we exclude asteroid 334 Chicago from the plot, we would have a weaker correlation.

60% of asteroids in the sharp group exhibit an absorption feature around 0.7-μm. This finding is an agreement with the results of Vilas (1994) who found an approximately 80% correlation between the 3-μm band and the 0.7-μm charge transfer band, attributed to oxidized iron in phyllosillicates.

4.2 The Ceres-like Group

The spectrum of 1 Ceres contains a distinct infrared absorption feature centered at a wavelength of ~3.05 μm that is superimposed on a broader absorption feature from ~2.8 to 3.7 μm (Lebofsky et al. 1981; Rivkin et al. 2006; Miliken and Rivkin 2009). The two asteroids in our

sample with a similar ~3.05 μm band, in addition to 1 Ceres, are located in the 2.5 and 3.3 AU region.

10 Hygeia's spectrum exhibits a 3-μm feature with a band center at 3.05 ± 0.01 μm and a band depth of 13.26 ± 0.10 %. Similarly in Ceres, the 3-μm feature in Hygiea is superimposed on a broader absorption from ~2.8 to 3.7 μm. Lebofsky et al. (1981) attributed the 3.05-μm absorption feature in Ceres to a very thin water ice frost. Additionally, King et al. (1992) attributed the 3.05-μm feature in 1 Ceres to NH_4-bearing phyllosilicates. Vernazza et al. (2005) suggested that the 3.05-μm feature is due to a mixture of irradiated organics and crystalline water ice. Furthermore, Rivkin et al. (2006) attributed this feature to iron-rich clay (i.e., serpentine cronstedite). Rivkin et al. (2006) also attributed the 3.3-3.4 and 3.8-3.9-μm features to carbonates. Miliken and Rivkin (2009) suggested that the 3.05-μm spectral feature in Ceres is due to the hydroxide brucite. They attribute other features in the spectrum to magnesium carbonates and serpentines.

324 Bamberga, which is a CP type (in the Tholen taxonomy), exhibits a similar feature at 3.05 ± 0.01 μm with a band depth of 16.55 ± 0.07 %. Both 1 Ceres and 10 Hygiea exhibit a broad feature around 1 μm. Yang and Jewitt (2010) attributed the presence of a similar broad absorption band centered around 1 μm in a B-type asteroid, 335 Roberta, to magnetite, which is an indicator of past aqueous alteration on the surface of this asteroid. The discovery of the 3-μm feature in both 10 Hygiea and 324 Bamberga suggests that Ceres's surface mineralogy is not unique.

4.3. The Europa-like Group

We identify here a new 3-μm group that has not been previously reported or discussed in the literature. This group includes asteroids 52 Europa, 31 Euphrosyne, and 451 Patientia,

characterized by a 3-μm feature with a band center ~3.15 μm and a band depth of ~14%. Jones et al. (1990) observed 52 Europa, but did not detect a feature in the 3-μm region. In searching the United States Geological Survey spectral library[2] for possible matches to Europa-like group, phyllosilicates that allow interlayer H_2O (along with OH), such as montmorillonite, appear as plausible explanations, suggesting that this group possibly has been aqueously altered. However, more laboratory work that includes spectral analyses of minerals under dry conditions (to remove absorbed water) and spectral modeling are needed to better characterize Europa-like group.

4.4 The Rounded Group

The rounded 3-μm band shape that distinguishes this group has been previously identified on 24 Themis (Rivkin and Emery 2010; Campins et al. 2010) and 65 Cybele (Licandro et al. 2011). Rivkin and Emery (2010) found that the spectrum of 24 Themis is matched very well by a spectral model of a mixture of ice-coated pyroxene grains and amorphous carbon, suggesting that the surfaces of these asteroids with rounded features include very fine water frost in the form of grain coatings. The characteristics of the rounded band on these asteroids (listed in Table A4) are very similar to those of 24 Themis. Detailed models similar to those shown in Rivkin and Emery (2010) match the data presented here quite well, with only small variations in mixing parameters (e.g., Figure A13).

Because ice will sublime at main-belt asteroid surfaces, Rivkin and Emery (2010) attributed the current presence of ice on the surface of 24 Themis to replenishment by a slow and steady outgassing from the interior of this asteroid, and to the recondensation of some amount of vapor as frost on regolith grains. The grain coatings in these models are so thin, and the

[2] http://speclab.cr.usgs.gov/spectral.lib06/ds231/datatable.html

absorption coefficient of H_2O in the visible so small, that the albedo is not increased by the required level of ice. Hence, the low albedos are still consistent with the amounts of surface frost suggested. For all asteroids observed in this study including the sharp and the rounded 3-μm groups, no correlation was found between albdeo and the intensity of the 3-μm absorption feature. Beck et al. (2011) suggest that goethite, an iron oxyhydroxide, as an alternative hypothesis to explain the 3-μm band in 24 Themis. However, at least in the case of 24 Themis goethite does not match the shorter wavelength spectrum (Pinilla-Alonso et al. 2011). The seven asteroids that fall in this group are concentrated in the $3.3 < a < 3.6$ AU and $3.6 < a < 4.0$ AU heliocentric bins, as are Themis and Cybele. Jones et al. (1990) found no hydrous asteroids beyond 3.4 AU. Their spectrophotometric data were apparently not sufficiently sensitive to detect this rounded band.

4.5 P- and D-type Asteroids

Jones et al. (1990) found all P- and D-type asteroids they studied to be featureless in the 3-μm region, except for 324 Bamberga, which showed a weak feature. 324 Bamberga is a CP type with a heliocentric distance of 2.68 AU. In addition, none of P- and D-type asteroids studied by Lebofsky et al. (1990) exhibits a 3-μm feature. In the present study, all P and D asteroids were found to exhibit a 3-μm absorption feature, except for 140 Siwa (P-type), which has a heliocentric distance of 2.73 AU and appears to have escaped extensive heating and aqueous alteration or have experienced extreme heating that dehydrated phyllosilicates. All observed P- and D- asteroids are located in the $3.0 < a < 4.0$ AU region and exhibit a rounded 3-μm H_2O feature, except for 324 Bamberga, which is a part of Ceres-like group. We did not observe any asteroids beyond 4 AU. Emery and Brown (2003) did not find any of the Trojan asteroids they observed to exhibit a 3-μm feature. Although most of their data were sufficiently sensitive to

detect absorptions as strong as those in asteroids 24 Themis and 65 Cybele (~10%), a few were not sufficiently sensitive and the total sample consisted of only 8 Trojans. Further observations are needed to firmly establish the presence or absence of these features among the Trojan asteroids.

4.6 Thermal Evolution of Outer Main Belt Asteroids

When placed in the context of the asteroid thermal evolution model of Grimm and McSween (1993), the distribution of the four 3-μm spectral groups reveals an interesting trend, and provides important hints about the alteration histories and thermal evolution of outer Main Belt asteroids spanning the $2.5 < a < 4.0$ AU region .

Figure A14 illustrates that many of the asteroids with the sharp 3-μm feature are concentrated around the vertical bar at 2.7 AU, which marks the approximate calculated boundary between bodies that melted or were thermally metamorphosed and those that experienced melting of ice and subsequent aqueous alteration. Figure A14 also reveals that asteroids with the rounded 3-μm feature, including 24 Themis and 65 Cybele, are concentrated around the vertical bar at 3.4 AU, which marks the calculated transition to unaltered asteroids that might still contain unmelted water ice.

The thermal evolution model of Grimm and McSween (1993) recognizes that planetesimals closer to the Sun accreted faster than those further out and thus had larger proportions of live ^{26}Al available to drive heating. In their model, this radiogenic heating is in turn responsible for aqueous alteration in CM/CI chondrite parent bodies. Grimm and McSween (1989) assumed that accretion occurred quickly compared with interior heating. Accretion times have shorter durations than the heat durations, which have a timescale of 1-10 Myr (Grimm and McSween 1989). Cohen and Coker (2000), who support this assumption, found that ^{26}Al decay

can generate adequate heat for aqueous alteration if the accretion starts within 3 Myr of nucleosynthesis.

Electromagnetic induction heating caused by a solar-wind plasma flow from the young Sun has also been suggested as a heat source responsible for aqueous alteration in CM/CI chondrite parent bodies (Sonnett 1979). However, further studies of T-Tauri stars showed that solar winds are not oriented toward the nebular disk where the plantesimnals form; instead, solar winds are concentrated at high latitude (Edwards et al. 1987). Hence, the electromagnetic induction heating model is no longer strongly supported (McSween et al. 2002).

4.7 The Nature of Aqueous Alteration on Outer Main Belt asteroids

Our telescopic observations have revealed evidence consistent with a thermal stratification of outer Main Belt asteroids. Most asteroids located in the $2.5 < a < 3.3$ AU region experienced a widespread aqueous alteration episode early in the solar system history, forming the sharp group. The $3.3 < a < 4.0$ AU region includes mostly unaltered asteroids that did not experience aqueous alteration, forming the rounded group. In the former group, the detection of hydrated minerals on the surface of asteroids suggests that aqueous alteration has affected carbonaceous chondrites and produced secondary minerals, which include hydroxylated silicates (i.e., phyllosilicates). In carbonaceous meteorites, these phyllosilicates are associated with other phases that were produced by the precipitation of hydrous fluids, such as carbonates and sulfates (Zolensky et al. 1989). The 3.3-3.4 and 3.8-3.9-μm features seen in Ceres-like group are more likely attributed to the presence of carbonates (Miliken and Rivkin 2009).

The detection of hydrated minerals on the surface of asteroids is important to link carbonaceous chondrites (e.g., CM chondrites) with their parent bodies. The hydrated minerals found in the meteroites could be due to the aqueous alteration that occurred in the interior of the

parent bodies or on their surfaces (Grimm and McSween 1989). On the basis of the assumption that CM chondrite parent bodies were formed as mixtures of water ice and anhydrous silicates, Grimm and McSween (1989) proposed two models for the aqueous alteration environment. The first model suggests that the interior of a CM chondrite parent body was petrologically homogeneous and altered throughout (at least 50% of the interior), and samples originated from subsequent catastrophic breakup. When the parent bodies were heated by ^{26}Al decay, water ice began to melt and react with anhydrous silicates to form hydrous silicates. This model applies to larger asteroids (D = 300 km) only (Grimm and McSween 1989).

The second model suggests that aqueous alteration occurred on the surface of the parent body where the regolith and water were in contact. According to Grimm and McSween (1989), liquid water was produced by the internal heating of the parent body and the melting of its interior ice. Hydrothermal circulation caused liquid water to reach the surface of the parent body. Aqueous alteration of the regolith could also be produced by venting of liquid/vapor water through fractures, or by vapor diffusion through preexisting pores and cracks. Grimm and McSween (1989) suggested that hydrothermal circulation into the regolith is unlikely to occur on small asteroids (D = 30 km), unlike water venting and vapor diffusion mechanisms.

Figure A15 shows that there is a positive correlation between the diameter and the 2.90-μm band depth for asteroids that exhibit the sharp OH 3-μm feature and have diameter larger than 300 km. This signature can be explained by the past occurrence of hydrothermal circulation on these asteroids, which caused liquid water to reach the surface and come in contact with the regolith (Grimm and McSween 1989). As the diameter of asteroids increases, the hydrothermal circulation increases and so the liquid water that reach the surface to produce aqueous alteration and hydrated minerals regolith (Grimm and McSween 1989). Hence, in this model, the 2.90-μm

band depth increases with increase of the diameter. Jones et al. (1990) did not find any correlation between hydrated silicate abundance and the diameter, but the observations presented here are higher sensitivity.

5.0 CONCLUSIONS

(1) We observed 28 outer Main Belt asteroids located in the 2.5 < AU < 4.0 AU region, using NASA IRTF and SpeX spectrograph/Imager and its two modes, prism and LXD. The target asteroids were selected from four heliocentric (semi-major axis) bins: 2.5 < a < 2.9 AU, 2.9 < a < 3.3 AU, 3.3 < a < 3.6 AU, and 3.6 < a < 4.0 AU. The observations include asteroids with different classes (C, P, D, G, and T), diameters (~99-400-km), and families/groups (Hygiea, Themis, Cybele, and Hilda).

(2) We identified four spectral groups based on the shape and position of the 3-μm absorption band: the sharp group, the Ceres-like group, the Europa-like group, and the rounded group.

(2.1) The sharp 3-μm band shape is inferred to be due to the presence of phyllosilicates on the surfaces. Asteroids with the sharp 3-μm feature are predominately located in the first and second semi-major axis bins. In this group, there is a weak indication that the 2.90-μm band depth may decrease with increasing heliocentric distance. If real, this would suggest that the abundance of hydrated silicates declines gradually among these asteroids with increasing heliocentric distance. 60% of asteroids in the sharp group exhibit an absorption feature around 0.7 μm. For asteroids with diameters ranging between 30 km and 300 km, the 2.90-μm band depth increases with the increase of the diameters in agreement with the model of Grimm and McSween (1989).

(2.2) The rounded 3-μm band shape, on the other hand, is inferred to be due to the presence of H_2O frost on the surfaces rather than hydrated phases. Asteroids that exhibit this feature are predominately located in the third and fourth semi-major axis bins. The transition from aqueously altered surfaces (the sharp group) to unaltered surfaces (the rounded group) corresponds to the boundary (~2.7 AU) predicted by the thermal model of Grimm & McSween (1993).

(2.3) Our observations have revealed two asteroids with a 3-μm band shape and associated longer wavelength absorptions that are nearly identical in shape and position to that found in the spectrum of Ceres. The surface composition of Ceres is apparently not as unique as once thought.

(2.4) We have also identified a new 3-μm spectral group that is characterized by a broad absorption with maximum depth near 3.15 μm. This "Europa-like" group currently includes three asteroids (52 Europa, 31 Euphrosyne, and 451 Patientia). Future work will include laboratory experiments and spectral modeling to better characterize the mineralogy represented by this newly discovered group.

(3) Asteroids in Ceres-like and Europa-like groups are characterized by large diameters and are concentrated in the first and second semi-major axis bins. It is unclear at this point whether these groups fit in the thermal alteration trend of the sharp and rounded groups, or whether different mechanisms are required.

(4) Our telescopic observations have revealed interesting trends that have placed some constraints on how, where, and when aqueous alteration occurred in the early solar system. We are conducting laboratory work that includes spectroscopy, petrology, and geochemistry of

CM/CI carbonaceous chondrites to better quantify the degree of aqueous alteration for outer Main Belt asteroids and to place more constraints on their meteorite analogs.

ACKNOWLEDGEMENTS

We acknowledge Richard Binzel (MIT), Bobby Bus (U. Hawaii), and Pierre Vernazza (ESO) for kindly providing their previously unpublished data obtained using the NASA Infrared Telescope Facility (IRTF). The IRTF is operated by the University of Hawaii under Cooperative Agreement no. NCC 5-538 with the National Aeronautics and Space Administration, Office of Space Science, Planetary Astronomy Program. We thank NASA IRTF staff for their assistance. We also thank Hap McSween for his help improving this manuscript.

REFERENCES

Abell, P. A. 2003. Near-IR reflectance spectroscopy of main belt and near-Earth objects: A study of their composition, meteorite affinities and source regions. Ph.D. thesis, Rensselaer Polytechnic Institute, Troy, New York, USA.

Beck, P., Quirico, E., Sevestre, D., Montes-Hernandez, G., Pommerol, A., and Schmitt, B. 2011. Goethite as an alterantive origin of the 3.1 μm band on dark asteroids. Astronomy and Astrophysics, 526, A85.

Bibring, J.P., Langevin, Y., Poulet, F., Gendrin, A., Gondet, B., Berthe, M., Soufflot, A., Drossart, P., Combes, M., Bellucci, G., Moroz, V., Mangold, N., Schmitt, B., OMEGA team. 2004. Prennial water ice identified in the south polar cap of Mars. Nature, 428, 629-630.

Bowell, E., Hapke, B., Domingue, D., Lumme, K., Peltoniemi, J., and Harris, A. W. 1989. Application of photometric models to asteroids. *In* Asteroids II, edited by BinzelR. P., GehrelsT., MatthewsM. S. Tucson: The University of Arizona Press. pp. 524–556.

Brearley, A.J. 2006. The action of water. In: Lauretta, D.S. and McSween Jr., H.Y. (Eds.). Meteorites and the Early Solar System II Arizona University Press, pp. 587-624.

Brown, R. H., Cruikshank, D. P., Pendleton, Y. J., and Veeder, G. J. 1997. Surface composition of Kuiper belt object 1993 SC. Science, 276, 937–939.

Bunch, T. E. and Chang, S. 1980. Carbonaceous chondrite phyllosilicates and height element geochemistry as indicators of parent body processes on surface conditions.Geochim. Cosmochim. Acta, 44**,** 1543- 1577.

Bus, S.I. and Binzel, R.P. 2002. Phase II of the Small Main-Belt Asteroid Spectroscopic Survey: The Observations**,** Icarus, 158**,** 1, 146-177.

Calvin W. M. and Clark R.N. 1991. Modeling the reflectance spectrum of Callisto 0.25 to 4.1-μm. Icarus, 89, 305-317.

Campins, H., Rieke, G.H., Lebofsky, M.J. 1983. Ice in Comet Bowell. Nature, 301, 405-406.

Campins, H., Hargrove, K., Pinilla-Alonso, N., Howell, E., Kelley, M., Licandro, J., Moth´e-Diniz, T., Fernndez, Y. & Ziffer, J. 2010. Water ice and organics on the surface of the asteroid 24 Themis. Nature, 464, 1320-1321.

Cohen, B. A. and Coker, R. F. 2000. Modeling of liquid water on CM meteorite parent bodies and implications for amino acid racemization. Icarus, 145, 369-381.

Cushing, M.C.2004. Spextool: A Spectral Extraction Package for SpeX, a 0.8-5.5 Micron Cross-Dispersed Spectrograph. ASP.

Cyr, K. E., Sears, W. D., and Lunine, J. I. 1998. Distribution and evolution of water ice in the

solar nebula: Implications for solar system body formation. Icarus, 135, 537–548.

DeMeo, F.E., Binzel, R.P., Slivan, S.M., Bus, S.J. 2009. An extension of the Bus asteroid taxanomy into the near-infrared. Icarus, 202, 160-180.

Dodson-Robinson, S.E., Willacy, K., Bodenheimer, P., Turner, N.J., Beichman, C.A. Ice lines, planetesimal composition and solid surface density in the solar nebula. Icarus, 200, 672-693.

Edwards, S., Cabrit, D., Strom, S. E., Heyer, I., Strom, K. M., and Anderson, E. 1987. Forbidden line and H-alpha profiles in T Tauri star spectra: A probe of anisotropic mass outflows and circumstellar disks. Astrophys. J., 321, 473–495.

Emery, J.P. and R.H. Brown, 2003. Constraints on the surface composition of Trojan asteroids from near-infrared (0.8 – 4.0 ìm) spectroscopy, Icarus, 164, 104-121.

Encrenaz T., Drossart P., Feuchtgruber H., Lellouch E., Bézard B., Fouchet T., and Atreya S. K. 1999. The atmospheric composition and structure of Jupiter and Saturn from ISO observations: A preliminary review. Planet. Space Sci., 47, 1225–1242.

Gaffey, M.J., Burbine, T.H., and Binzel, R.P. 1993a. Asteroid spectroscopy: Progress and perspective. Meteoritics, 28, 161-187.

Gaffey, S. J., McFadden, L. A., Nash, D., and Pieters, C. M. 1993b. Ultraviolet, visible, and near-infrared reflectance spectroscopy: Laboratory spectra of geologic materials. In: Pieters, C.M. and Englert, A.J. (eds.). Remote Geochemical Analysis: Elemental and Mineralogical Composition. Cambridge Univ., Cambridge, pp. 43-77.

Grimm, R. E. and McSween, H. Y. 1989. Water and the thermal evolution of carbonaceous chondrite parent bodies. Icarus, 82, 244–280.

Grimm, R. E. and McSween, H. Y. 1993. Heliocentric zoning of the asteroid belt by aluminum-26 heating. Science, 259, 653–655.

Harris, A. W. 1998. A thermal model for near-Earth asteroids. Icarus 131:291–301.

Harris, A.W., Lagerros, J.S.V. 2002. Asteroids in the thermal infrared. In: Bottke Jr., W.F., Cellino, P., Paolicchi, P., Binzel, R.P. (eds.). Asteroids III. Univ. of Arizona, 205–218.

Hiroi, T., Zolensky, M.E., and Pieters, C.M. 2001. The Tagish Lake Meteorite: A possible sample of a D-type asteroid. Science, 293, 2234-2236.

Howell, E. S., Britt, D. T., Bell, J. F., Binzel R. P., and Lebofsky L. A. 1994. Visible and near-infrared spectral observations of 4179 Toutatis. Icarus, 111, 468–474.

Jones, T. D., Lebofsky, L. A., Lewis, J. S., and Marley, M. S. 1990. The composition and origin

of the C, P, and D asteroids: Water as a tracer of thermal evolution in the outer belt, Icarus, 88, 172-192.

Kanno, A., Hiroi, T., Nakamura, R., Abe, M., Ishiguro, M., Hasegawa S., Miyasaka, S., Sekiguchi, T., Terada, H., and Igarashi, G. 2003. The first detection of water absorption on a D-type asteroid. Geophys. Res. Lett., 30, PLA 2-1 (CiteID 1909, DOI10.1029/2003GL017907).

King, T.V.V., Clark, R.N., Calvin, W.M., Sherman, D.M., Brown, R.H., 1992. Evidence for ammonium-bearing minerals on Ceres. Science, 255, 1551–1553.

Larson, H. P., Fink, U., Treffers, R., and Gautier T. N. (1975) Detection of water vapor on Jupiter. Astrophys. J. Lett., 197, 137–140.

Lebofsky, L.A. 1980. Infrared reflectance spectra of asteroids: A search for water of hydration. The Astronomical Journal, 85**,** 573-585.

Lebofsky L. A., Feierberg M. A., Tokunaga A. T., Larson H. P., and Johnson J. R. 1981. The 1.7- to 4.2-micron spectrum of asteroid 1 Ceres: Evidence for structural water in clay minerals. Icarus, 48, 453–459.

Lebofsky, L. A., Sykes, M. V., Tedesco, E. F., Veeder, G. J., Matson, D. L., Brown, R. H.,

Gradie, J. C., Feierberg, M. A., and Rudy, R.J. 1986. A refined ‘standard’ model for asteroids based on observations of 1 Ceres and 2 Pallas. Icarus, 68, 239–2

Licandro, J., Campins, H., Kelley, M., Hardgrove, K., Pinilla-Alonso, N., Cruikshank, Rivkin, A.S., Emery, J. 2010 . 65 Cybele: detection of small silicate grains, water-ice and organics. 2011. Astronomy and Atrophysics, 525, A34.

Lunine, I.J. 2006. Origin of water ice in the Solar System. In: Lauretta, D.S. and McSween Jr., H.Y. (Eds.). Meteorites and the Early Solar System II Arizona University Press, pp. 309-319-624.

McCord, T. B., Hansen, G. B., Matson, D. L., Johnson, T. V., Crowley, J. K., Fanale, F. P., Carlson, R. W., Smythe, W. D., Martin, P. D., Hibbitts, C. A., Granahan, J. C., and Ocampo, A. 1999. Hydrated salt minerals on Europa’s surface from the Galileo near-infrared mapping spectrometer (NIMS) investigation. J. Geophys. Res., 104, 11827–11852.

McSween Jr., H.Y. 1979. Alteration in CM carbonaceous chondrites inferred from modal and chemical variations in matrix. Geochim. Cosmochim. Acta, 43, 1761-1170.

McSween Jr., H. Y., Ghosh, A., Grimm, R. E., Wilson L., and Young, E. D. 2002. Thermal evolution models of asteroid. In: Bottke Jr., W.F., Cellino, P., Paolicchi, P., Binzel, R.P. (eds.). Asteroids III. Univ. of Arizona, pp. 559–571.

Miliken, R.E. and Rivkin, A.S. 2009. Brucite and carbonate assemblages from altered olivine-rich materials on Ceres. Nature Geosciences, 2, 258-261.

Montgomery, D., C. and Peck, E., A. 1992. Introduction to linear regression analysis (2^{nd} ed.). Wiley series in probability and mathematical statistics.

Mumma, M.J., Weaver, H.A., Larson, H.P., Williams, M., Davis, D.S. 1986. Detection of water vapor in Halley's comet. Science, 232, 1523-1528.

Mustard, J.F. et al., 2008. Hydrated silicate minerals on Mars observed by the Mars Reconnaissance Orbiter CRISM instrument. Nature 454, 305–309.

Pieters, C.M. and McFadden, L.A. 1994. Meteorite and asteroid reflectance spectroscopy: Clues to early solar system processes. Annu. Rev. Earth Planet. Sci, 22, 457-497.

Pinilla-Alonso, N. 2011. Ice vs Goethite on Themis. Workshop on Water in Asteroids and Meteorites, Observatoire de Paris, Paris, France.

Rayner, J.T., Toomey, D.W., Onaka, P.M., Denault, A.J., Strahlberger, W.E., Vacca, W.D., Cushing, M.C., Wang, S. 2003. SpeX: a medium-resolution 0.8-5.5 micron spectrograph and imager for the NASA Infrared Telescope Facility. Publ. Astron. Soc. Pacific, 155, 362-382.

Rayner, J.T., Onaka, P.M., Cushing, M.C., Vacca, W.D. 2004. Four years of good SpeX. SPIE

5492, 1498-1509.

Reddy, V., Emery, J. P., Gaffey, M. J., Bottke, W. F., Cramer, A. and Kelley, M. S. 2009). Composition of 298 Baptistina: Implications for the K/T impactor link. Meteoritics & Planetary Science, 44: 1917–1927. doi: 10.1111/j.1945-5100.2009.tb02001.x.

Rivkin, A.S. and Emery, J.P. 2010. Detection of ice and organics on an asteroidal surface. Nature , 64, 1322-1323.

Rivkin, A. S., Howell, E. S.,Vilas, F., Lebofsky, L. A. 2002. Hydrated Minerals on Asteroids: The Astronomical Record. In: Bottke Jr., W.F., Cellino, P., Paolicchi, P., Binzel, R.P. (eds.). Asteroids III. Univ. of Arizona, 235-253.

Rivkin, A.S., Binzel, R.P., Bus, S.J. 2005. Constraining near-Earth object albedos using near-infrared spectroscopy. Icarus, 175, 175-180.

Rivkin, A.S., Volquardsen, E.L., Clark, B.E. 2006. The surface composition of Ceres: Discovery of carbonates and iron-rich clays, Icarus, 185, 563-567.

Rubin, A. E. Mineralogy of meteorite groups. 1996. Meteoritics and Planetary Science, 32, 231-247.

Sonnett, C. P., Colburn, D. S., and Schwartz, K. 1968. Electrical heating of meteorite parent

bodies and planets by dynamo induction from a premain sequence T Tauri “solar wind.” Nature, 219, 924–926.

Taylor, J.R. 1982. An introduction to error analysis. University Science Books, 55-56.

Tedesco, E.F., Williams, J.G., Matson, D.L., and Veeder, G.J., 1989. A three-parameter asteroid taxonomy. The Astronomical Journal, 97, 580-606.

Tedesco, E.F., Noah, P.V., Noah, M., and Price, S.D. 2002. The supplemental IRAS minor planet survey. The Astronomical Journal, 123, 1056-1085.

Tomeoka, K. and Buseck, P. R. 1985. Indicators of aqueous alteration in CM carbonaceous chondrites: Microtextures of a layered mineral containing Fe, S, O and Ni. Geochim. Cosmochim. Acta, 49, 2149-2163.

Tholen, D.J., 1984. Asteroid taxonomy from cluster analysis of photometry, Ph.D. thesis, University of Arizona.

Vernazza, P., Mothé-Diniz, T., Barucci, M.A., Birlan, M., Carvano, J.M., Strazzulla, G., Fulchignoni,M., Migliorini, A., 2005. Analysis of near-IR spectra of 1 Ceres and 4 Vesta, targets of the Dawnmission. Astron. Astrophys. 436,1113–1121.

Vilas, F. and Gaffey, M.J. 1989. Phyllosilicate absorption features in main-belt and outer-belt

asteroids from reflectance spectroscopy. Science, 246, 790-792.

Vilas, F., Hatch, E.C., Larson, S.M., Sawyer, S.R., and Gaffey, M.J. 1993. Ferric iron in primitive asteroids; a 0.43-μm absorption feature. Icarus, 102, 255-231.

Vilas, F., Jarvis, K.S., and Gaffey, M.J. 1994. Iron alteration minerals in the visible and near-infrared spectra of low-albedo asteroids. Icarus, 109, 274-283.

Walsh, K.J., Morbidelli, A., Raymond, S.N., O'Brien, D.P., Mandell, A.M. 2011. A low mass for Mars from Jupiter's early gas-driven migration. Nature, 475, 206-209.

Weaver, H.A., Mumma, M.J., Larson, H.P., Davis, D.S., Post-perihelion observations of water in comet Halley. Nature, 324, 441-444.

Yang, B. and Jewitt, D., 2010. Identification of magnetite in B-type asteroids. The Astronomical Journal, 140, 692-698.

Zolensky, M.E. and McSween Jr., H.Y. 1988. Aqueous alteration. In: Kerridge, F. and Mattews, M (eds). Meteorites and the Early Solar System. Univ. of Arizona, Tuscon, 114-143.

Zolensky, M. E., Bourcier, W. L., and Gooding, J. L. 1989. Aqueous alteration on the hydrous asteroids: Results of EQ3/6 computer simulations. *Icarus*, 78, 411–425.

Appendix A

Table A1. Physical properties. Source: http://ssd.jpl.nasa.gov/sbdb.cgi.

Asteroid	a(AU)	d(km)[a]	Class[b]	Albedo[a]	Family/Group
190 Ismene	3.99	159	P	0.066	Hilda
153 Hilda	3.97	170.6	P	0.062	Hilda
361 Bononia	3.96	141.7	DP	0.045	Hilda
334 Chicago	3.89	158.5	C	0.062	
107 Camilla	3.49	222.6	C	0.053	Cybele
121 Hermione	3.44	209.0	C	0.048	Cybele
76 Freia	3.41	183.7	P	0.036	Cybele
790 Pretoria	3.41	170.4	P	0.038	Cybele
401 Ottilia	3.35	99.1	--	0.041	Cybele
1015 Christa	3.21	96.9	C	0.046	
31 Euphrosyne	3.16	256	C	0.0543	
511 Davida	3.16	326.1	C	0.054	
104 Klymene	3.15	123.7	C	0.057	Themis
10 Hygiea	3.14	407.1	C	0.072	Hygiea
130 Elektra	3.12	182.2	G	0.076	
120 Lachesis	3.11	174.1	C	0.046	
48 Doris	3.11	221.8	CG	0.062	
52 Europa	3.10	302.5	CF	0.058	
451 Patientia	3.06	225	CU	0.076	
704 Interamnia	3.06	316.62	F	0.074	
308 Polyxo	2.75	140.7	T	0.048	
36 Atalante	2.75	105.6	C	0.065	
187 Lamberta	2.73	130.4	C	0.057	
140 Siwa	2.73	109.8	P	0.067	
54 Alexandra	2.71	165.7	C	0.055	
34 Circe	2.69	113.5	C	0.054	
324 Bamberga	2.68	229.4	CP	0.063	
91 Aegina	2.59	109.8	CP	0.042	

[a]Tedesco et al. (1989) and Tedesco et al. (2002).
[a]Tholen (1984).

Table A2. Observing parameters for asteroids observed with the LXD mode of SpeX.

Asteroid	Date(UT)	Time(UT)	int (min)	Airmass	Standard Star	Spectral Type	B-V	V-K
190 Ismene	09/05/11	8:33-12:56	190	1.2-1.4	HD 216492	G0	0.47	1.3
153 Hilda	08/23/09	12:56-15:32	120	1.0-1.1	SAO 92660	G0	0.63	1.55
361 Bononia	01/22/10	10:32-14:19	180	1.1-1.2	SAO 61747	G5	0.61	1.55
334 Chicago	01/22/10	04:41-10:20	220	1.2-1.5	HD 29601	G5	0.65	---
107 Camilla	08/23/09	05:08-08:31	128	1.2-1.8	HD 155882	G0V	0.59	1.47
121 Hermione	01/21/10	04:43-09:41	180	1.9-1.2	HD 29714	G2V	0.65	1.58
76 Freia	04/16/09	08:34-11:36	96	1.1-1.5	HD 103459	G5	0.68	1.52
790 Pretoria	08/24/09	11.09-14:02	120	1.0-1.5	HD 223322	G0	0.58	1.38
401 Ottilia	01/21/10	09:48-14:07	180	1.0-1.4	SAO 80246	G0	0.59	1.34
1015 Christa	05/20/11	04:33-09:25	180	1.0-1.1	HD 118981	G0	0.58	1.48
31 Euphrosyne	09/04/11	11:55-14:48	100	1.6-1.0	HD 19617	G5	0.66	1.60
511 Davida	05/19/11	11:12-15:39	160	1.4-1.6	SAO 161836	G0	0.93	2.10
104 Klymene	04/11/10	04:50-09:39	140	1.0-1.7	HD 73708	G2V	0.61	1.66
10 Hygiea	04/09/10	04:44-08:59	180	1.1-1.3	HD 75528	G1V	0.63	1.53
130 Elektra	05/19/11	05:11-09:53	160	1.0-1.6	SAO 99574	G0	0.74	1.63
120 Lachesis	05/20/11	13:29-15:42	100	1.6-1.3	HD 203366	G4V	0.56	1.50
48 Doris	08/07/10	06:03-11:03	200	1.4-1.9	HD 171266	G3V	0.65	1.61
52 Europa	05/01/11	05:10-06:11	40	1.3-1.2	HD 106423	G0	0.57	1.36
451 Patientia	09/05/11	13 :29-15 :28	90	1.2-1.4	SAO 148056	GO	--	1.23
704 Interamnia	14/09/11	9:14-11:10	80	1.6-1.7	HD 177908	G0	0.58	1.53
308 Polyxo	04/11/10	11:16-15:40	200	1.4-1.6	SAO 159606	G3V	0.59	1.55
36 Atalante	08/09/10	11:01-15:43	180	1.3-1.3	HD 7128	G5	0.63	1.77
187 Lamberta	08/08/10	11:13-15:30	180	1.3-1.4	HD 116	G0	0.59	1.37
140 Siwa	09/25/09	05:51-07:16	80	1.4-1.8	HD 193298	G2V	0.60	1.54
54 Alexandra	08/07/10	11:14-15:29	180	1.2-1.1	SAO 91793	G0	0.63	1.58
34 Circe	08/09/10	05:42-10:52	180	1.7-1.5	HD 180060	G3V	0.58	1.60
324 Bamberga	05/01/11	06:21-07:17	40	1.1-1.1	HD 94706	G5	0.61	1.48
91 Aegina	04/09/10	10:31-13:26	140	1.2-1.6	HD 116367	G5	0.63	1.5

Table A3. Observing parameters for asteroids observed with the prism mode of SpeX.

Asteroid [a]	Date (UT)	Time (UT)	int (min)	Airmass	Standard Star	Spectral Type	B-V	V-K
190 Isemne	04/15/2009	15:04-15:32	32	1.2-1.3	HD165445	G3V	0.60	1.48
361 Bononia	01/21/10	14:50-15:33	32	1.2-1.4	HD 87680	G2V	0.62	1.54
334 Chicago	04/07/03	7:07-7:19	32	1.1-1.2	SAO 79521	G2V	0.67	1.52
107 Camilla	03/29/07	5:59-6:20	24	1.0	HD 69809	G0	0.64	1.49
790 Pretoria	08/24/09	14.18-14:45	32	1.2-1.3	HD 223322	G0	0.58	1.38
401 Ottilia	01/21/10	14:17-14:44	16	1.5-1.8	SAO 80246	G0	0.59	1.34
1015 Christa	09/06/11	5:41-6:05	16	2.2-2.7	HD 125712	G5	0.32	1.08
31 Euphrosyne	09/05/11	15:20-15:40	32	1.0-1.1	HD 19617	G5	0.66	1.60
511 Davida	09/18/11	4:51-5:35	64	1.3-1.4	HD 162255	G3V	0.61	1.58
104 Klymene	05/01/11	08:42-09:05	16	1.9-1.1	HD 119026	G0	0.57	1.46
120 Lachesis	09/05/11	6:41-7:00	16	1.4	HD 19529	G8	1.02	2.44
48 Doris	04/19/10	15:37-15:54	12	1.2	HD 180060	G3V	0.58	1.6
451 Patientia	09/19/11	10:11-10:39	32	1.4-1.3	SAO 148019	G5	0.59	1.49
308 Polyxo	04/10/10	13:27-14:36	48	1.2-1.4	SAO 159606	G3V	0.59	1.55
187 Lamberta	12/06/10	06:04-06:17	16	1.2-1.3	HD 219201	G5	0.60	1.55
140 Siwa	03/29/07	5:39-5:55	24	1.0	HD 56513	G2V	0.63	1.66
54 Alexandra	12/06/10	05:43-05:53	8	1.0	HD 222718	G5	0.61	1.66
324 Bamberga	04/30/11	06:21-07:17	40	1.1-1.1	HD 94706	G5	0.61	1.48
91 Aegina	04/10/10	08:15-13:26	32	1.3	HD 115153	G5	0.66	1.74

[a] Prism spectra of the following asteroids were obtained from the MIT-UH-IRTF Joint Campaign for NEO Reconnaissance database:153 Hilda, 368 Haidea, 121 Hermione, 130 Elektra, 36 Atalante, 34 Circe, 52 Europa, 10 Hygiea, 76 Freia, and 704 Interamnia.

Table A4. Results

Asteroid	Type[a](Type[b])	IR slope[c] $(\mu m)^{-1}$	0.7-μm Band Depth[d] (%)	3.00-μm Band Depth (%)	$R_{2.90}$	$R_{3.05}$	$R_{2.90}/R_{3.05}$	3-μm Band Center (μm)	3-μm Band Shape
24 Themis[e]	C, B, L, Cb, or X (C)	0.0599±0.0035	Featurless	18.22±2.66	0.973±0.002	0.953±0.002	1.021±0.002	3.08±0.01	Rounded
190 Ismene	Xc, Cc, L, T, or K (P)	0.1624±0.0008	Featureless	8.98±5.74	1.022±0.003	1.012±0.006	1.010±0.007	3.11±0.02	Rounded
153 Hilda	Xc, Cc, L, T, or K (P)	0.1754±0.0005	Featureless	11.36±11.05	1.082±0.016	1.033±0.010	1.047±0.018	3.12±0.01	Rounded
361 Bononia	D (DP)	0.2802±0.0009	Featureless	6.83±3.90	0.973±0.002	0.952±0.002	1.022±0.003	3.09±0.01	Rounded
334 Chicago	C, B, L, Cb, or X (C)	0.1489±0.0008	Featureless	9.33±8.50	0.991±0.006	1.018±0.005	0.973±0.008	<2.85	Sharp
107 Camilla	Xc, Cc, L, T, or K (C)	0.1338±0.0011	Featureless	13.68±7.26	0.995±0.013	0.976±0.007	1.019±0.015	3.08±0.01	Rounded
121 Hermione	Xc, Cc, L, T, orK (C)	0.1266±0.0018	3.49±0.02	24.02±7.70	0.775±0.003	0.845±0.002	0.917±0.005	<2.85	Sharp
76 Freia	D (P)	0.1715±0.0011	Featureless	12.29±7.63	1.043±0.024	0.967±0.026	1.079±0.035	3.09±0.02	Rounded
790 Pretoria	Xc, Cc, L, T, or K (P)	0.1618±0.0005	Featureless	11.28±5.61	1.064±0.005	1.047±0.005	1.016±0.007	3.03±0.01	Rounded
401 Ottilia	Xc, Cc, L, T, or K (–)	0.1857±0.0015	--	7.58±6.61	1.061±0.009	1.035±0.007	1.025±0.011	3.11±0.02	Rounded
1015 Christa	K, L, or Sq (C)	0.2197±0.0020	Featureless	19.75±18.84	0.926±0.026	1.020±0.021	0.908±0.035	<2.85	Sharp
31 Euphrosyne	D (C)	0.2659±0.0017	Featureless	13.63±4.56	--	--	--	3.15±0.01	Europa-like
511 Davida	Cc, B, L, Cb, or X (C)	0.1118±0.0012	Featureless	19.32±9.42	0.905±0.005	0.949±0.004	0.954±0.007	<2.85	Sharp
104 Klymene	C, B, L, Cb, or X (C)	0.0275±0.0013	11.82±7.78	11.82±10.18	0.827±0.022	0.960±0.018	0.861±0.033	<2.85	Sharp
10 Hygiea	C, B, L, Cb, or X (C)	0.0499±0.0010	Featureless	12.09±7.76	--	--	--	3.05±0.01	Ceres-like
130 Elektra	Xc, Cc, L, T, or K (G)	0.0894±0.0015	4.62±0.02	36.90±9.57	0.732±0.023	0.812±0.017	0.901±0.038	<2.85	Sharp
120 Lachesis	C, B, L, Cb, or X (C)	0.1568±0.0009	Featureless	14.11±13.23	0.885±0.012	0.974±0.009	0.909±0.016	<2.85	Sharp
48 Doris	Xc, Cc, L, T, or K (CG)	0.0179±0.0013	6.25±0.01	23.50±3.65	0.779±0.020	0.834±0.016	0.934±0.032	<2.85	Sharp
52 Europa	C, B, L, Cb, or X (CF)	0.1283±0.0020	Featureless	11.48±0.99	--	--	--	3.15±0.01	Europa-like
451 Patientia	C, B, L, Cb, or X(CU)	0.0832±0.0010	Featureless	12.66±7.12	--	--	--	3.15±0.01	Europa-like
704 Interamnia	Indeterminate (F)	0.0650±0.0067	Featureless	10.37±4.91	0.970±0.005	1.006±0.004	0.964±0.007	<2.85	Sharp
308 Polyxo	Xc, Cc, L, T, or K (T)	0.2130±0.0021	Featureless	14.08±3.31	0.887±0.004	0.954±0.003	0.930±0.005	<2.85	Sharp
36 Atalante	Xc, Cc, L, T, or K (C)	0.1251±0.0010	3.05[f]	21.49±6.82	0.874±0.005	0.995±0.004	0.878±0.007	<2.85	Sharp
187 Lamberta	Xc, Cc, L, T, or K (C)	0.0792±0.0009	1.89±0.07	18.56±18.58	0.868±0.007	0.907±0.006	0.957±0.010	<2.85	Sharp
140 Siwa	Xc, Cc, L, T, or K (P)	0.1304±0.0006	Featureless	1.60±6.77	--	--	--	--	Featureless
54 Alexandra	Xc, Cc, L, T, or K (C)	0.2046±0.0012	2.37[f]	26.13±5.28	0.787±0.004	0.893±0.002	0.881±0.006	<2.85	Sharp
34 Circe	Xc, C,c L, T, or K (C)	0.0624±0.0014	2.99±0.02	13.15±6.75	0.891±0.008	0.942±0.006	0.946±0.011	<2.85	Sharp
324 Bamberga	Xc, Cc, L, T, or K(CP)	0.1865±0.0015	Featureless	8.40±5.62	--	--	--	3.05±0.01	Ceres-like
91 Aegina	Xc, Cc, L, T, or K (C)	0.0535±0.0011	1.72±0.04	27.48±26.99	0.808±0.005	0.872±0.004	0.927±0.008	<2.85	Sharp

[a] Bus-DeMeo taxonomy (DeMeo et al. 2009).
[b] Tholen taxonomy (Tholen 1984).
[c] IR slopes were calculated using an algorithm described by DeMeo et al. (2009)
[d] Data from the Small Bodies Data Ferret: http://sbn.psi.edu/ferret/
[e] Themis spectra from Rivkin and Emery (2010).
[f] Uncertainty is not provided by the Small Bodies Data Ferret for this asteroid

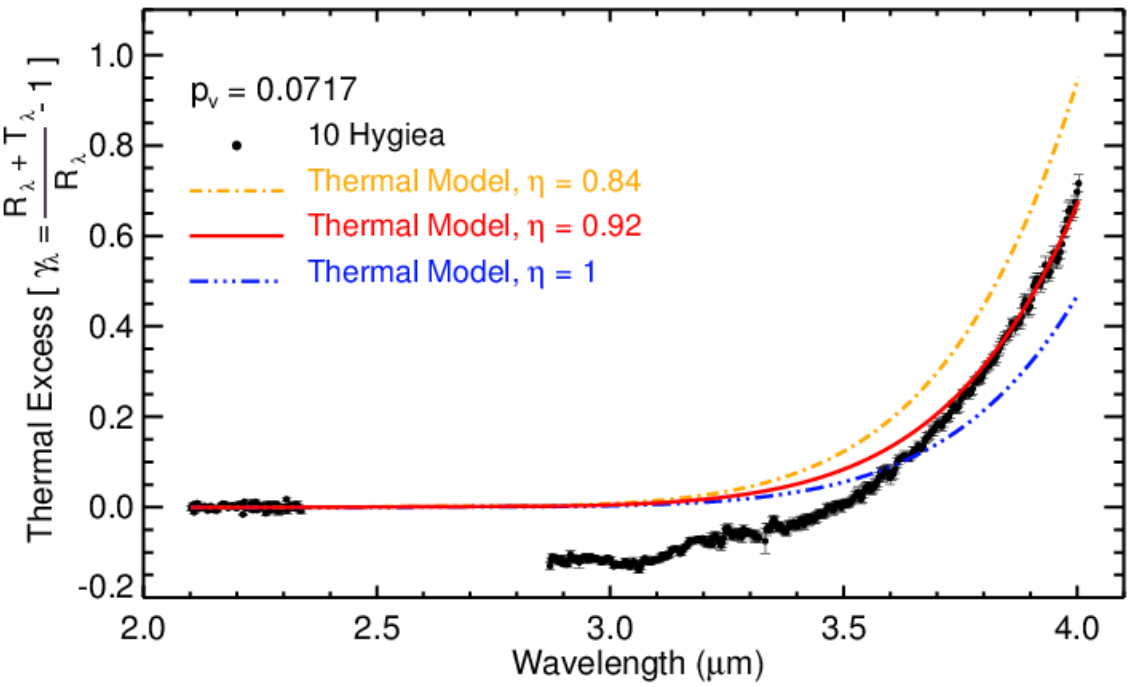

Figure A1. Uncorrected spectrum of 10 Hygiea with thermal models, using different values of the beaming parameter (η).

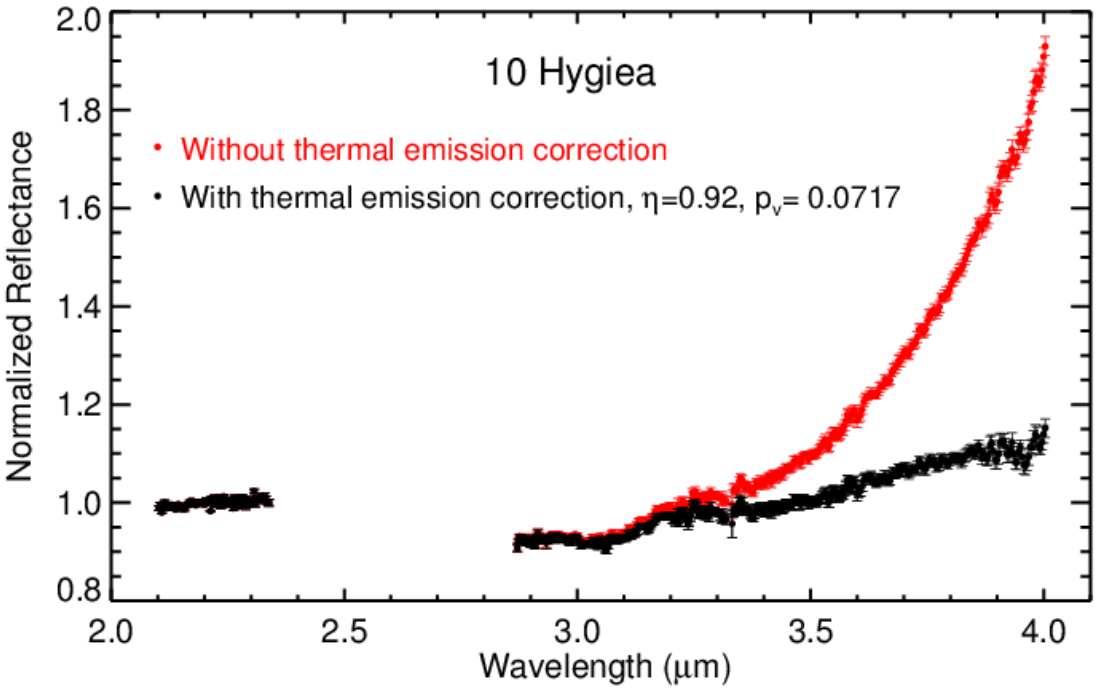

Figure A2. Spectrum of 10 Hygiea uncorrected and corrected, using thermal model of a beaming parameter η = 0.92.

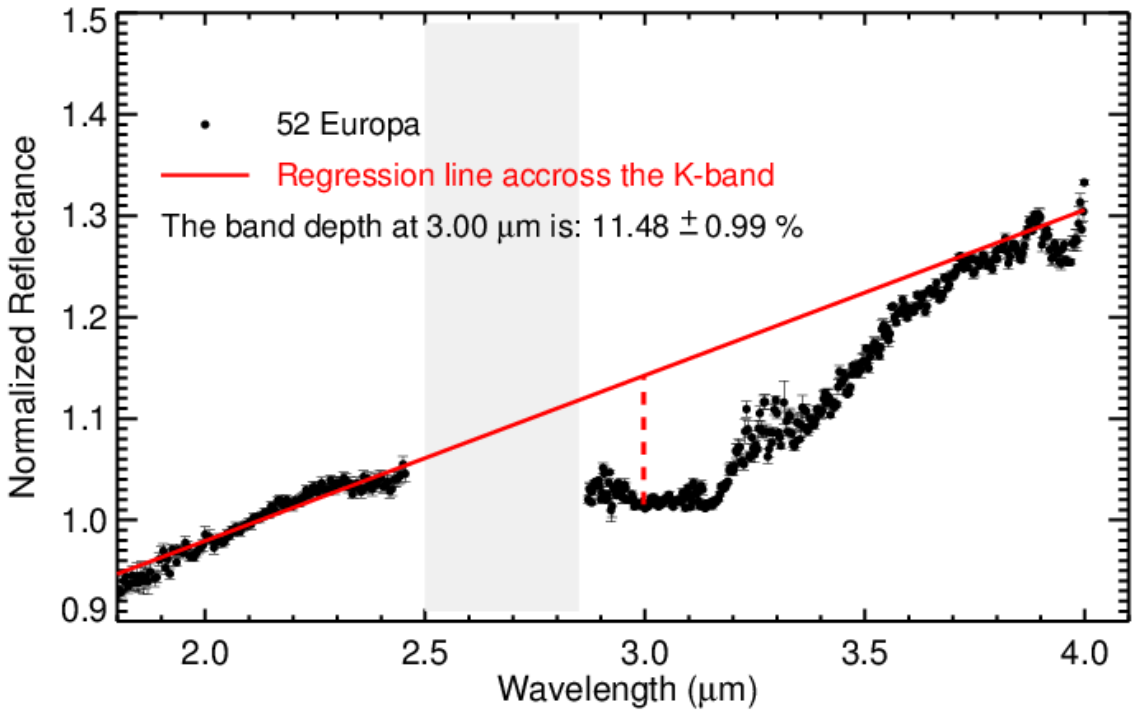

Figure A3. The band depth is calculated by using a regression line across the K-band of the spectrum of 52 Europa. The band depth at 3.00 µm is: 11.48 ± 0.99 %. The dashed line shows the band depth at 3.00 µm.

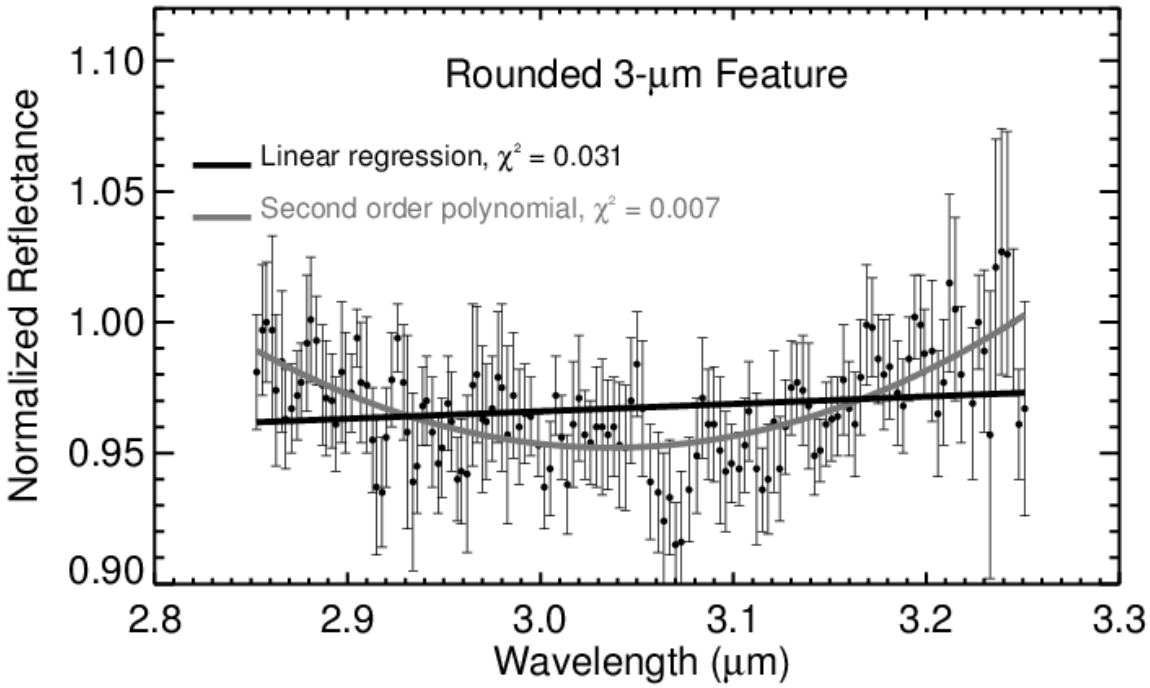

Figure A4. Determination of the best fit for the rounded 3-µm feature of 361 Bononia. The calculated chi-squared of the second order polynomial fit (in gray) across the 2.85-3.25-µm region has a lower value than one calculated for the linear regression fit (in black). Hence, the former fit is better than the latter. In this chi-squared test, the predicted data are the spectrum data and the observed data are the trendline data. The same technique was used for the sharp 3-µm feature.

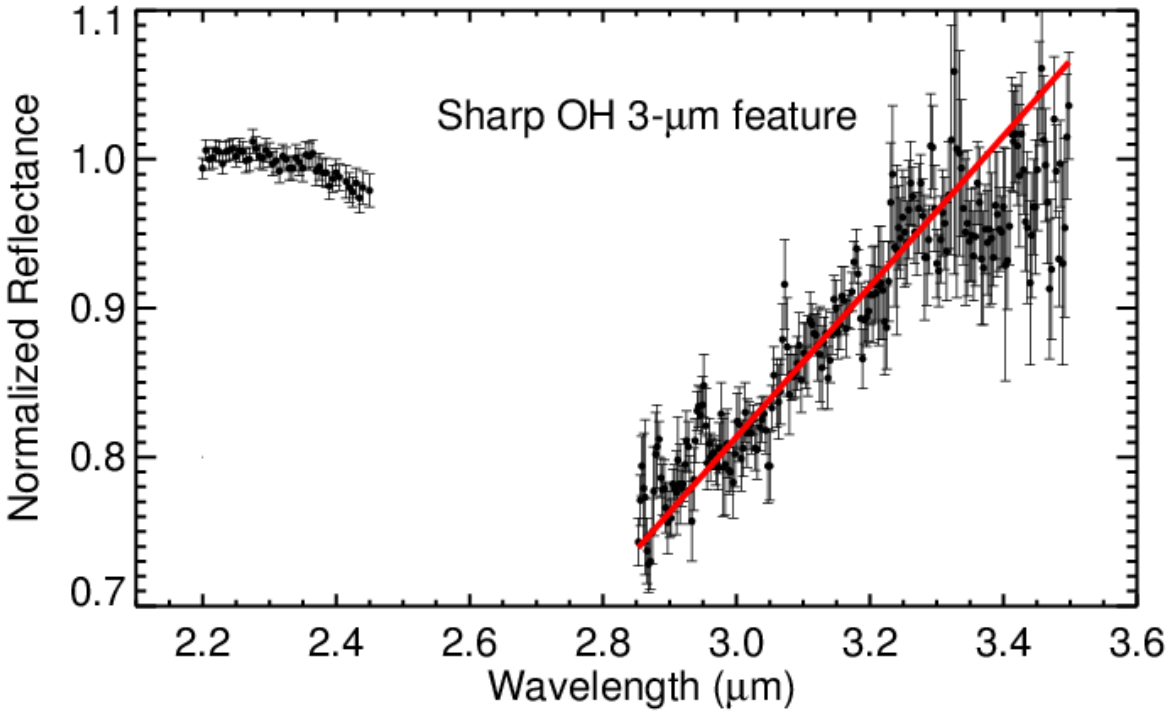

Figure A5. Isolated sharp 3-lm feature in the spectrum of 121 Hermione. The best fit for this feature is a linear regression across the 2.85-3.25-µm region (in red).

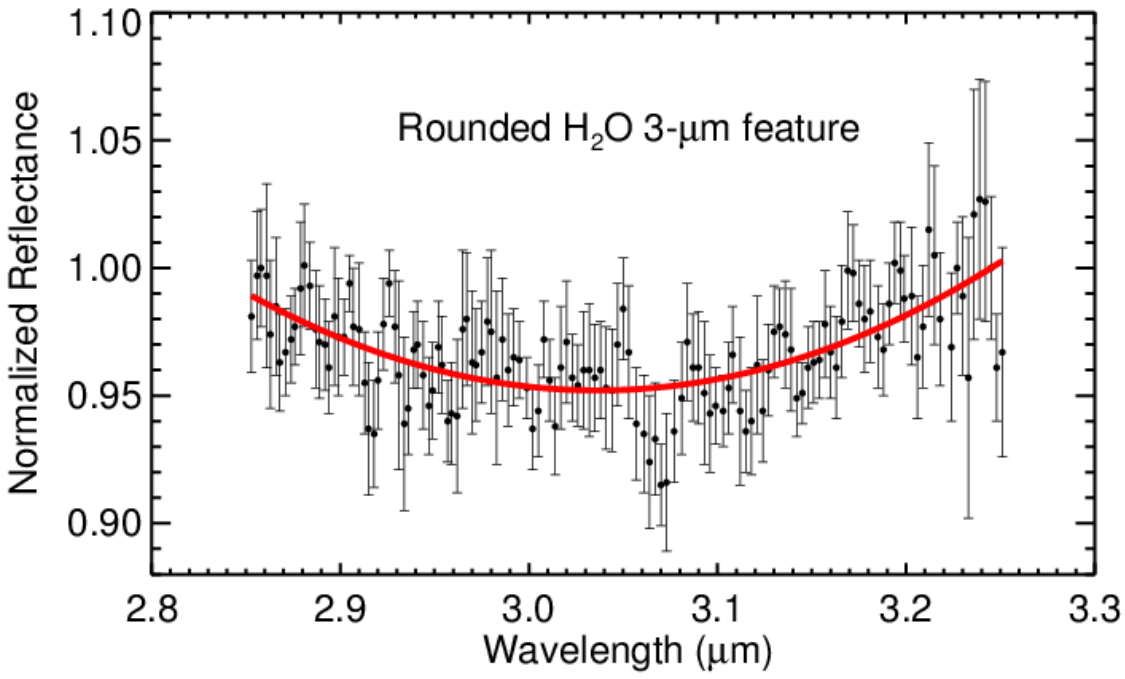

Figure A6. Isolated rounded 3-µm feature in the spectrum of 361 Bononia. The best this feature is a second order polynomial across the 2.85-3.25-lm region (in red).

Figure A7. The group with sharp 3-μm features. All spectra have been normalized to unity at 2.2 μm. The gray bars on each plot mark wavelengths of strong absorption by water vapor in Earth's atmosphere.

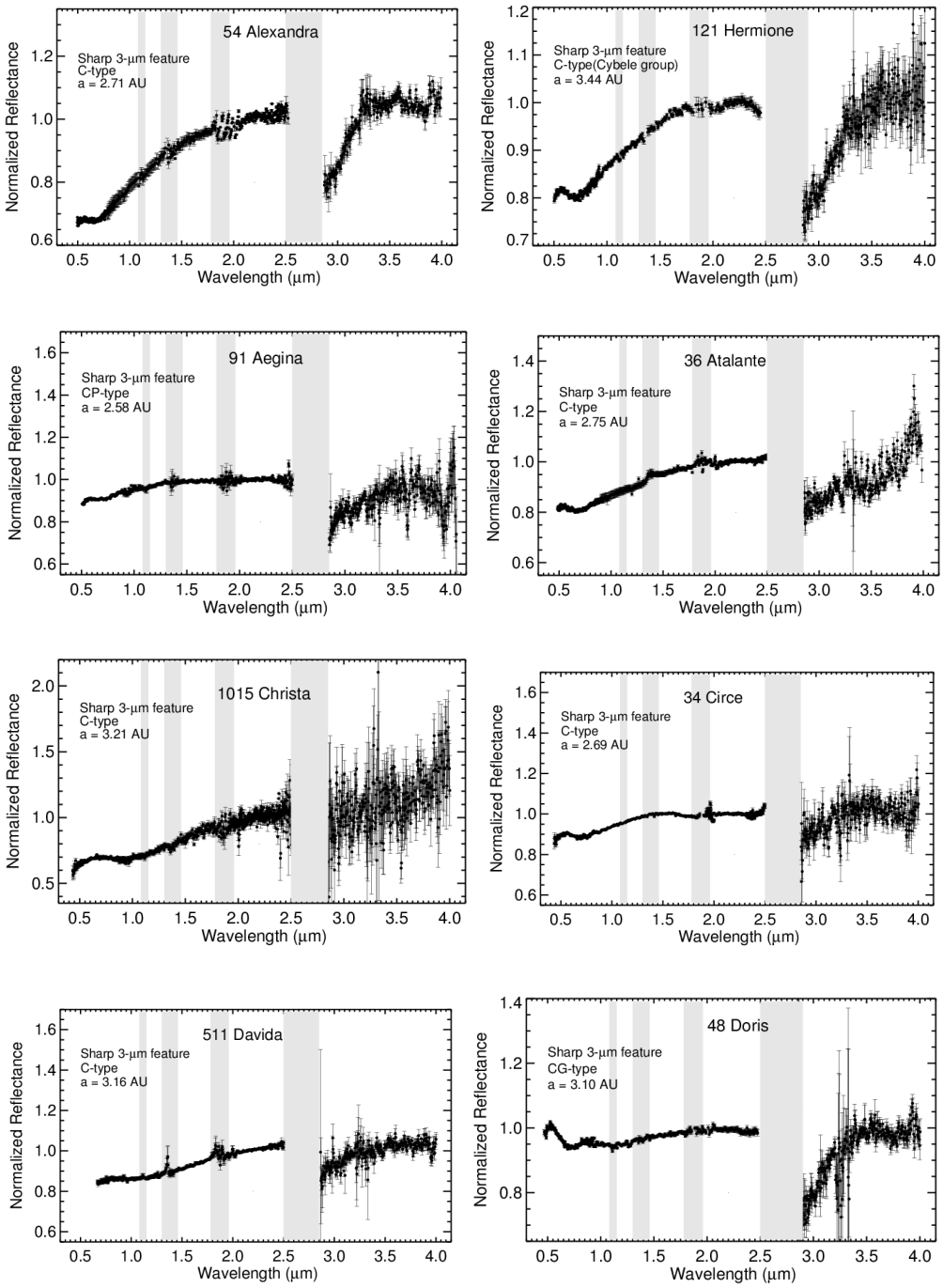
54 Alexandra
Sharp 3-μm feature
C-type
a = 2.71 AU
121 Hermione
Sharp 3-μm feature
C-type(Cybele group)
a = 3.44 AU
91 Aegina
Sharp 3-μm feature
CP-type
a = 2.58 AU
36 Atalante
Sharp 3-μm feature
C-type
a = 2.75 AU
1015 Christa
Sharp 3-μm feature
C-type
a = 3.21 AU
34 Circe
Sharp 3-μm feature
C-type
a = 2.69 AU
511 Davida
Sharp 3-μm feature
C-type
a = 3.16 AU
48 Doris
Sharp 3-μm feature
CG-type
a = 3.10 AU
Normalized Reflectance
Wavelength (μm)

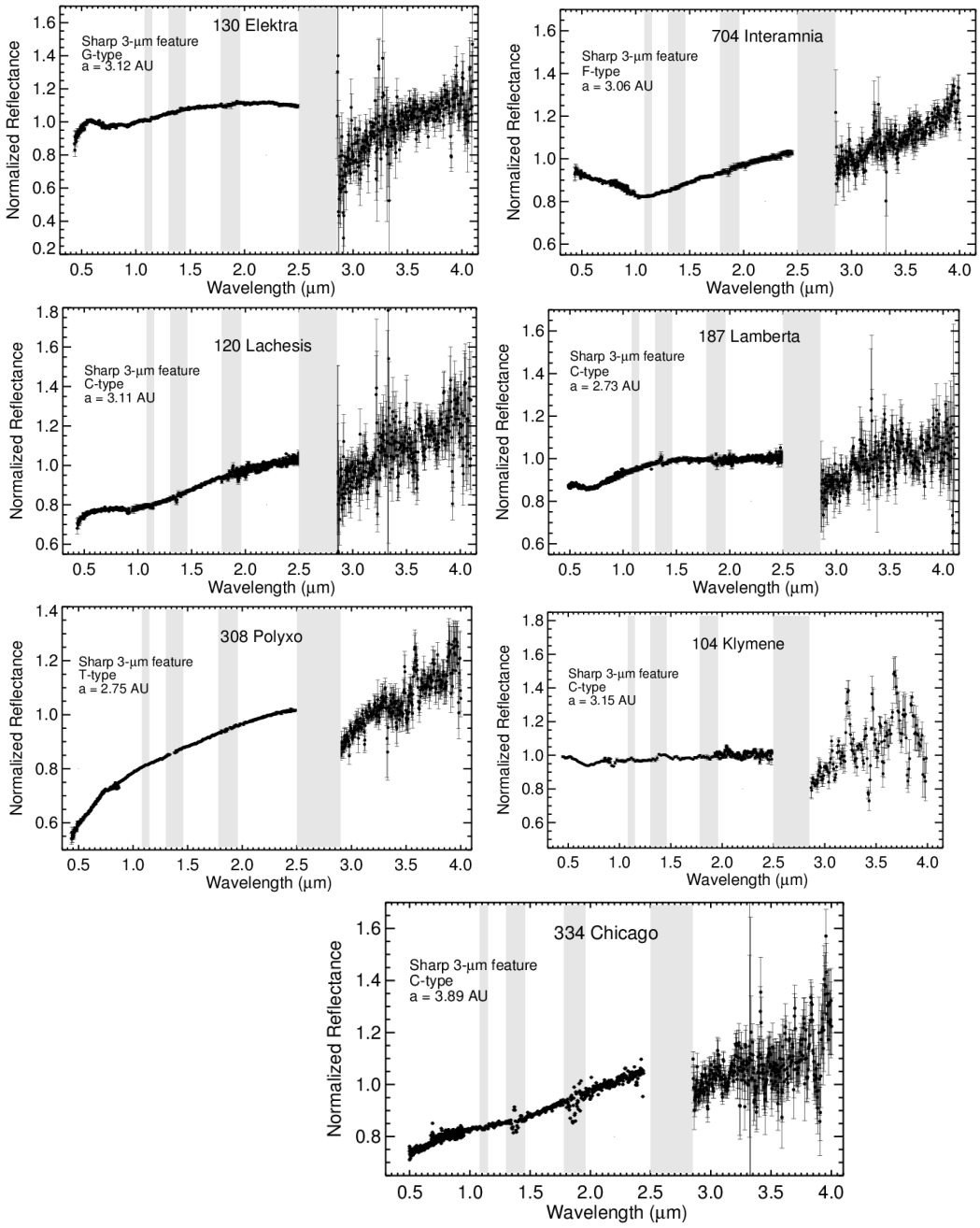
130 Elektra
Sharp 3-μm feature
G-type
a = 3.12 AU
704 Interamnia
Sharp 3-μm feature
F-type
a = 3.06 AU
120 Lachesis
Sharp 3-μm feature
C-type
a = 3.11 AU
187 Lamberta
Sharp 3-μm feature
C-type
a = 2.73 AU
308 Polyxo
Sharp 3-μm feature
T-type
a = 2.75 AU
104 Klymene
Sharp 3-μm feature
C-type
a = 3.15 AU
334 Chicago
Sharp 3-μm feature
C-type
a = 3.89 AU
Normalized Reflectance
Wavelength (μm)

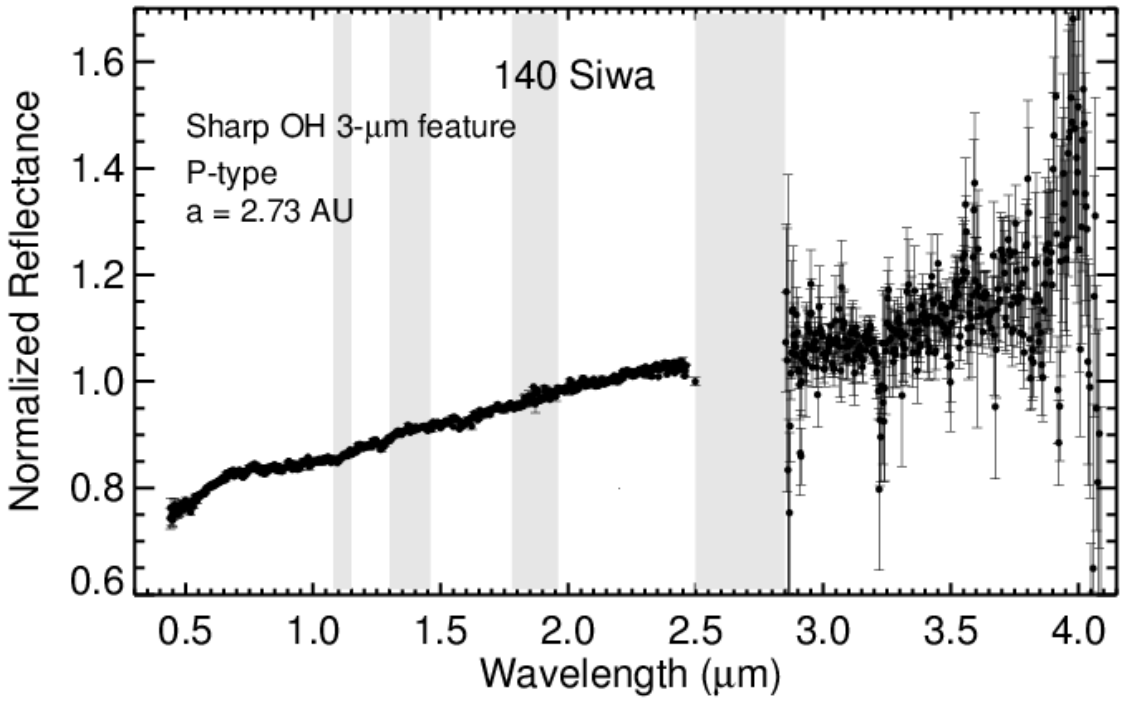

Figure A8. 140 Siwa does not show any feature above the noise level in the 3-µm region. This spectrum has been normalized to unity at 2.2 µm. The gray bars on each plot mark wavelengths of strong absorption by water vapor in Earth's atmosphere.

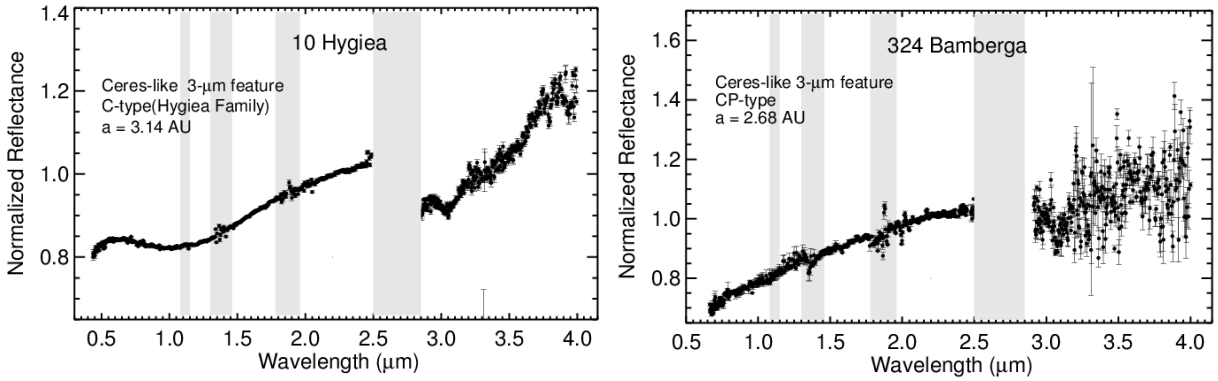

Figure A9. The Ceres-like group with a 3-μm feature centered at 3.05 ± 0.01 μm. All spectra have been normalized to unity at 2.2 μm. The gray bars on each plot mark wavelengths of strong absorption by water vapor in Earth's atmosphere.

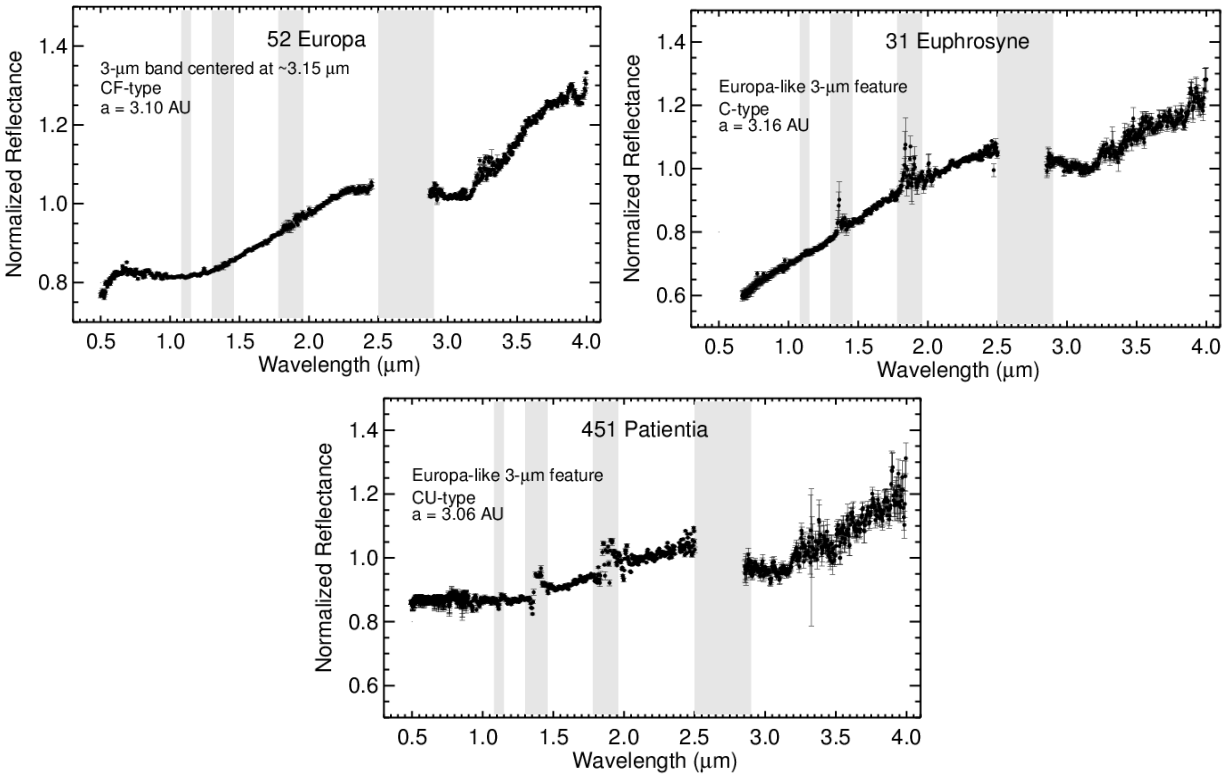

Figure A10. The Europa-like group with a 3-µm feature centered at 3.15 ± 0.01 µm. All spectra have been normalized to unity at 2.2 µm. The gray bars on each plot mark wavelengths of strong absorption by water vapor in Earth's atmosphere.

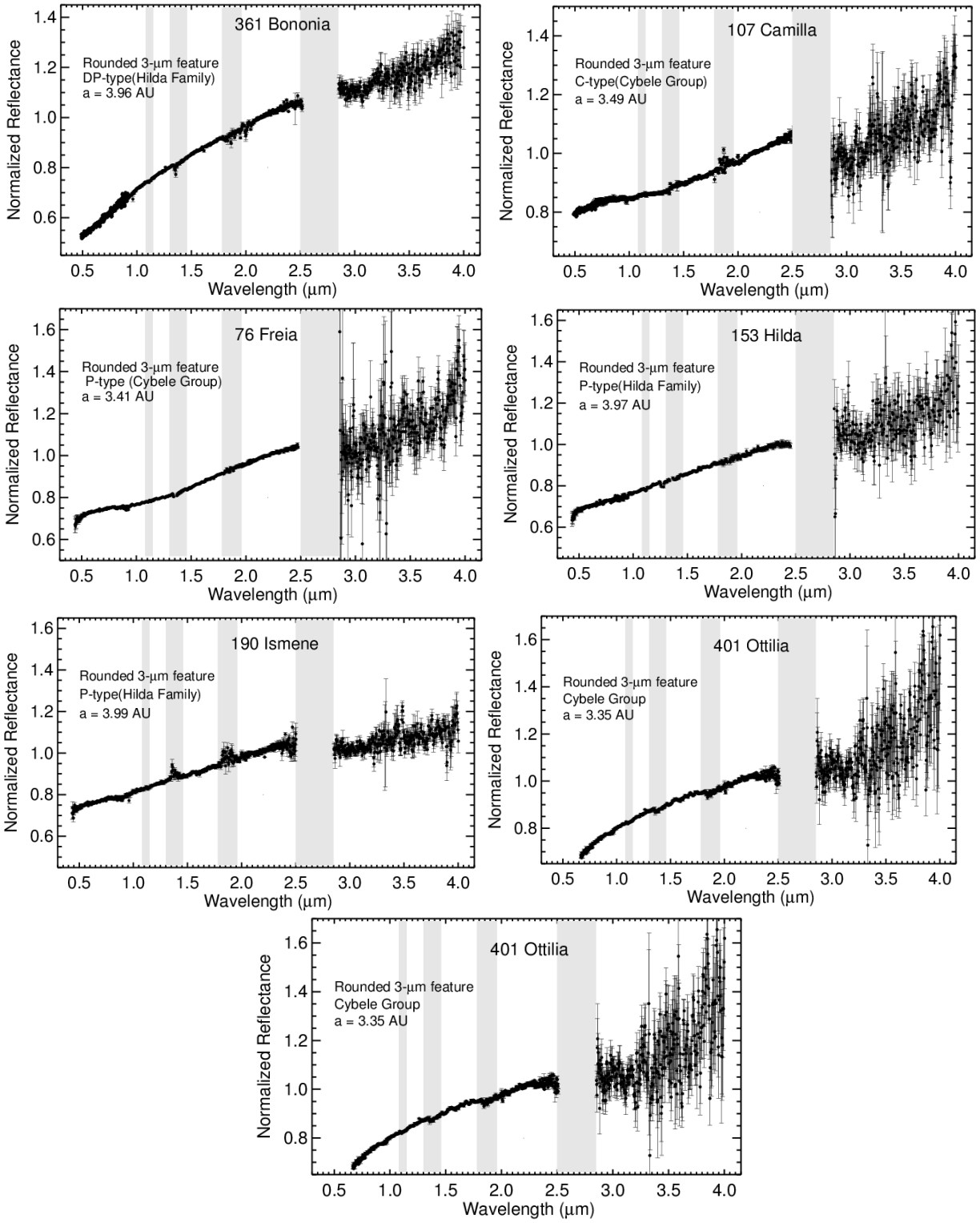

Figure A11. The rounded 3-µm feature. All spectra have been normalized to unity at 2.2 µm. The gray bars on each plot mark wavelengths of strong absorption by water vapor in Earth's atmosphere.

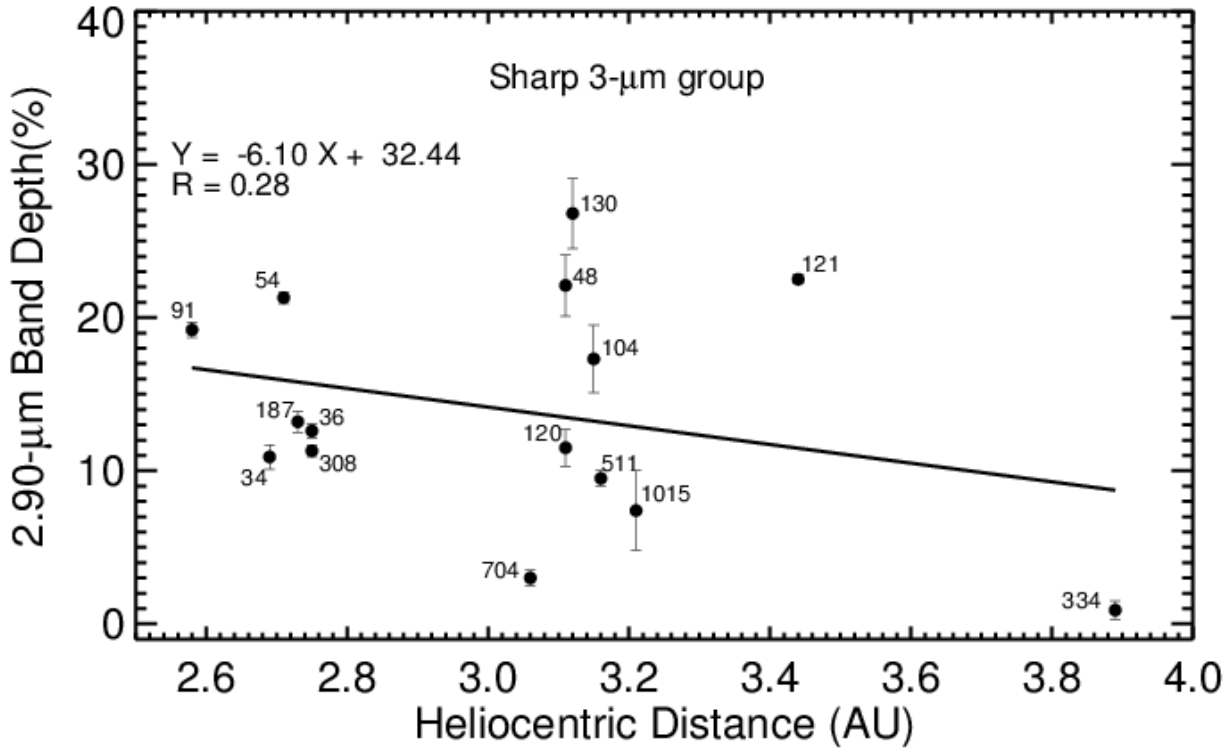

Figure A12. Heliocentric distance vs. the band depth at 2.90 µm for asteroids that exhibit the sharp OH 3-µm feature. The reflectance was calculated by fitting a linear regression line across the 2.85–3.25-µm region. 2.90-µm band depth decrease with the increase of the heliocentric distance. The R (linear-correlation coefficient) value of 0.28 corresponds to a probability of ~0.60 (1σ) that the variables are correlated. If we exclude 121 Hermione and 130 Electra (binaries) from the plot, the R value would be 0.64, corresponding to a probability of ~0.95 (2σ) that the variables are correlated. However, if we exclude 334 Chicago from the plot we would have a weaker correlation.

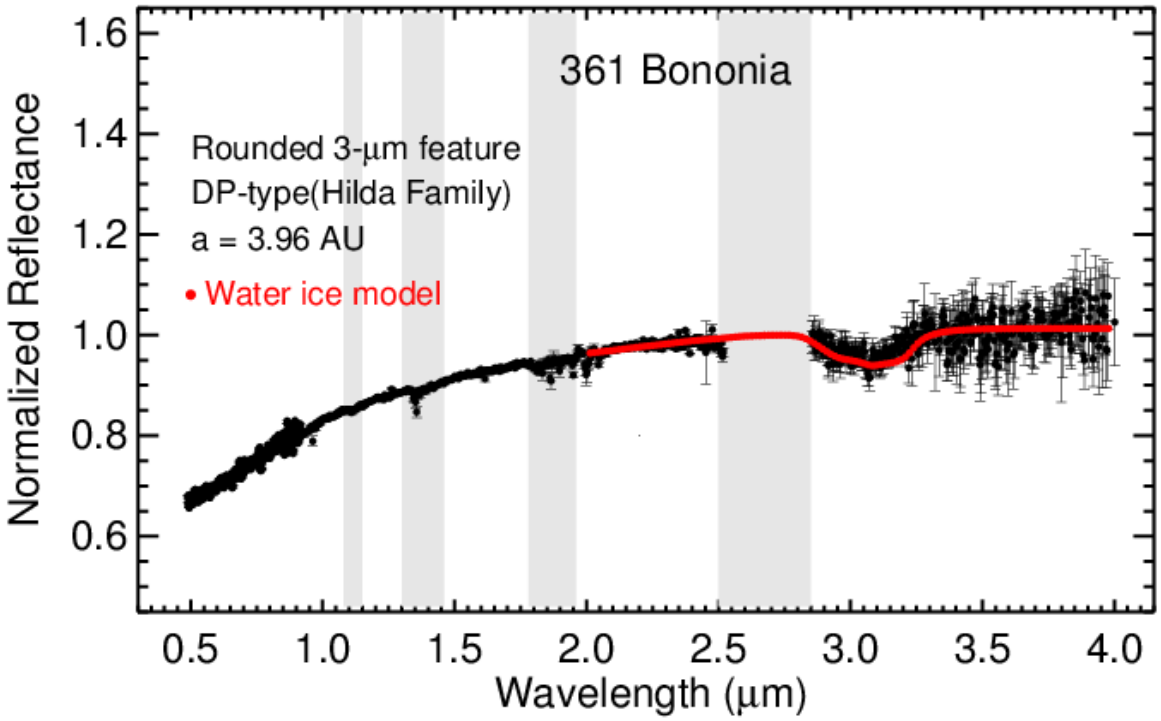

Figure A13. The spectrum of 361 Bononia, which is characterized by a round 3-µm feature, is matched very well by the spectral model of Rivkin and Emery (2010) of a mixture of water ice-coated pyroxene grains and amorphous carbon (in red).

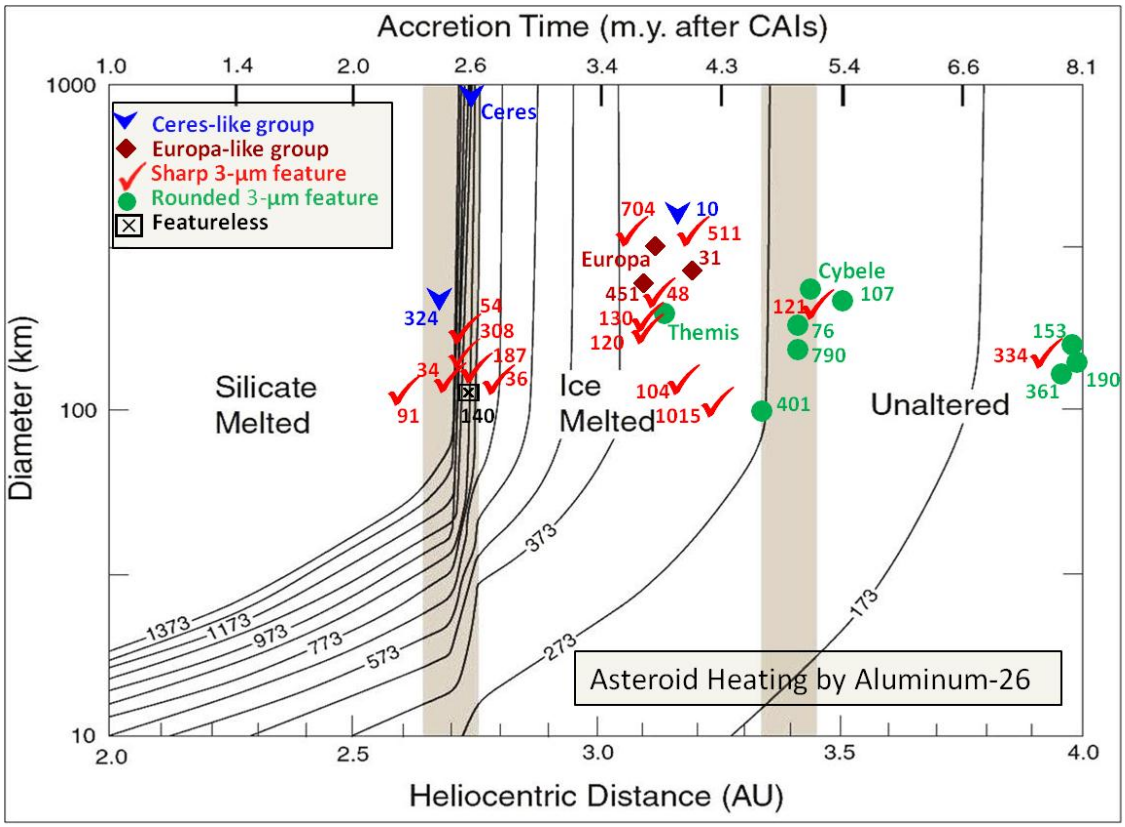

Figure A14. Asteroids analyzed in this study plus 24 Themis (Rivkin and Emery 2010; Campins et al. 2010), 65 Cybele (Licandro et al. 2011), and 1 Ceres (Rivkin et al. 2006), are plotted in the context of the thermal model of Grimm and McSween (1993).

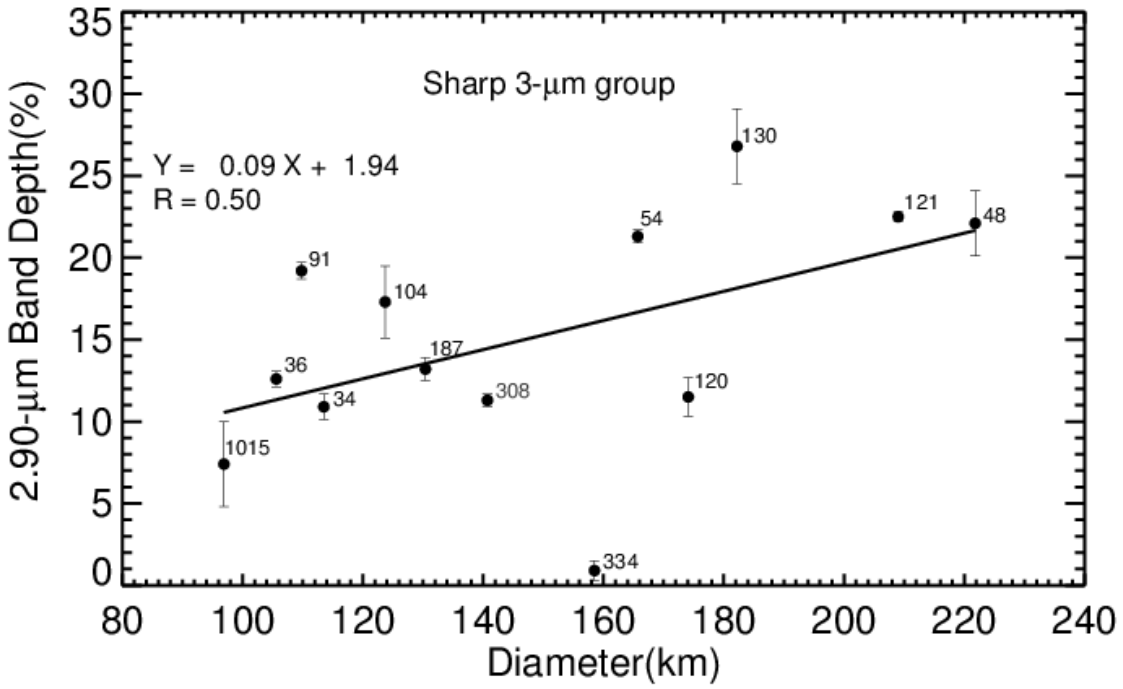

Figure A15. Diameter vs. the band depth at 2.90 µm for asteroids (D < 300 km) exhibit the sharp OH 3-µm feature. The reflectance was calculated by fitting a linear regression line across the 2.85-3.25-µm region. 2.90-µm band depth increases with the increase of the diameter. The R (linear-correlation coefficient) value of 0.50 corresponds to a probability of ~0.95 (2σ) that the variables are correlated.

Chapter 2

Nature and Degree of Aqueous Alteration in CM and CI Carbonaceous Chondrites

This chapter is a reformatted version of a paper of the same name submitted to Meteoritics and Planetary Science in December 2012.

Takir D., Emery J.P., McSween Jr. H. Y., Hibbitts C.A., Clark R.N., Pearson N., and Wang A. (in review) Nature and Degree of Aqueous Alteration in CM and CI Carbonaceous Chondrites. *Meteoritic & Planetary Science*.

Abstract

In the present study, we investigate the petrological, geochemical, and spectral parameters that relate to the degree of aqueous alteration in nine CM and one CI (Ivuna) carbonaceous chondrites. Our underlying hypothesis is that the position and shape of the 3-μm band is diagnostic of phyllosilicate mineralogy. We measured reflectance spectra of the chondrites under dry conditions and vacuum to remove adsorbed water and mimic the space environment, for subsequent comparison with reflectance spectra of asteroids. We have identified three spectral CM groups in addition to Ivuna. "Group 1", which is the least altered group, is characterized by 3-μm band centers at longer wavelengths and is consistent with cronsdetite (Fe-serpentine). "Group 3", which is the most altered group, is characterized by 3-μm band centers at shorter wavelengths and is consistent with antigorite (serpentine). "Group 2" is an intermediate group between Group 1 and 3. Ivuna exhibits a unique spectrum that is distinct from the CM meteorites and is consistent with lizardite and chrysotile (serpentine). The petrological and geochemical parameters, which were determined using microprobe analyses and microscope observation, are found to be consistent with the three spectral groups. These results indicate that the distinct parent body aqueous alteration environments experienced by these carbonaceous chondrites can be distinguished using reflectance spectroscopy. High-quality

ground-based telescopic observations of Main Belt asteroids can be expected to reveal not just whether an asteroid is hydrated, but also details of the alteration state.

1.0 INTRODUCTION

Aqueous alteration is possibly the most widespread process that has affected primitive solar system materials and chondritic meteorites (Brearley 2006). The CM (Mighei-like) and CI (Ivuna-like) carbonaceous chondrites were affected by varying degrees of fluid-assisted alteration (McSween 1979a; Bunch and Chang 1980; Tomeoka and Buseck 1985; Zolensky and McSween 1988; Brearley 2006). Indications of aqueous alteration are obtained from mineralogic (Browning et al. 1996; Zolensky et al. 1993), geochemical (McSween 1979a), oxygen and hydrogen isotopic (Clayton 1999; Eiler and Kitchen 2004), and textural (Lee 1993; Browning et al. 2000) analyses of chondrites.

CM and CI carbonaceous chondrites are widely thought to derive from the C-complex asteroids (Bell et al. 1989; Gaffey et al. 1993). If so, the meteorites and asteroids should have similar mineralogies. Infrared (IR) reflectance spectroscopy of CM and CI chondrites and their possible parent bodies can be useful in identifying hydrated phases, which exhibit a variety of spectral features. For asteroid and meteorite spectroscopy, absorptions around 0.7 μm and 3.0 μm are particularly diagnostic. The former absorption is attributed to a $Fe^{2+} \rightarrow Fe^{3+}$ charge transfer in phyllosilicates, and the latter to structural water- and hydroxyl-bearing minerals (Vilas and Gaffey 1989; Lebofsky 1980; Rivkin et al. 2002).

Laboratory analyses of CM and CI chondrites, in addition to telescopic observations of outer Main Belt asteroids, have the potential to place crucial constraints on how and where this aqueous alteration occurred, and offer a unique glimpse at the effects of asteroidal processing on early solar system materials. In a previous paper (Takir and Emery 2012), we presented near-infrared (0.7 to 4.0 μm) spectra of 28 outer Main Belt asteroids. An analysis focused on the 3-μm band in those data revealed four spectral groups, each of which is, presumably, related to

distinct surface mineralogy. The goal of the present study is to develop reliable 3-μm spectral indicators that will be used to interpret phyllosilicate mineralogy on the surface of these asteroids. To that end, we have undertaken combined petrologic, geochemical, and spectroscopic analyses of CM and CI chondrites.

The first part of the investigation consists of a study of degree of hydration using previously defined alteration parameters (i.e., Mineralogical Alteration Index: MAI, and petrologic subtype) for nine CM carbonaceous chondrites: LAP 02277, MIL 07700, QUE 97990, QUE 99038, LAP 03786, MAC 02606, MET 00639, Cold Bokkeveld, and Bells (Table B1). We apply and compare the previously published alteration scales of Browning et al. (1996) and Rubin et al. (2007), which utilized petrographic observations and electron microprobe analyses to quantify the degree of aqueous alteration. The analyses include samples previously studied by Browning et al. (1996) and by Rubin et al. (2007) to test the consistency of the two alteration scales. We also compare some results from the XRD-based alteration scale of Howard et al. (2009, 2011) to investigate the consistency of all three aqueous alteration scales, and to identify the most reliable aspects of each scale.

The second part of the investigation evaluates IR reflectance spectral properties (e.g., band center and shape) of the same CM chondrites, as well as one CI chondrite (Ivuna). Comparisons of asteroid and meteorite spectra in the 3-μm region have been difficult because meteorite spectra have been measured under ambient terrestrial conditions, and therefore were contaminated by adsorbed water (Miyamoto and Zolensky 1994; Sato et al. 1997; Rivkin 2003). Here, we present IR reflectance spectra measured under dry and vacuum conditions to remove adsorbed water and mimic the space environment, for subsequent comparison with asteroid reflectance spectra. Our reflectance study differs from that of Beck et al. (2010), who measured

IR transmission spectra of heated CM and CI chondrites at elevated temperatures up to 575 K. Due to the scattering of reflected illumination by granular particles, the shape and even position of absorption features can differ between transmission and reflectance measurements. Our study is important to investigate the implications of aqueous alteration for outer Main Belt asteroids ($2.5 < a < 4.0$ AU), which are observed in reflectance using ground-based telescopes (Takir and Emery 2012).

2.0 METHODOLOGY

2.1. Petrologic and Geochemical Analyses of CM and CI Chondrites

Characterization of the ten CM and CI chondrites included detailed petrographic observations and electron microprobe (EMP) analyses, following procedures outlined by Browning et al. (1996) and Rubin et al. (2007). Polished thin sections were examined with a petrographic microscope, in both transmitted and reflected light. Compositions of matrix material were analyzed with a CAMECA SX-100 electron microprobe at the University of Tennessee, using a 2 μm beam size, 10 nA beam current, and 15 keV accelerating voltage. Counting times for all elements were generally 20-30 s. Standard PAP corrections (Pouchou and Pichoir 1987) were applied. Precision and accuracy were monitored with natural and synthetic standards at intervals during each analytical session, and drift was within counting error. Detection limits (3σ above background) are typically < 0.03 wt. % for SiO_2, TiO_2, Al_2O_3, MgO, CaO, Na_2O, K_2O, and < 0.05 wt. % for FeO, MnO, Cr_2O_3, and NiO. We also made multi-element X-ray maps of representative regions of the ten carbonaceous chondrites for better characterization of their mineralogy.

2.1.1. Browning et al. Scale

Browning et al. (1996) used petrographic and mineralogical criteria to track the degree of alteration in CM chondrites. These criteria are based on the relative progress of coupled substitutions in the progressive alteration of Fe-serpentine (cronstedtite) to Mg-serpentine, which increases as alteration advances. This reaction, which defines the MAI, can be expressed as:

$$2\,(Fe^{3+}, Al^{3+})_{\text{cronstedtite}} = Si^{4+} + (Mg^{2+}, Fe^{2+})_{\text{serpentine}} \quad . (1)$$

Browning et al. (1996) proposed two additional indicators of aqueous alteration, the abundance of isolated anhydrous mineral fragments in the matrix and the relative percentage of chondrule alteration. These indicators were based on the assumption that, as alteration proceeds, anhydrous olivine and pyroxene, present as isolated mineral grains in the matrix and within chondrules, progressively alter to serpentine and therefore decrease in abundance. Browning et al. (1996) found correlations between these three indicators of degree of alteration in CM chondrites. The authors also found good correlations between MAI and key bulk properties of CM chondrites, including bulk contents of H and trapped planetary (non-radiogenic) ^{36}Ar. Applying this model to seven CM falls, Browning et al. (1996) established the following relative order of increasing alteration: Murchison ≤ Bells < Pollen ≤ Murray < Nogoya < Mighei < Cold Bokkeveld. Eiler and Kitchen (2004) also found a strong correlation between MAI and bulk δD in CM chondrites. The hydrogen isotopic change presumably reflects reaction of silicates with an aqueous fluid having a different isotopic composition.

2.1.2. Rubin et al. Scale

Rubin et al. (2007) studied eleven CM chondrites and proposed an alteration sequence that ranges downward from moderately altered petrologic type-2.6 chondrites to highly altered type-2.0 chondrites. This downward numbering scheme reflects the increasing degree of

alteration in going from type-3, to type-2, to type-1 carbonaceous chondrites, a reinterpretation (McSween 1979b) of that part of the Van Schmus and Wood (1967) chondrite classification. Rubin et al. (2007) utilized qualitative petrologic observations including the formation of phyllosilicates, alteration of chondrule mesostases, production of large clumps of serpentine-tochilinite intergrowths, oxidation of metallic Fe-Ni, alteration of mafic silicate phenocrysts in chondrules, changes in tochilinite composition (increase in the phyllosilicate/sulfide ratio), and changes in carbonate mineralogy.

2.1.3. Howard et al. Scale

Howard et al. (2009, 2011) used position sensitive detector X-ray diffraction (PSD-XRD) and X-ray pattern stripping to quantify the modal mineralogy of 13 CM2 and CM1 chondrites. They found a negative correlation between the modal abundances of anhydrous Fe-Mg silicates (olivine and pyroxene) and total phyllosilicates. This variation in modal mineralogy was used as an index of aqueous alteration. An inverse relationship between the abundance of Mg-serpentine and Fe-serpentine suggested that the transition from Fe-rich to Mg-rich serpentine occurs as aqueous alteration progresses.

2.2. Visible and Near-infrared Spectroscopy

2.2.1. Infrared Spectroscopy of Meteorites

Meteorite chips (100-140 mg) were ground into fine powders, using a dry ceramic mortar and pestle. Because we were limited by the sample sizes, we were not able to sieve the samples and precisely measure their grain size distributions. IR reflectance spectra of meteorites were measured at the USGS in Denver and the Johns Hopkins University Applied Physics Laboratory (APL) under dry and vacuum conditions. At APL, we used a high vacuum chamber system with a Bruker Vertex 70 spectrometer and an external MCT detector to measure meteorite spectra

(Figure B1). The samples were measured in bi-directional reflectance with an incidence angle of 15^{o}, an emission angle of 45^{o}, and a phase angle of 60^{o}. Samples were placed in a copper sample holder that has a $MgFl_2$ window, with powdered anhydrous $MgFl_2$ used as a IR reflectance standard, and a thermocouple for accurate temperature measurement. The chamber was sealed and pumped down to 10^{-7}-10^{-8} torr. The meteorite samples were heated to 475 K through a combination of conductive and radiative heating and then cooled to ~150 K using liquid N_2 conductive cooling. Spectra were measured *in situ* during the heating and cooling process.

At USGS, we used a Nicolet Fourier Transform Infrared (FTIR) Interferometer Spectrometer covering the range from ~1.3 to 15.5 μm at 4 wavenumber resolution (any use of trade names is for descriptive purposes only and does not constitute endorsement by the authors' institutions). The samples were measured while in a small, 15-cm diameter stainless steel environment chamber through a 5-cm diameter sapphire window. The samples were measured in bi-directional reflectance with an incidence angle of ~20^{o} an emission angle of ~35 degrees and azimuth angle ~60^{o}, giving a phase angle of ~20^{o}. The entire environment chamber was heated up to 475 K and temperature measured with an Lakeshore temperature meter with platinum temperature sensor. The environment chamber, heating stage, optics and FTIR spectrometer were maintained in a dry nitrogen environment and the sample was held under vacuum, pressure was typically limited by outgassing of the sample as it dehydrated. The samples noticeably shrunk during a dehydration run. Here we assume that these heating experiments of were conducted at perfect asteroid-like conditions. Although there might be some small amounts of adsorbed water present in meteorite powders, this remaining adsorbed water is spectrally insignificant and hence does not affect the 3-μm band in meteorite spectra.

We also used an Analytical Spectral Devices (ASD) portable field spectrometer (model FR) at the University of Tennessee, covering the range from 0.35 to 2.5 μm (hereafter called VNIR spectra) to measured spectra under ambient conditions at incidence angle (i) of ~30^o and an emission angle (e) of ~30^o. More than 50 VNIR spectra were measured and averaged for each sample. Spectra were measured relative to Spectralon, which has a several percent absorption at ~2.13 μm and a blue slope in the 2-2.5 μm region (Weidner and Hsia 1981). Therefore, all VNIR spectra were corrected according to the following equation (Clark et al. 2002):

$$R_{absref} = \left(\frac{I_{sample}}{I_{ref}}\right) R_{ref}, \qquad (2)$$

where R_{absref} is the corrected reflectance, I_{sample} is the light measured by the instrument from the sample, I_{ref} is the light measured by the instrument from the reference under the same incident lighting conditions, and R_{ref} is the absolute reflectance of the reference material (i.e., Spectralon).

2.2.2. Supporting Measurements

To demonstrate that hydroxyl groups remained stable at 450 K, X-ray powder diffraction patterns of serpentine (lizardite) powder unheated and heated at 475 K for 12 hours were obtained. The unheated and heated XRD patterns are quite similar (Figure B2).

Spectra of serpentine (lizardite) and saponite mixed with carbon black (~1 %) were also measured under dry conditions and vacuum to aid interpretation of meteorite spectra. Mixtures of small amounts of spectrally featureless carbon black and clays produce qualitatively similar spectra to those of carbonaceous chondrites in the 3-μm region (Larson et al. 1979; Clark 1983). Serpentine and saponite were obtained from Wards Scientific Co. To characterize additional spectral absorptions in the chondrites, we also measured L-tyrosine amino acid (0.12 %) and

decane alkane (4%) mixed with Hawaiian Basalt (USGS BHVO-2F, Clark et al. 2013 spectral library in preparation) under ambient conditions. L-tyrosine amino acid was purchased from Now Foods Co. and labeled as 100 % pure. Decane alkane is from Sigma-Aldrich and is 98% pure (Clark et al. 2009). In addition, magnetites in CM and CI chondrites were examined at USGS using a FEI Quanta 450 field emission scanning electron microscope (SEM) in high vacuum mode at a voltage of 5-20 kV. Backscattered electron images of individual grains were acquired with a voltage contrast detector, and secondary electron images were acquired with an Everhart-Thornley detector.

To provide additional interpretations of meteorite spectra, Raman spectra of powdered CM and CI chondrites (randomly oriented fine grains) were also obtained, using a HoloLab 5000 Raman spectrometer (Kaiser Optical Systems Inc.) at Washington University in St. Louis. The spectrometer uses the 532 nm line of a frequency-doubled Nd:YAG laser for excitation with Stokes-Raman shifted spectral coverage of 50-4300 cm^{-1} and spectral resolution of ~4-5 cm^{-1}. Further details on HoloLab 5000 can be found in Wang et al. (2007).

2.2.3. Calculations of Band Parameters

Following a standard technique described by Cloutis et al. (1986), absorption features in the 3-μm, 2.3-μm, and 0.7-μm regions were isolated, and each was divided by a straight-line continuum. The continuum was determined by two maxima at 2.63-2.65 μm and 3.07-3.85 μm for the 3-μm band, by two maxima at 2.20-2.25 μm and 2.35-2.40 μm for the 2.3-μm band, and by two maxima at 0.60-0.65 μm and 0.75-0.85 μm for the 0.7-μm band. For spectra with strong and well-defined features around 3.4-3.5 μm, the continuum for the 3-μm band was determined by two maxima at 2.63-2.65 μm and around 3.3 μm.

The following band parameters were used to analyze spectra of CM and CI chondrites: the band center, band depth, and band area. The band center was determined by applying a sixth-order polynomial fit to the central part of the feature. Band depth, D_b, was calculated using the following equation:

$$D_b = \frac{R_c - R_b}{R_c}, \qquad (3)$$

where R_b is the reflectance at the band center and R_c is the reflectance of the continuum at the band center (Clark and Roush 1984). The band area was calculated by integrating the spectral curve below the straight-line continuum. An average of five measurements, determined by varying the positions of band maxima, was used for each band paramter. Uncertainty for each parameter was determined by the 2σ standard deviation that represents variability from the average.

3.0 RESULTS

3.1. Petrologic and Geochemical Properties

3.1.1. Browning et al. Scale

Applying the previously published scale of Browning et al. (1996), we determined the MAI for the nine CM chondrites. Table B2 shows the estimated chemical formulae of average matrix serpentines and MAI for the CM chondrites analyzed in this study. The MAI is the average of MAIs for the matrix analyses in an individual CM chondrite. Standard deviations for each cation do not represent analytical errors but illustrate the compositional variability of matrix serpentines. Atomic formulae were determined from microprobe analyses, which were corrected for small amounts of sulfide, following the algorithm outlined in Browning et al. (1996).

3.1.2. Rubin et al. Scale

We also applied the previously published scale of Rubin et al. (2007). Tables 3 and 4 summarize our results on various petrologic properties, including oxidation of metallic Fe-Ni, alteration of chondrule phenocrysts, changes in tochilonite compositions, and carbonate mineralogy. Using the criteria outlined by Rubin et al. (2007), petrologic subtypes (±0.1) were assigned to the nine CM chondrites. The petrologic subtypes vary between 2.6 and 2.1, representing the least altered and most altered chondrites, respectively. The aqueous alteration scales of Browning et al. (1996) and Rubin et al. (2007) for the same chondrites weakly correlate with each other, and where XRD data on the same meteorites are available, also with the scale of Howard et al. (2009, 2011) (Figure B3).

3.2. Spectral properties of CM and CI Chondrites

Figures B4a-j show IR reflectance spectra of nine CM chondrites and one CI chondrite measured at ambient, and at dry and vacuum conditions. All spectra exhibit an apparent 3-μm band. Some spectra also show a very weak absorption feature at ~2.3 μm with band depth less than 1 %. The 3-μm band center shifts to shorter wavelengths under dry conditions for some samples, mainly due to the removal of adsorbed water.

Figure B5 illustrates red-sloped VNIR spectra of these CM and CI chondrites. A few VNIR spectra exhibit a very weak 0.7 μm absorption feature with a band depth less than 1 %. QUE 99038 and MIL 07700 exhibit 1-μm and 2-μm features and no 2.3-μm feature. Ivuna's VNIR spectrum shows a shoulder at ~0.6 μm, an overall red slope between 0.4 and 2.3 μm, and an absorption feature at ~1.9 μm. Table B5a and B5b includes the 3-μm, 2.3-μm, and 0.7-μm band centers and depths for these chondrites and additional minerals, respectively.

4.0 DISCUSSION

4.1. Mineralogical Alteration Index

Velbel and Palmer (2012) suggested that the application of the MAI is problematic because it includes Al, which is not a good indicator of aqueous alteration in CM chondrites. According to these authors, the main problems with the MAI are mathematical, since division by zero occurs where Si obtains its stoichiometric value of 2 in pure serpentine, and by the biases caused by data screening. Under certain circumstances, these potential problems could result in very large values of MAI (greater than 2), leading to the elimination of valid phyllosilicate analyses.

We were able to apply the MAI to the nine CM chondrites without encountering any of the problems raised by Velbel and Palmer (2012). After reducing electron microprobe data of the matrices in CM chondrites, following the procedure described by Browning et al. (1996), all calculated Si cations were found to be far less than 2 (Table B2). For CM chondrites, experience indicates that it is unrealistic to expect pure serpentine with a Si cation of value 2 (Zolensky et al. 1993). Data screening as outlined by Browning et al. (1996) is necessary in order to exclude cation totals that are representative of non-serpentine phyllosilicates, carbonates, and oxides. The expression used by Browning et al. (1996) to determine the amount of Fe^{3+},

$$Fe^{3+} = (2 * (2 - Si)) - Al, \qquad (5)$$

remains valid, assuming a loss of Si is accommodated by coupled substitutions that deplete all the available Al. Moreover, Figure B9 in Velbel and Palmer (2012) shows an extremely weak correlation ($R^2 = 0.09$) between the chemical index of alteration (CIA) and Si/Al ratio, making it difficult to draw any conclusion about the mobility of Si relative to Al during leaching of CMs. Therefore, the criticisms raised by Velbel and Palmer (2012) have not convinced us to abandon

the application of the Browning et al. (1996) scale, as applied specifically to CM chondrites. We also note that there is a typographical error in Table 2 of Browning et al. (1996); the MAIs listed in column 12 should be subtracted from 2 because the MAI is defined as:

$$MAI = 2 - \frac{Fe^{3+}}{2 - Si} \quad . \qquad (6)$$

4.2. Diversity in the 3-µm Band in CM and CI Chondrites

CM and CI chondrites display three distinct types of spectra. This spectral classification is generally not affected by the grain size distribution of the samples because spectra are mainly distinguished by the 3-µm band center. "Group1" that includes QUE 97990, MIL 00700, and QUE 99038, possesses a 3-µm band centered ~2.77-2.80 µm (Figures B4a-c). "Group 2" includes Bells, LAP 03786, MAC 02606, and Cold Bokkeveld. This group has a 3-µm band centered ~2.76-2.78 µm, with a shoulder near ~2.72 µm (Figures B4d-g). "Group 3", which includes LAP 02277 and MET 00639, exhibits a 3-µm band centered ~2.72 µm (Figures B4h-i).

4.2.1. Spectral Interpretations

Spectra of Group 1 exhibit 3-µm band centers that are at longer wavelengths than most serpentines or smectites (e.g., saponite), the matrix mineral compositions commonly discussed for CM matrices. The longer-wavelength band center is, however, consistent with cronstedtite (Figure B6a), a serpentine for which Fe^{3+} replaces some Si in the tetrahedral site. Two Group 1 meteorites, QUE 99038 and MIL 00770, exhibit absorptions at ~1 µm and ~2 µm, attributed to Fe^{2+} in the M2 crystallographic site in olivine and pyroxene (Burns 1993) (Figure B6b), indicating a high fraction of anhydrous silicates in these samples. Raman spectra confirm the high concentrations of olivine in QUE 99038 (Figure B6c).

Group 2 samples show a particularly strong 3.1-μm feature in ambient spectra, attributed to adsorbed water. This feature goes away as the sample is desiccated in vacuum at elevated temperatures. In addition, dry spectra of this group exhibit a 3.4-3.5-μm feature, attributed to C-H stretching of aliphatic organic compounds (Clark et al. 2009). The organics features become sharper as heating proceeds. MAC 02606 has a unique spectrum in that it exhibits strong CO_3 absorptions in the 3.4-3.5-μm and 3.8-4.0-μm regions, attributed to carbonates (Clark et al. 2007) (Figure B6d). Carbonates were also detected in MAC 02606, using multi-element X-ray maps and microprobe analyses. Raman spectra show that the carbonate in this sample is dominated by dolomite (Figure B6e). All samples in Group 2 also exhibit a 2.3 μm feature, usually, but not uniquely, attributed to Mg-OH stretch (Clark et al. 1990). The 2.3-μm feature was not affected by heating the samples, providing additional confidence that the structural OH was not altered.

Spectra of Group 3 exhibit band centers and shapes that are more consistent with typical serpentines. In particular, the band position of the serpentine antigorite matches that of the two Group 3 meteorites (Figure B6f). Ambient spectra of this group do exhibit a much weaker 3.1-μm feature (attributed to adsorbed water) than the other groups. Dry spectra of this group do not show any indications of organic features at 3.4 – 3.5 μm.

Ivuna, which is the only CI included in the present study, is distinct from all of the CM groups, with a 3-μm band centered at ~2.71 μm that is consistent with serpentine (lizardite and chrysotile) (Figure B6g). Ivuna is also unique because it exhibits a distinctive water feature at ~1.9 μm, which becomes weaker as the sample is desiccated. Osawa et al. (2005) also reported that Ivuna and another CI chondrite, Orgueil, exhibit a narrow feature at ~2.71 μm, under ambient conditions. They attributed this feature to serpentine (lizardite) rather than saponite.

However, Zaikowski (1979) attributed the 2.71 μm feature in Orgueil, also under ambient conditions, to chlorite and chamosite rather than serpentine or saponite.

4.2.2. Geochemical Analyses

Figure B7, a ternary diagram of SiO_2+Al_2O_3, FeO, and MgO, compares our analyzed matrix compositions in CM chondrites and Ivuna. The matrix compositions lie along an approximately linear trend that extends from near the composition of cronstedtite (representing the least altered material) towards the SiO_2-MgO join near the composition of Mg-serpentine (representing the most altered material). This trend is typical for carbonaceous chondrites (e.g., Brearley 1997). The matrix composition of QUE 97990, which is assigned to subtype 2.6, plots near cronstedtite in agreement with the spectral analysis, providing more evidence that this meteorite is the least altered sample in the present study. The matrix compositions of CM and CI chondrites plot along the cronstedtite-serpentine join far from saponite, vermiculite, and montmorillonite, suggesting that the former mineral is more abundant in these chondrites in agreement with the spectroscopic investigation. Although these geochemical analyses generally support our spectral investigation and alteration sequence, they do not uniquely distinguish the spectral classes identified in CM and CI chondrites.

4.3. Alteration Parameters and Spectral Properties of CM Chondrites

Figure B8 summarizes the results of the petrological, geochemical, and spectral investigation of the CM chondrites and Ivuna. Group 1 is the least altered group, Group 3 is the most altered group (before Ivuna), and Group 2 is an intermediate group. The 3-μm band center decreases with the increase of alteration. Group 1, which has 3-μm band centers at longer wavelength, is consistent with Fe-rich serpentine minerals such as cronstedtite. Group 3, which has 3-μm band centers at shorter wavelength, is consistent with Mg-rich serpentine minerals

such as antigorite. Group 1 has a petrological subtype that ranges from 2.6-2.3 and a lower MAI that varies from 0.33-0.67, consistent with the low degree of alteration in this group. Group 3 has a petrological subtype that ranges from 2.2-2.1 and a higher MAI that varies from 0.90-1.04, consistent with the high degree of alteration in this group. This group includes LAP 02277 with a subtype of 2.1, which has been classified as a CM1 (Russell et al. 2005). Group 2 represents the transition between Group 1 (least altered) and Group 3 (most altered). MAC 02606 in Group 2 has a very low MAI of 0.35, possibly because it contains unusually high concentrations of carbonates.

Most researchers believe that CM chondrites experienced alteration processes on or within their parent asteroids (e.g., McSween 1979a, 1987; Brearley 2006), although arguments for solar nebula alteration have also been presented (e.g., Metzler et al. 1992). CM parent body alteration has been described as occurring in four stages (Tomeoka et al. 1989): (1) formation of tochilinite by interaction of Fe metal (kamacite) with a S-bearing fluid (sulfide) that moved through cracks in chondrules and aggregates, (2) formation of phyllosilicates from Fe-rich matrix olivine, and "spinach" from mesostasis glasses in chondrules and aggregates, (3) formation of magnesium cronstedtite by interaction of Si (released from the alteration of olivine and pyroxene) with tochilinite, and formation of tochilinite-cronstedtite intergrowths, (4) while tochilinite continued to be consumed, magnesium cronstedtite increased its Mg and Si contents by interacting with existing serpentine to form Fe-serpentine, which then altered to form Mg-serpentine. Unlike the scale of Rubin et al. (2007), the scale of Browning et al. (1996) includes only the second part of the fourth stage of alteration (alteration of Fe-serpentine to Mg-serpentine). Hence, it is possible that the MAI parameter alone does not capture all the petrologic

parameters that are expressed by the diversity of the 3-μm band and by the complex and multistage aqueous alteration experienced by CM chondrites.

4.4. Organic Compounds in CM and CI chondrites

The association of aqueous alteration and organic compounds in carbonaceous chondrites has been reported in several studies (e.g., Bunch and Chang 1980; Cronin and Chang 1993). The abundance of organics is likely related to the aqueous alteration process during which phyllosilicates enabled the adsorption and trapping of organic material through subsequent mineral growth (Pearson et al. 2002).

4.4.1. Aliphatic Organics

Our spectral investigation has revealed that aliphatic organics features in Group 2 and Ivuna develop into sharper and more pronounced features as heating proceeds. This increase in observed spectral contrast of the organic features appears to be due to the removal of the spectrally masking effects of the adsorbed water that is dark at those wavelengths. It seems from the spectrally detected aliphatic organic compounds in Group 2 rather than the Group 3 that abundant organics may be associated with mineral diversity in these groups (Figure B6f).

We suggest four possible explanations for the spectral appearance of organics in dry spectra in Group 2 and Ivuna: (1) adsorbed water, before it is removed by heating, spectrally masks organic features, (2) removal of adsorbed water compositionally altered the mix of organic compounds, (3) new organic compounds formed during heating, or (4) the deposition of organics onto the sample or sample window from elsewhere in the vacuum system. We do not observe any new organic absorption features being created, nor any features decreasing in strength (relative to other C-H absorptions) that would be indicative of bulk compositional changes. Also, the sample holder is the warmest component in the system and thus not likely to

'cold-trap' organics in the vacuum system. Hence, there appear to be no major changes in the organic compounds within the sample. This also means that the organic compounds appear stable during the heating and vacuum runs. Therefore, of the four suggested explanations, the first one is the most likely explanation for the appearance of organics in both Group 2 and Ivuna.

4.4.2. Amino Acids

Among the organic compounds in carbonaceous chondrites are amino acids, which are building blocks of life (e.g., Botta and Bada 2002; Pizzarello et al. 2006). Relative concentrations of amino acids in carbonaceous chondrites have been used to understand the nature of aqueous alteration processes experienced on the parent body (e.g., Botta el al. 2007). Glavin et al. (2011) found that carbonaceous chondrites with higher degrees of aqueous alteration have lower abundance of amino acids, suggesting that alteration influenced their formation. Furthermore, Monroe and Pizzarello (2011) suggested that repeated aqueous alteration processes on parent bodies might have altered or destroyed the original organic inventory of carbonaceous chondrites.

The amino acids exhibit diversity in their molecular structures and concentrations among carbonaceous chondrites. Botta et al. (2007) found that the abundance of amino acids in CM1 chondrites is significantly lower than in CM2s. LAP 02277 (CM1), also studied here (Group 3), shows a unique amino acid distribution that cannot be related to any of the other classes studied by Botta et al. (2007). In addition, Ehrenfreund (2001) showed that the amino acids in CIs, including Ivuna, are distinct from those in CM2s, and suggested that these classes had different parent bodies and were processed under different physical and chemical conditions. Oxygen isotope analyses also showed that CI and CM chondrites were altered at different temperatures and water/rock ratios (Clayton and Mayeda 1984, 1999). It is therefore likely that CM and CI

chondrites have had distinct organic precursor compounds and thus their parent bodies were different.

Changes of aliphatic organic compounds in CM and CI carbonaceous chondrites with heating above room temperature are not well documented, but Cronin and Pizzarello (1983) noted a change in amino acids. The abundance of some amino acids, such as β-alanine, increased while the abundance of others, such as γ-aminobutyric acid, decreased. We found no N-H absorptions at ~ 3.1 μm in any of our spectra, nor any C-H absorptions specifically attributable to amino acids (Figure B9).

4.5. Magnetite in CM and CI Chondrites

Magnetite has been identified in many CM and CI chondrites as framboidal aggregates with polygonal morphology (Jedwab 1971, Kerridge et al. 1979, Tomeoka and Buseck 1985). It is widely accepted that magnetite is a product of parent body aqueous alteration (e.g., Kerridge et al. 1979), although arguments for solar nebula formation have also been presented (e.g., Jedwab 1971). Magnetite was probably deposited in the matrix after the migration of Fe, S, and Ni from serpentine-tochilinite intergrowths (Tomeoka and Buseck 1985). McSween (1979a) also noted that magnetite abundance probably increases with alteration.

Using high resolution SEM, we searched for magnetite in the ten CM and CI chondrites. We identified relatively abundant framboidal magnetite grains in three samples of Group 2: Bells, assigned to subtype 2.1, Cold Bokkeveld, subtype 2.2, MAC 02606, subtype 2.1, in addition to Ivuna. Framboidal magnetite grains found in CM chondrites are similar to ones in Ivuna with the same polygonal morphology (Figure B11). We also note that the broad adsorbed water feature at ~3.1 μm (in ambient spectra) and the sharper aliphatic organics feature (in dry

spectra) are present in all of these four samples. This suggests that magnetite forms in an environment that enables the adsorption of water.

6.0 CONLUSIONS

We have measured reflectance spectra of nine CM and one CI chondrites under dry and vacuum conditions to remove adsorbed water and mimic the space environments. These chondrites are classified into three groups, mainly on the basis of the 3-μm band center. Group 1, which is characterized by 3-μm band centers at 2.76-2.80 μm, is consistent with the endmember Fe-serpentine (cronstedite). Group 3, which is characterized by 3-μm band centers at ~2.72 μm, is consistent with the endmember Mg-serpentine (antigorite). Group 2 represents an intermediate mineralogy between the two endmembers. Ivuna, which is the only CI chondrite analyzed in the present study, has a unique 3-μm band centered ~2.71 μm, is consistent with lizardite and chrysotile. This diversity in the 3-μm band suggests distinct pre-terresterial aqueous alteration conditions for these chondrites, which provide clues to parent body alteration.

We applied two previously published alteration scales by Browning et al. (1996) and Rubin et al. (2007) to nine CM carbonaceous chondrites. We found good agreements between the petrological and geochemical parameters, and spectral characteristics of these chondrites. The petrological subtype in Group 1 varies from 2.6-2.3 (least altered group) and in Group 3 from 2.1-2.2 (most altered) in agreement with the spectral analyses. Geochemical analysis also shows that QUE 97990 (Group 1), which is the least altered sample, is cronstedtite-rich. More spectral analyses on the intermediate phases between endmembers Fe-serpentine and Mg-serpetine are needed to better characterize the mineralogy in Group 2.

For Group 2 and Ivuna, the organic absorptions became more pronounced at elevated temperatures, possibly because the adsorbed water, before it is removed by heating, spectrally masks the organic feature. Hence, both Group 2 and Ivuna are characterized by adsorptive surfaces. Magnetite abundance is relatively higher in chondrites that show the broad adsorbed water feature at ~3.1 μm (in ambient spectra) and the pronounced aliphatic organics feature (in dry spectra). These results suggest that magnetite forms in an environment that enables adsorption of volatiles. CM and CI chondrite spectra show no evidence for amino acids, probably due to their low abundance.

This study has direct implications for the interpretation of ground-based telescope spectra of outer Main Belt asteroids (Takir and Emery 2012). The consistency between petrological and geochemical parameters, which were determined using microprobe and microscope analyses, and the spectral properties of CM meteorites indicates that distinct parent body aqueous alteration environments can be distinguished using reflectance spectroscopy. High-quality ground-based telescopic observations of outer Main Belt asteroids can be expected to reveal not just whether an asteroid is hydrated, but also details of the alteration state.

This study may also have some implications for: (1) the interpretation of the dark material on Vesta, which is thought to be from the infall of carbonaceous volatile-rich material (McCord et al. 2012), (2) the interpretation of spectra of Ceres that will be visited by the Dawn spacecraft in 2015, (3) the interpretation and analysis of spectra and the returned sample from asteroid 1999 RQ36 that will be visited by the OSIRIS-Rex spacecraft, and (4) the interpretation of the dark material in the Saturn system (Clark et al. 2012).

ACKNOWLEDGEMENTS

We thank Allan Patchen for assistance with the electron microprobe, Bill Deane and Michael DeAngelis for assistance with serpentine preparation and XRD measurements, Jeff Moersch for providing the ASD spectrometer, Yali Lu for assistance with Raman spectra measurements, Heather Lowers at USGS for assistance with the SEM measurements, and Genesis Berlanga for assistance with reflectance spectra measurements at APL. This work was partly supported by NASA Cosmochemistry grant NNX10AH48G to HYM and by NASA Planetary Astronomy grant NNX08AV93G to JPE. Clark and Pearson were funded by the NASA Cassini mission to Saturn, VIMS team (Clark - team member).

REFERNCES

Bell J.F., Davis D.R., Hartmann W.K., and Gaffey M.J. 1989. Asteroids: The big picture. In *Asteroid II,* edited by Binzel R.P., Gehrels T., and Matthews M.S. Tucson: University of Arizona Press, pp. 921-945.

Beck P., Quirico E., Montes-Hernandez G., Bonal L., Bollard J., Orthous-Daunay F. R., Howard K. T., Schmitt B., Brissaud O.,Deschamps F., Wunder B. and Guillot S. 2010. Hydrous mineralogy of CM and CI chondrites from infrared spectroscopy and their relationship with low albedo asteroids. *Geochimica et Cosmochimica. Acta* 74:4881–4892.

Botta O. and Bada J.L. 2002. Extraterrestrial organic compounds in meteorites. *Survey of Geophys*ics 23:411-465.

Botta O., Zita M., and Ehrenfreund P. 2007. Amino acids in Antarctic CM1 meteorites and their relationship to other carbonaceous chondrites. *Meteoritics & Planetary Science* 42:81-92.

Brearley A.J. 1997. Phyllosilicates in the matrix of the unique carbonaceous chondrite, LEW 85332 and possible implications fir aqueous alteration of CI chondrites. *Meteoritics and Planetary Science* 32:377-388.

Brearley A.J. 2006. The action of water. In *Meteorites and the Early Solar System II,* edited by Lauretta D. and McSween H.Y. Tucson: University of Arizona Press, pp. 587-624.

Browning L.B., McSween H.Y., and Zolensky M.E. 1996. Correlated alteration effects in CM carbonaceous chondrites. *Geochimica et Cosmochimica Acta* 60:2621-2633.

Browning L.B., McSween H. Y., and Zolensky M. E. 2000. On the origin of rim textures surrounding anhydrous silicate grains in CM carbonaceous chondrites. *Meteoritics & Planetary Science* 35:1015-1023.

Bunch T. E. and Chang S. 1980. Carbonaceous chondrite phyllosilicates and light element geochemistry as indicators of parent body processes on surface conditions. *Geochimica et Cosmochimica Acta* 44:1543-1577.

Burns R.G. 1993. Origin of electronic spectra in minerals in the visible to near-infrared region. In *Topics in Remote Sensing 4: Remote Geochemical Analysis: Elemental and Mineralogical composition,* edited by Pieters C.M. and Englert P.A.J., 3-29. Cambridge: Cambridge University Press, pp. 3-29.

Clark R. N. 1983. Spectral properties of mixtures of montmorillonite and dark carbon grains: Implications for remote sensing minerals containing chemically and physically adsorbed water. *Journal of Geophysical Research* 88:10635-10644.

Clark R.N. and Roush T.L.1984. Reflectance spectroscopy: Quantitative analysis techniques for remote sensing applications. *Journal of Geophysics Research* 89:6329-6340.

Clark R.N., King T.V.V., Klewja M., Swayze G.A., Vergo N. 1990. High spectral resolution reflectance spectroscopy of minerals. *Journal of Geophysics Research* 95:12653-12680.

Clark R. N., Swayze G. A., Livo K. E., Kokaly R. F., King T. V. V., Dalton J. B., Vance J. S., Rockwell B. W., Hoefen, T., and McDougal R. R., Surface Reflectance Calibration of Terrestrial Imaging Spectroscopy Data: a Tutorial Using AVIRIS. 2002. Proceedings, XXth Airborne Earth Science Workshop, JPL Publication 02-1.

Clark R.N, Swayze G.A., Wise R., Livo E., Hoefen T., Kokaly R., and Sutley S.J. 2007. USGS digital spectral library splib06a, Data Series, 231, U.S. Geol. Surv., Reston, Va. (http://speclab.cr.usgs.gov/spectral.lib06).

Clark R.N., Curchin J.M., Hoefen T.M., and Swayze G.A. 2009. Reflectance spectroscopy of organic compounds I: Alkanes: *Journal of Geophysical Research* 114, p. E03001.

Clark R.N., Pearson N., Takir D., Emery J.P., McSween H.Y.Jr, Cruikshank D.P., Hendrix A.R. 2012. Nano-Iron on Outer Solar System Satellites, Implications for Space Weathering (abstract # 53B-05). 45th American Geophysical Union Fall meeting.

Clayton R.N. and Mayeda T.K. 1984. The oxygen isotope record in Murchison and other carbonaceous chondrites. *Earth and Planetary Science Letters* 67:151-161.

Clayton R.N. and Mayeda T.K. 1999. Oxygen isotope studies of carbonaceous chondrites. Geochimica et Cosmochimica Acta 63:2089-2104.

Cronin J. R. and Pizzarello S. 1983. Amino acids in meteorites. *Advances in Space Research.* 9: 5-18.

Cronin J.R. and Chang S. 1993. Organic matter in meteorites: Molecular and isotopic analyses of the Murchison meteorite. In *Chemsitry of Life's Origins,* edited by Greenburg J.M. and Pirronello V. Dordrecht, The Netherlands: Kluwer, pp. 209-258.

Ehrenfreund P., Glavin D. P., Botta O., Cooper G., and Bada J. L. 2001. Extraterrestrial amino Acids in Orgueil and Ivuna: Tracing the parent body of Cl type carbonaceous chondrites. *Proceedings of the National Academy of Sciences, USA* 98:2138–2141.

Eiler J.M. and Kitchen N. 2004. Hydrogen isotope evidence for the origin and evolution of the CM chondrites. Geochimical et Cosmochimica Acta 68:1395-1411.

Gaffey M.J., Burbine T.H., and Binzel R.P. 1993. Asteroid spectroscopy: Progress and perspectives. *Meteoritics,* 28:161-187.

Glavin D.P. and Dworkin J.P. 2009. Enrichment of the amino acid L-isovaline by aqueous alteration on CI and CM meteorite parent bodies. *Proceedings of the National Academy of Sciences, USA* 106:5487-5492.

Glavin D. P., Callahan M. P., Dworkin J. P., and Elsila J. E. 2011. The Effects of Parent Body Processes on Amino Acids in Carbonaceous Chondrites. *Meteoritics & Planetary Science* 45:1948-1972.

Hibbitts C.A., Hagaman S., and Greenspon A. 2012The adsorption of gases onto refractory materials: CO_2 onto clays and their relevance to the icy galilean satellites (abstract #2400). 43rd Lunar and Planetary Science Conference. CD-ROM

Hiroi T., Zolensky M.E., and Pieters C.M. 2001. The Tagish Lake Meteorite: A possible sample of a D-type asteroid. *Science* 293:2234-2236.

Howard K.T, Benedix G.K., Bland P.A., Cressey G. 2009. Modal mineralogy of CM2 chondrites by X-ray diffraction (PSD-XRD). Part 1: Total phyllosilicate abundance and the degree of aqueous alteration. *Geochimica et Cosmochimica Acta* 73:4576-4589.

Howard K.T., Benedix G.K., Bland P.A., Cressey G. 2011. Modal mineralogy of CM chondrites by X-ray diffraction (PSD-XRD): Part 2. Degree, nature and settings of aqueous alteration. *Geochimica et Cosmochimica Acta* 75:2735-2751.

Jedwab J. 1971. La magnetite de la meteorite d'orgueil vu au microscope electronic a balayage. *Icarus* 15:319-340.

Kebukawa Y., Nakashima S., Otsuka T., Nakamura-Messenger K., and Zolensky M.E. 2009. Rapid contamination during storage of carbonaceous chondrites prepared for micro FTIR measurements. *Meteoritics & Planetary Science* 44:545-557.

Kerridge J. F., Mackay A. L., and Boynton W. V. 1979. Magnetite in CI carbonaceous meteorites - Origin by aqueous activity on a planetesimal surface. *Science* 205:395-397.

Larson H. P., Feierberg M.A., Fink U., and Smith H.A. 1979. Remote spectroscopic identification of carbonaceous chondrite mineralogies: Applications to Ceres and Pallas. *Icarus* 39:257-271.

Lebofsky L.A. 1980. Infrared reflectance spectra of asteroids: A search for water of hydration. *The Astronomical Journal* 85**:**573-585.

Lee M. 1993. The petrography, mineralogy and origins of calcium sulphate within the Cold Bokkeveld CM carbonaceous chondrite. *Meteoritics* 28:53-62.

Metzler K., Bischoff A., and Stoffler D. 1992. Accretionary dust mantles in CM chondrites: evidence for solar nebula processes. *Geochimica et Cosmochimica Acta* 56:2873-2897.

McCord T.B., Li J-Y, Combe J.-P, McSween H.Y., Jaumann R., Reddy V, Tosi F., Williams D.A., Blewett D.T., Turrini D., Palomba E., Pieters C.M., De Sanctis M.C., Ammannito E., Capria M.T.., Le Corre L., Longobardo A., Nathues A., Mittlefehldt D.W., Schröder S.E., Hiesinger H., Beck A.W., Capaccioni F., Carsenty U., Keller H.U., Denevi B.W., Sunshine J.M., Raymond C.A., and Russell C.T. 2012. Dark material on Vesta from the infall of carbonaceous volatile-rich material. *Nature* 491:83-86.

McSween H.Y. Jr. 1979a. Alteration in CM carbonaceous chondrites inferred from modal and chemical variations in matrix. *Geochimica et Cosmochimica Acta* 43:1761-1170.

McSween H. Y. Jr. 1979b. Are carbonaceous chondrites primitive or processed? A review. Reviews of Geophysics and Space Physics 17:1059-1078.

McSween H. Y. Jr. 1987. Aqueous alteration in carbonaceous chondrites: Mass balance constraints on matrix mineralogy. *Geochimica et Cosmochimica Acta* 51:2469-2477.

Monroe A. A. and Pizzarello S. 2011. The soluble organic compounds of the Bells meteorite: Not a unique or unusual composition. *Geochimica et Cosmochimica Acta* 75: 7585-7595.

Miyamoto M. and Zolensky M.E. 1994. Infrared diffuse reflectance spectra of carbonaceous chondrites: Amount of hydrous minerals. *Meteoritics* 29:849-853.

Osawa T., Kagi H., Nakamura T. and Noguchi T. 2005. Infrared spectroscopic taxonomy for carbonaceous chondrites from speciation of hydrous components. *Meteoritics & Planetary Science* 40:71-86.

Pearson V.K., Kearsley A.T., Sephton M.A., and Glimour I. 2002. Organic-Inorganic spatial relationships in carbonaceous chondrites (abstract #1311). 33rd Lunar and Planetary Science Conference. CD-ROM

Pouchou J.L. and Pichoir F. 1987. In: *Basic Expression of "PAP" Computation for Quantitative EPMA,* edited by Brown J.D. and Packwood R.H., eds. Proceeding. 11th ICXOM, University of Western Ontario, London, Ontario, pp. 249-253.

Pizzarello S., Cooper G.W., and Flynn G.J. 2006. The nature and distribution of the organic material in carbonaceous chondrites and interplanetary dust particles. In *Meteorites and the Early Solar System II,* edited by Lauretta D. and McSween Jr. H.Y. Tucson: University of Arizona Press. pp. 625-651.

Pieters C.M. and McFadden L.A. 1994. Meteorite and asteroid reflectance spectroscopy: Clues to early solar system processes. *Annual Review of Earth and Planetary Science* 22:457-497.

Rivkin A. S., Howell E. S.,Vilas F., and Lebofsky L. A. 2002. Hydrated minerals on asteroids: The astronomical record. In *Asteroids III*, edited by Bottke Jr. W.F., Cellino P., Paolicch P., and Binzel, R.P. Tucson: University of Arizona Press, pp. 235-253.

Rivkin A. S., Davies J.K., Johnson J.R., Ellison S.L., Trilling D.E., Brown R.H., and Lebofsky L.A. 2003. Hydrogen concentrations on C-class asteroids derived from remote sensing. *Meteoritics & Planetary Science* 38:1383-1398.

Rubin A.J., Trigo-Rodríguez J.M., Huber H., and Wasson J.T. 2007. Progressive aqueous alteration of CM carbonaceous chondrites. *Meteoritics & Planetary Science* 71:2361-2382.

Russell S. S., Zolensky M., Righter K., Folco L., Jones R., Connolly H. C., Grady M. M., and Grossman J. N. 2005. *Meteoritics & Planetary Science* 40:A201–A263.

Ryskin Y.A. 1974. The vibrations of protons in minerals: hydroxyl, water and ammonium. In *The infrared spectra of minerals* , edited by V.C. Farmer. London: The Mineralogical Society Monograph 4, pp.137-181.

Salisbury J. W., Walter L. S., Vergo N., and and D'Aria D. 1991. Infrared (2.1-25 μm) Spectra of Minerals.Baltimore: Johns Hopkins University Press, 267 p.

Sandford S. A., Allamandola L. J., Tielens A. G. G. M., Sellgren K., Tapia M., and Pendleton Y. 1991. The interstellar C-H stretching band near 3.4 microns constraints on the composition of organic material in the diffuse interstellar-medium. *The Astrophysical Journal* 371:607-620.

Sato K., Miyamoto M., and Zolensky M.E.1997. Absorption bands near three micrometers in diffuse reflectance spectra of carbonaceous chondrites: Comparison with asteroids. *Meteoritic & Planetary Science* 32:503-507.

Takir D., and Emery J.P. 2012. Outer Main Belt asteroids: Identification and distribution of four 3-um spectral groups. *Icarus* 219:641-654.

Tomeoka K. and Buseck P. R.1985. Indicators of aqueous alteration in CM carbonaceous chondrites:Microtextures of a layered mineral containing Fe, S, O and Ni. *Geochimica et Cosmochimica Acta* 49:2149-2163.

Tomeoka K., McSween H.Y., Jr., and Buseck P. R.1989. Mineralogical alteration of CM carbonaceous chondrites: A Review. *Proceedings of the National Institute of Polar Research Symposium* 2:221-234.

Velbel M.A. and Palmer E.E. 2012. Fine-grained serpentine in CM2 carbonaceous chondrites and its implications for the extent of aqueous alteration on the parent body: A review. *Clays and Clay Minerals* 59:416-432.

Van Schmus W. R., and Wood J. A. 1967. A chemical-petrologic classification for the chondritic meteorites. *Geochimica et Cosmochimica Acta* 31:747-765.

Vilas F. and Gaffey M.J. 1989. Phyllosilicate absorption features in main-belt and outer-belt asteroids from reflectance spectroscopy. *Science* 246:790-792.

Weidner V. R. and Hsia J.J. 1981. Reflection properties of pressed polytetrafluoroethylene powder. The Journal of the Optical Society of America 71:856-859.

Wang A., Freeman J.J., Jolliff B.L., and Chou I. 2006. Sulfates on Mars: A systematic Raman spectroscopic study of hydration states of magnesium sulfates. *Geochimica et Cosmochimica Acta* 70:6118-6135.

Zaikowski A. 1979. Infrared-spectra of the Orgueil (C-1) chondrite and serpentine minerals. Geochimica et Cosmochimica Acta 3:943-945.

Zolensky M.E. and McSween H.Y.Jr.1988. Aqueous alteration. In *Meteorites and the Early Solar System,* edited by F. Kerridge and M. Mattews. Tucson: University of Arizona, pp. 114-143.

Zolensky M.E., Barret R., and Browning L.B. 1993. Mineralogy and composition of matrix and chondrule rims in carbonaceous chondrites. *Geochimica et Cosmochimica Acta* 57:3123-3148.

Appendix B1

Table B1. Carbonaceous chondrites analyzed in this study.

Meteorite	Type[c]	Section number	Fall or find[c]	Weathering grade[c]
LAP 02277[a]	CM1	10	Find	A
MIL 07700[a]	CM2	11	Find	A
QUE 97990[a]	CM2	35	Find	BE
QUE 99038[a]	CM2	23	Find	A/B
LAP 03786[a]	CM2	14	Find	A/B
MAC 02606[a]	CM2	7	Find	A
MET 00639[a]	CM2	15	Find	A
Cold Bokkeveld[b]	CM2	182-1	Fall	--
Bells[b]	C2-ung	5293-2	Fall	--
Ivuna[b]	CI1	2478-7413	Fall	--

[a]Sections are from NASA Johnson Space Center (JSC), Houston.
[b]Sections are from the Smithsonian Institution, Washington, DC.
[c]Data from the Meteoritical Bulletin Database.

Table B2. Estimated chemical formulae of average CM matrix serpentines for nine CM chondrites and Mineralogical Alteration Indices (MAI) of Browning et al. (1996).

	QUE 97990 (n =6)	MIL 07700 (n = 15)	QUE 99038 (n =13)	Bells (n = 3)	LAP 03786 (n = 7)	MAC 02609 (n = 2)	Cold Bokkeveld (n = 7)	LAP 02277 (n = 45)	MET 00639 (n = 13)
Si	1.65(0.17)	1.52(0.08)[a]	1.53(0.07)	1.50(0.12)	1.61(0.11)	1.57(0.03)	1.89(0.03)	1.84(0.04)	1.80(0.07)
Al	0.17(0.02)	0.20(0.06)	0.15(0.06)	0.20 (0)	0.17(0.05)	0.15(0.01)	0.13(0.02)	0.15(0.01)	0.16(0.03)
Cr	0.02(0.01)	0.01(0.01)	0.01(0)	0.01 (0)	0.02(0.01)	0.01(0)	0.02(0.01)	0(0)	0.01(0)
Fe^{2+}	0.78(0.31)	0.88(0.23)	0.74(0.08)	0.83 (0.07)	0.77(0.33)	0.73(0.20)	0.72(0.13)	0.71(0.05)	0.87(0.13)
Fe^{3+}	0.52(0.34)	0.76(0.16)	0.78(0)	0.79 (0.25)	0.60(0.17)	0.70(0.07)	0.10(0.01)	0.16(0.08)	0.24(0.14)
Mn	0.01(0)	0.01(0)	0.01(0)	0.01 (0)	0.01(0)	0.01(0)	0.01(0)	0.01(0)	0.01(0)
Mg	1.51(0.24)	1.43(0.29)	1.70(0.05)	1.42 (0.05)	1.56(0.40)	1.57(0.18)	1.92(0.18)	2.09(0.03)	1.73(0.11)
Ca	0.03(0.02)	0.02(0.01)	0.01(0)	0.02 (0.02)	0.03(0.04)	0.05(0.02)	0.02(0.01)	0(0)	0.02(0.02)
Na	0.10(0.03)	0.06(0.02)	0(0)	0.07 (0.02)	0.06(0.02)	0.05(0.01)	0.02(0.01)	0.01(0.01)	0.04(0.01)
Ni	0.07(0.03)	0.02(0.02)	0.02(0.01)	0.05 (0.05)	0.02(0.02)	0.04(0)	0.08(0.03)	0(0)	0.03(0.02)
MAI	**0.67(0.48)**	**0.43(0.13)**	**0.33(0.09)**	**0.41 (0.11)**	**0.45(0.08)**	**0.35(0.04)**	**1.21(0.32)**	**1.04(0.31)**	**0.90(0.33)**

[a] Numbers in parentheses correspond to 2σ standard deviations that represent the range of matrix serpentine compositions in the nine CM chondrite.

Table B3. . Tochilonite compositions (wt. %) in CM chondrites.

	QUE 97990 (n = 26)	MIL 07700 (n = 47)	QUE 99038 (n = 14)	Bells (n=10)	LAP 03786 (n =60)	MAC 02609 (n = 8)	Cold Bokkeveld (n =14)	LAP 02277 (n=8)	MET 00639 (n = 23)
SiO_2	19.7(23)	25.6(13)[a]	28.3(16)	25.8(49)	25.7(27)	30.4(35)	22.8(92)	28.2(23)	24.2(34)
TiO_2	0.04(2)	0.07(02)	0.16(12)	0.06(3)	0.29(33)	0.10(4)	0.09(3)	0.79(16)	0.06(04)
Al_2O_3	3.05(57)	2.63(23)	3.03(73)	4.00(63)	2.50(48)	2.22(24)	3.14(26)	1.89(49)	2.19(56)
"FeO"	51.9(59)	31.6(30)	34.6(23)	34.6(75)	28.5(53)	26.4(57)	34.7(81)	26.2(33)	38.3(55)
Cr_2O_3	0.08(8)	0.29(6)	0.40(16)	0.28(11)	0.26(15)	0.53(18)	0.87(95)	0.48(22)	0.24(7)
MnO	0.18(3)	0.21(3)	0.20(2)	0.16(6)	0.22(5)	0.21(6)	0.22(3)	0.23(3)	0.19(4)
MgO	7.91(52)	17.2(18)	20.9(12)	15.2(50)	15.7(30)	17.0(15)	12.5(55)	18.6(63)	16.8(25)
CaO	0.19(13)	0.46(38)	0.10(4)	0.84(27)	0.77(52)	0.73(26)	0.86(82)	4.18(23)	0.14(11)
Na_2O	0.50(29)	0.53(9)	0.05(3)	0.38(24)	0.70(32)	0.55(10)	0.20(13)	0.10(5)	0.28(6)
K_2O	0.06(4)	0.05(2)	0.02(2)	0.09(4)	0.04(6)	0.09(3)	0.09(4)	0.02(1)	0.02(2)
P_2O_5	0.02(2)	0.14(23)	0.24(6)	0.11(3)	0.31(93)	0.05(4)	0.67(66)	0.08(15)	0.02(6)
NiO	0.81(52)	1.24(45)	0.60(16)	1.49(11)	1.30(16)	1.30(58)	3.25(99)	3.52(98)	1.47(54)
S	3.13(4)	2.82(55)	0.28(11)	2.64(75)	2.58(4)	4.41(45)	2.11(72)	6.52(85)	5.06(67)
Total	86.76	81.96	88.83	85.02	78.32	82.90	80.84	89.13	87.76
S/SiO_2	0.17	0.11	0.01	0.11	0.10	0.15	0.17	0.23	0.22
"FeO"/SiO_2	**2.70**	**1.23**	**1.23**	**1.43**	**1.13**	**0.89**	**1.59**	**0.94**	**1.63**

[a] Numbers in parentheses correspond to 1σ standard deviations from the mean in terms of least units cited. The ''FeO'' concentration includes FeO in phyllosilicates, Fe^{3+} in cronstedtite and Fe^{2+}in sulfide.

Table B4. Diagnostic characteristics of progressive alteration in CM chondrite petrologic subtypes of Rubin et al. (2007).

	QUE 97990	MIL 07700	QUE 99038	Bells	LAP 03786	MAC 02606	Cold Bokkeveld	LAP 02277	MET 00639
Chondrule mesotasis	Phyllosilicate	Phyllosilicate	Phyllosilicate	Phyllosilicate	Phyllosilicate	Phyllosilicate	Phyllosilicate	Phyllosilicate	Phyllosilicate
Matrix phyllosilicates	Abundant	Abundant	Abundant	Abundant	Abundant	Abundant	Abundant	Abundant	Abundant
Metalic Fe-Ni	1 vol %	0.03-0.3 vo l %	0.03-0.3 vol %	≤ 0.02 vol %	0.03-0.3 vol %	≤ 0.02 vol %	0.03-0.3 vol %	≤ 0.02 vol %	0.03-0.3 vol %
Mafic silicate phenocrysts in chondrules	Unaltered	2-15 vol % altered	Unaltered	85-99 vol % altered	15-85 vol % altered	85-99 vol % altered	15-85 vol % Altered	85-99 vol % altered	15-85 vol % altered
Large PCP clumps	15-40 vol %	15-40 vol %	15-40 vol %	2-5 vol %	15-40 vol %	2-5 vol %	15-40 vol %	2-5 vol %	15-40 vol %
PCP compositions: "FeO"/SiO_2	2.70	1.23	1.23	1.13	1.43	0.89	1.59	0.94	1.63
Sulfide	po + pn	po + pn	po + pn	po + pn	po + pn	po + pn	po + pn	po + pn	po + pn
Carbonate	Ca	Ca	Ca	Ca & complex	Ca	Ca & complex	Ca	Ca	Ca
Petrologic subtype	**2.6**	**2.3**	**2.4**	**2.1**	**2.2**	**2.1**	**2.2**	**2.1**	**2.2**

The ‘‘FeO’’ concentration includes FeO in phyllosilicates, Fe^{3+} in cronstedtite and Fe^{2+}in sulfide.; po: pyrrhotite; pn: pentlandite.

Table B5a. The 3-μm feature parameters for meteorite spectra measured in dry conditions and the 2.3-μm and 0.7-μm parameters for meteorite spectra measured in ambient conditions.

	3-μm Band			2.3-μm Band		0.7-μm Band	
	Center (μm)	Depth (%)	Area(μm-^{1})	Center (μm)	Depth (%)	Center (μm)	Depth (%)
QUE 97990	2.796±0.001	31.95±0.91	0.10±0.03	2.31±0.002	0.46±0.17	0.732±0.014	0.73±0.23
MIL 00770	2.784±0.001	4.52±0.13	0.01±0.01	n.d	n.d	n.d	n.d
QUE 99038	2.773±0.010	16.85±0.49	0.11±0.01	n.d	n.d	n.d	n.d
Bells	2.778±0.002	41.88±0.71	0.15±0.03	2.299±0.004	0.39±0.15	0.738±0.003	1.36±0.44
LAP 03786	2.775±0.001	39.58±0.22	0.12±0.01	2.328±0.005	0.49±0.10	0.730±0.005	0.60±0.18
MAC 02606	2.770±0.006	16.16±0.37	0.04±0.01	2.311±0.009	0.48±0.05	n.d	n.d
Cold Bokkeveld	2.759±0.003	32.73±0.28	0.09±0.01	2.319±0.001	0.51±0.08	n.d	n.d
LAP 02277	2.723±0.001	31.77±0.45	0.05±0.01	2.306±0.025	0.62±0.22	0.727±0.001	1.63±0.25
MET 00639	2.722±0.00	17.78±0.39	0.02±0.01	n.d	n.d	n.d	n.d
Ivuna	2.715±0.001	40.71±0.15	0.06±0.01	2.316±0.003	0.67±0.08	n.d	n.d

n.d.: not detected.
Uncertainty for each parameter was determined by the 2σ standard deviation that represents variability from the average.

Table B5b. The 3-μm feature parameters for cronstedtite, the three Mg-serpentine polymorphs, and saponite.

	3-μm Band center (μm)	2.3-μm Band center (μm)
Cronstedtite[a]	2.852±0.002	2.327±0.002
Antigorite[b]	2.720±0.001	2.316±0.001
Lizardite[b]	2.713±0.001	2.331±0.003
Chrysotile[b]	2.710±0.001	2.300±0.016
Saponite(dry)	2.722±0.001	2.328±0.006
Lizardite(dry)	2.711±0.015	2.326±0.003

Uncertainty for each parameter was determined by the 2σ standard deviation that represents variability from the average.
[a]Spectrum from Clark et al. (2007) measured at ambient conditions with a strong adsorbed water feature.
[b]Spectra from Salisbury et al. (1991) measured at ambient conditions.

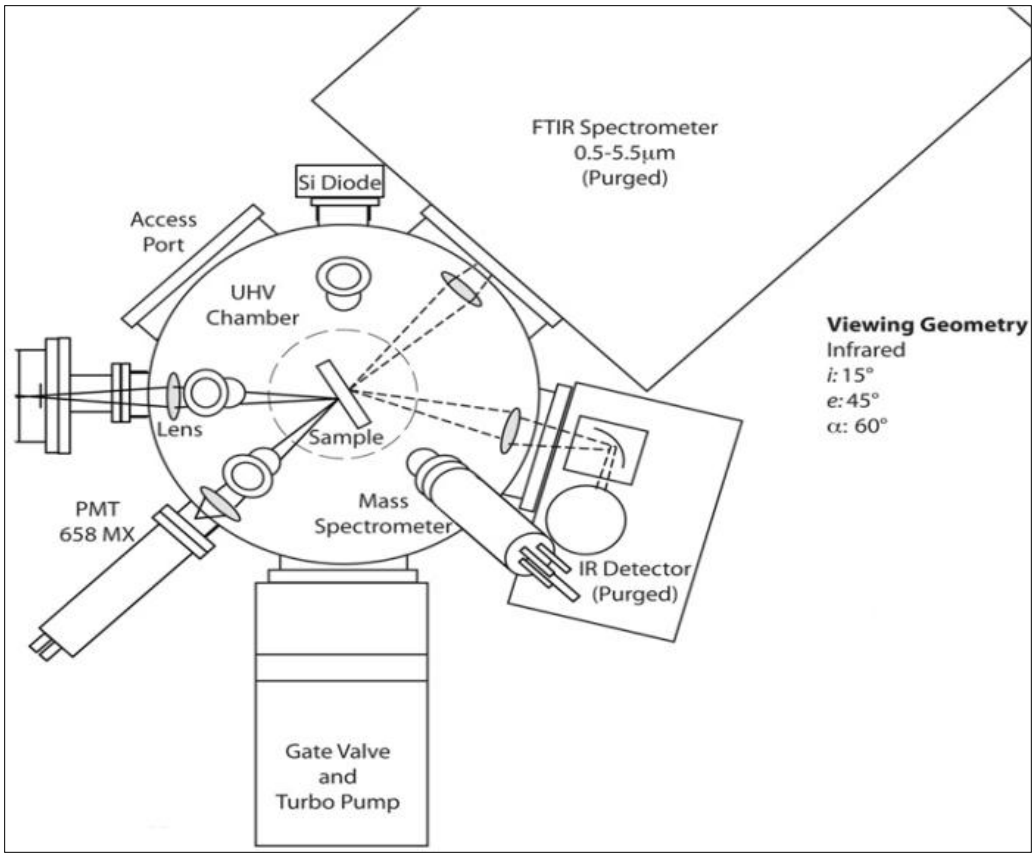

Figure B1. Optical design of the high vacuum chamber system with a Bruker Vertex 70 and an external MCT detector used to measure meteorite spectra under dry and vacuum conditions (Hibbitts et al. 2012).

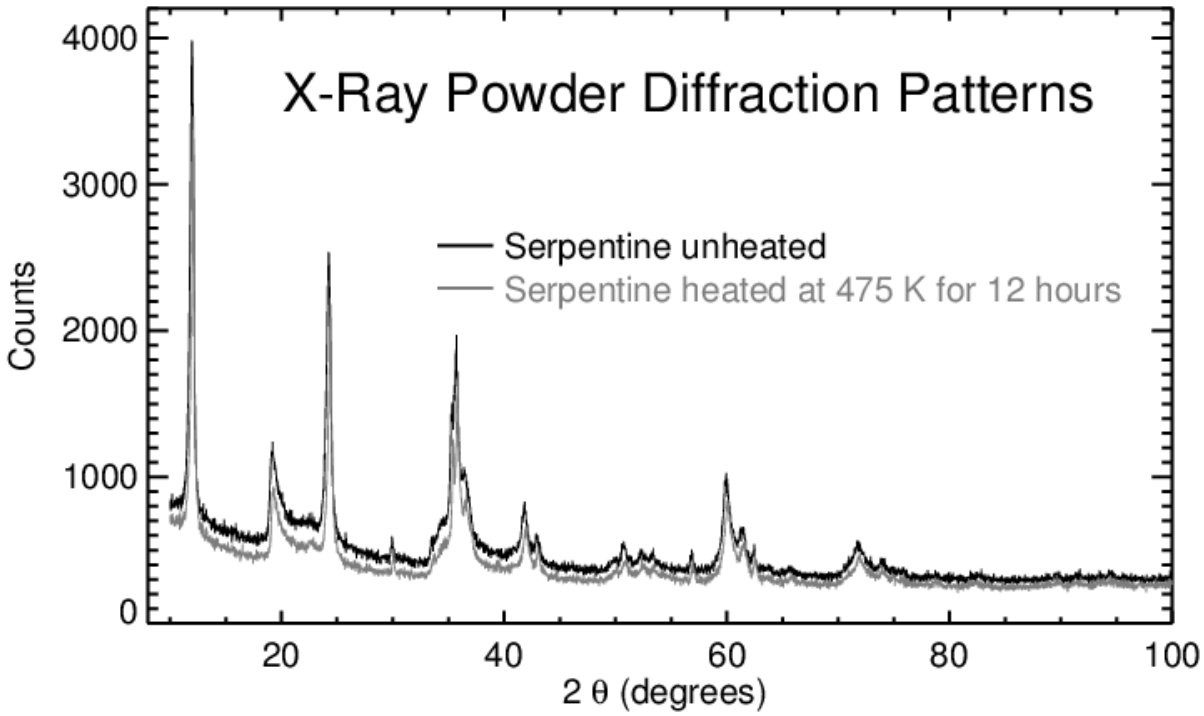

Figure B2. X-ray powder diffraction patterns of serpentine unheated (black) and heated at 475 K for 12 hours (gray). The similarity of the two diffraction patterns indicates that hydroxyl groups are not affected by modest heating.

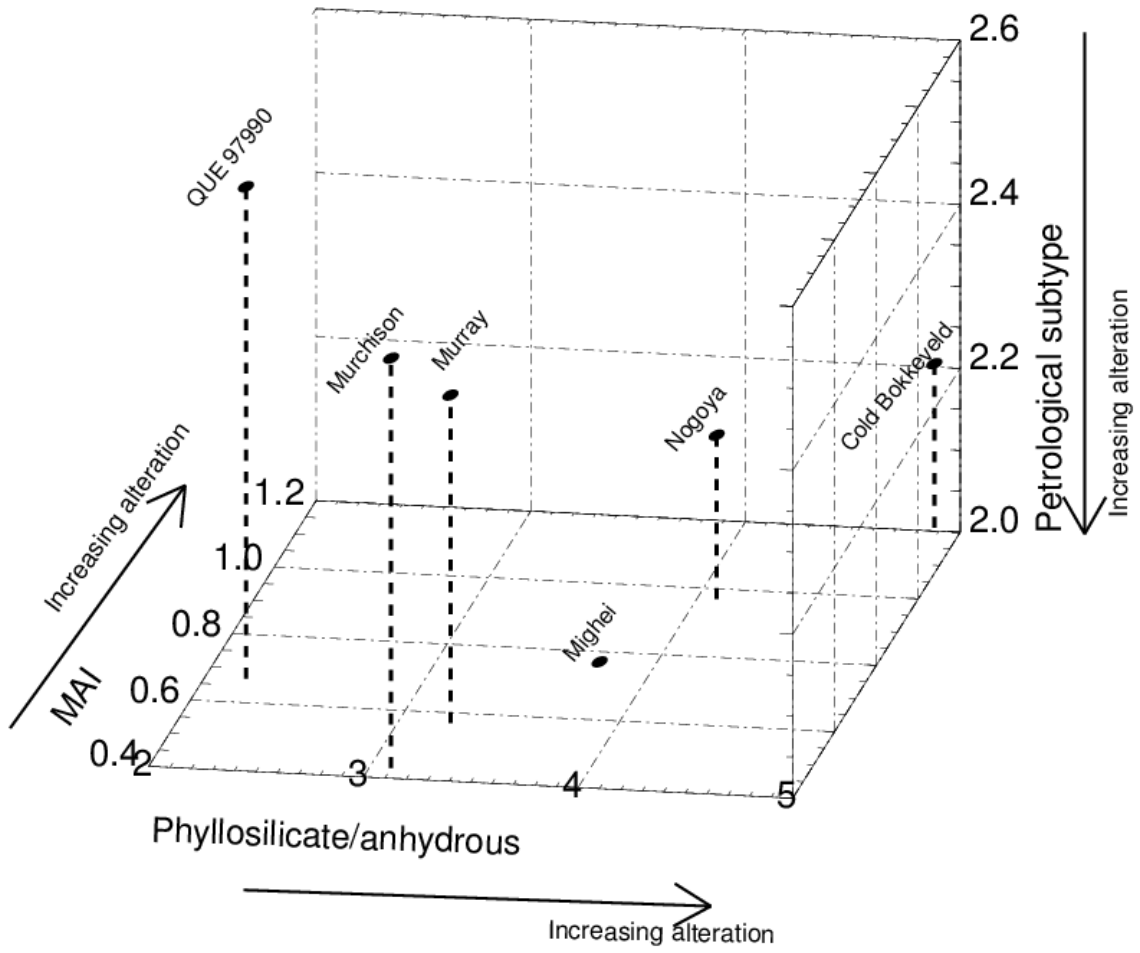

Figure B3. A 3D plot comparing the results of three alteration scales. The x-, y-, and z-axes represent the Howard, Browning, and Rubin scales, respectively. The plot includes samples analyzed by Browning et al. (1996), Rubin et al. (2007), and Howard et al. (2009, 2011). The plot includes two samples (QUE 97990 and Cold Bokkeveld) that were also analyzed by Rubin et al. (2007) and Howard et al. (2009, 2011). Mighei was not part of the Rubin et al. (2007) sample nor the current work, so it has been assigned the petrological subtype of 2.0 in the plot.

Figure B4a-j. Average IR reflectance spectra of CM and CI chondrites measured at ambient (solid), and dry and vacuum conditions (dashed). Several spectra were averaged for each temperature and pressure step. The atmospheric water represented by a gray bar marks the region of strong absorption by water vapor in Earth's atmosphere in which we cannot observe asteroids. Note the significant spectral effect of adsorbed water for the sample measured under ambient conditions. All spectra have been normalized to unity at 2.2 μm. See Appendix B2 for plots of spectra during the entire heating and depressurization sequence. Except for spectra of QUE 99038, which were measured at USGS, all other spectra were measured at APL.

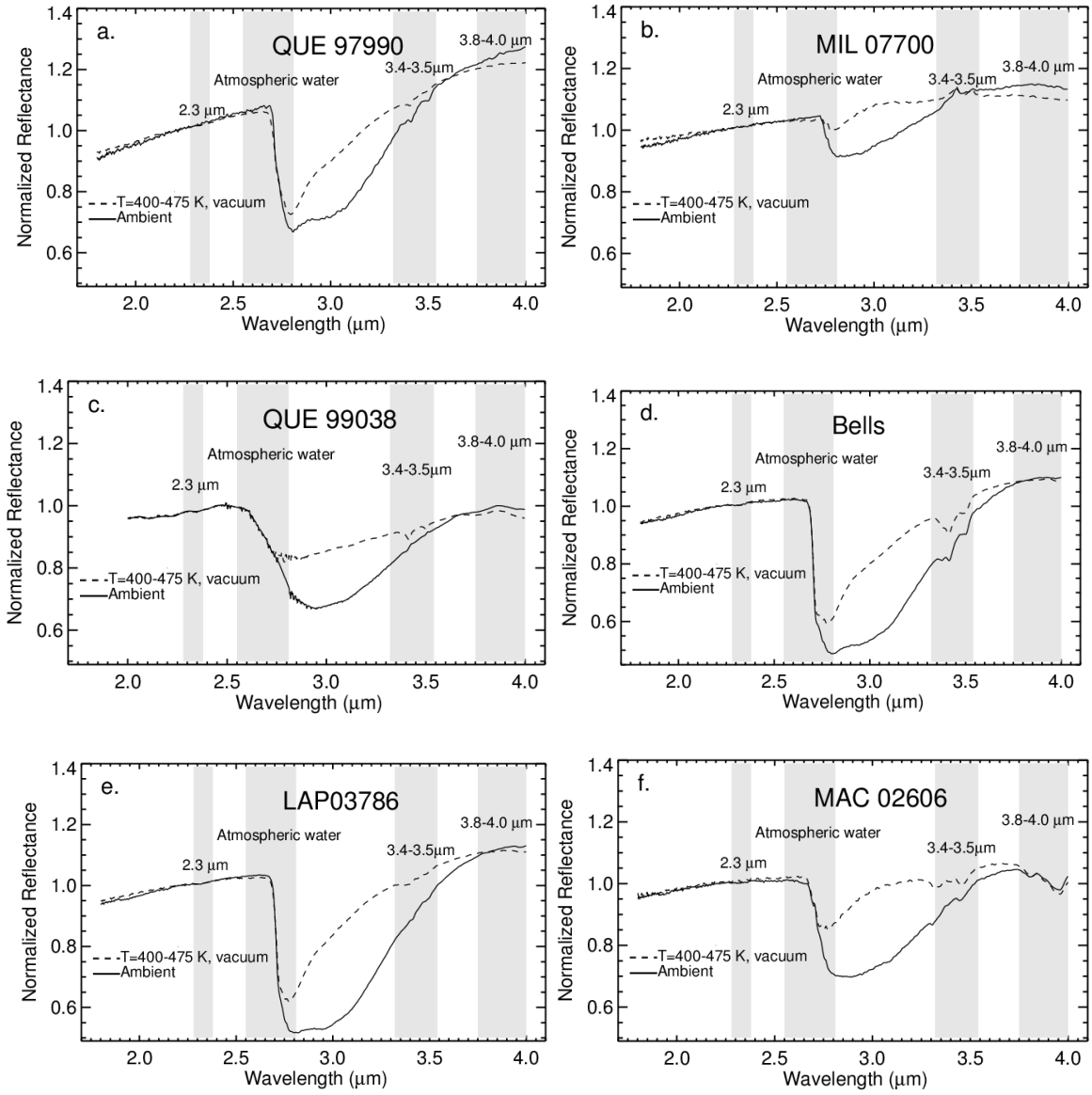

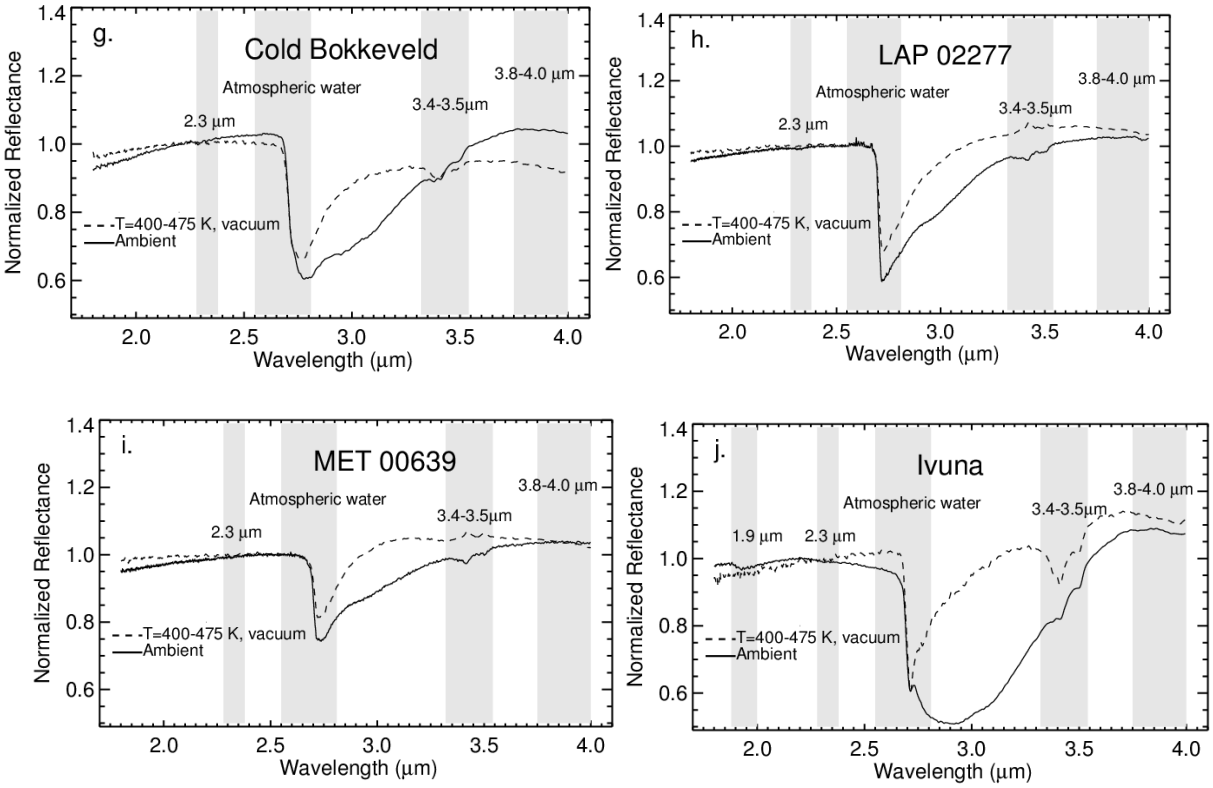
g.
Cold Bokkeveld
Atmospheric water
2.3 µm
3.4-3.5µm
3.8-4.0 µm
T=400-475 K, vacuum
Ambient
Normalized Reflectance
Wavelength (µm)
h.
LAP 02277
Atmospheric water
2.3 µm
3.4-3.5µm
3.8-4.0 µm
T=400-475 K, vacuum
Ambient
Normalized Reflectance
Wavelength (µm)
i.
MET 00639
Atmospheric water
2.3 µm
3.4-3.5µm
3.8-4.0 µm
T=400-475 K, vacuum
Ambient
Normalized Reflectance
Wavelength (µm)
j.
Ivuna
Atmospheric water
1.9 µm
2.3 µm
3.4-3.5µm
3.8-4.0 µm
T=400-475 K, vacuum
Ambient
Normalized Reflectance
Wavelength (µm)

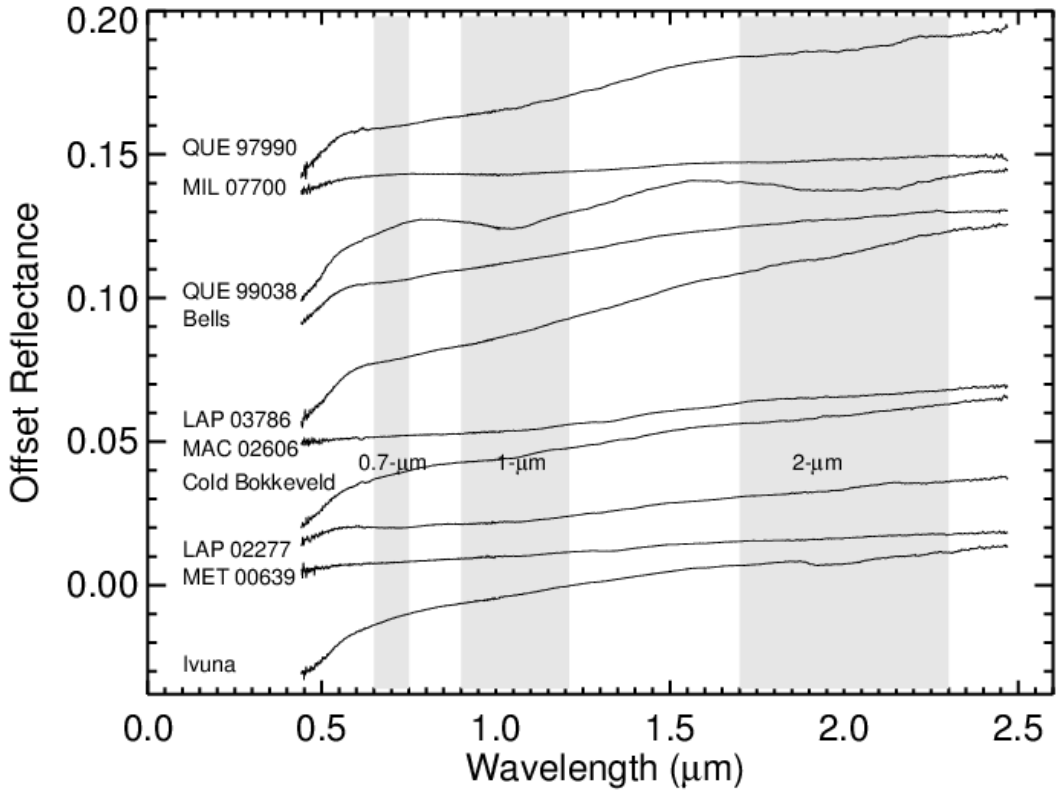

Figure B5. VNIR reflectance spectra of CM and CI carbonaceous chondrites. Some spectra show a very weak 0.7-µm feature (band depth less than 1%), and 1-µm and 2-µm features.

Figure B6.a. Spectrum of QUE 99790 (Group 1) is consistent with cronstedtite both measured at ambient conditions. The cronstedtite spectrum is from the USGS spectral library (Clark et al. 2007) and is affected by a strong adsorbed water feature. **6Bb.** Silicate-rich QUE 99038 and MIL 00770, which exhibit absorptions at ~1 μm and ~2 μm in VNIR spectra, attributed to olivine and pyroxene. **6Bc.** Raman spectrum also shows olivine in QUE 99038. **6Bd**. MAC 02606 (Group 2) exhibits a unique strong CO_3 absorptions in the 3.4-3.5-μm and 3.8-4.0-μm regions. **6Be**. Raman spectrum shows that the type of carbonates in MAC 02606 is dolomite. **6Bf**. Not-Serpentine-like group, which includes Bells, is distinguishable by a 3-μm band center that varies from 2.76 to 2.80 μm. This group is also distinguishable by ambient spectra that exhibit a broad feature at ~3.1 μm, attributed to adsorbed water, which is removed at dry conditions and vacuum. Group 3, which includes LAP 02277, is distinguishable by a narrower and shallower 3-μm band centered at ~2.72 μm, consistent with serpentine (antigorite). **6Bg.** Ivuna, the only CI chondrite analyzed in the present study, is distinct from all of the CM groups, with a very narrow 3-μm band centered at ~2.71 μm, consistent with lizardite and chrysotile and not saponite. Ivuna also exhibits a distinctive water feature at ~1.9 μm, which goes away at elevated temperatures and vaccum as adsorbed water is removed from the sample.

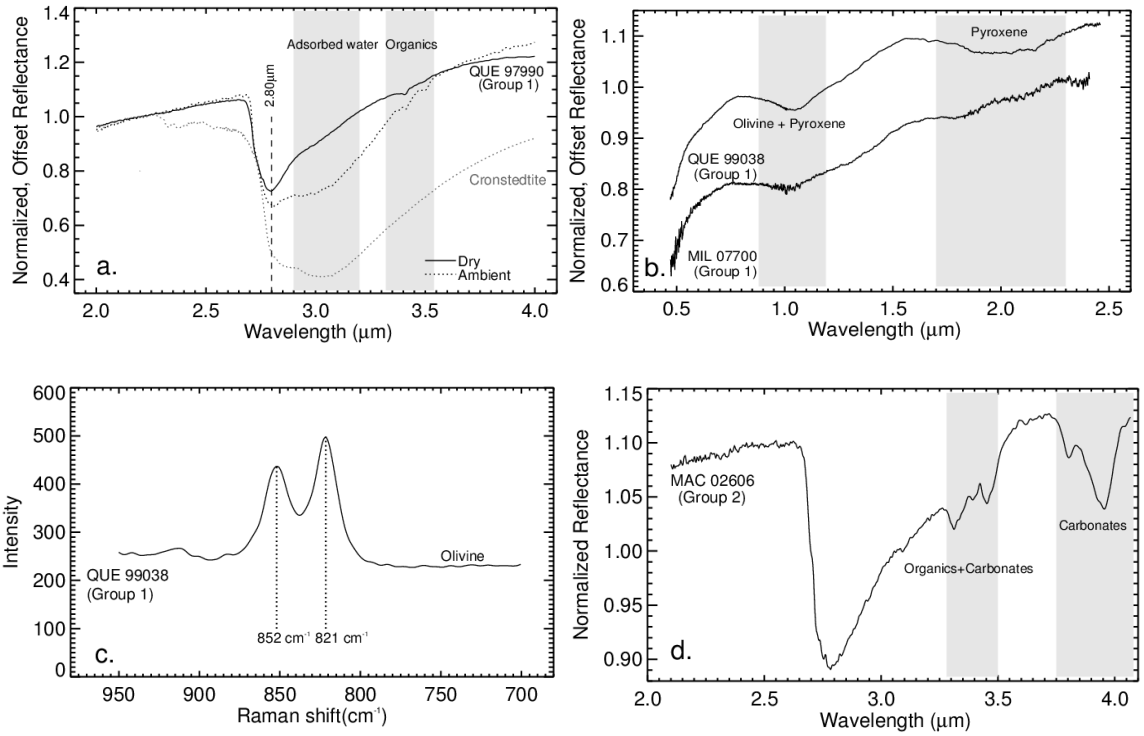

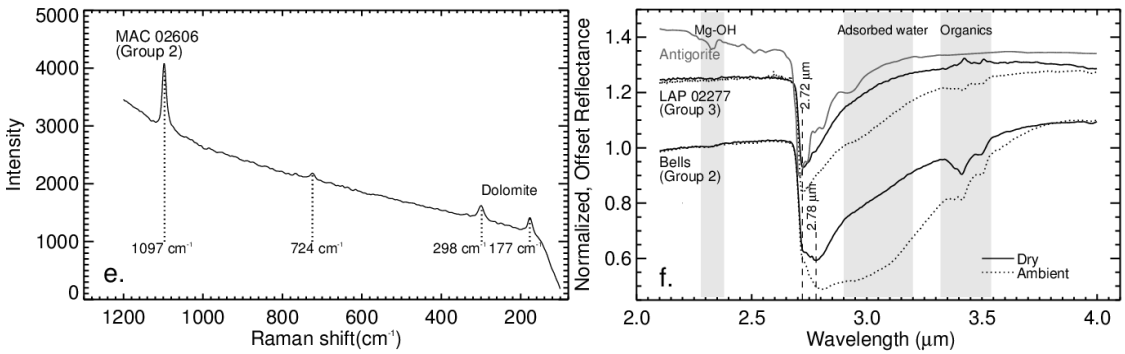
MAC 02606
(Group 2)
Dolomite
1097 cm-1
724 cm-1
298 cm-1
177 cm-1
e.
Intensity
Raman shift(cm-1)
Mg-OH
Antigorite
Adsorbed water
Organics
LAP 02277
(Group 3)
2.72 µm
2.78 µm
Bells
(Group 2)
f.
Dry
Ambient
Normalized, Offset Reflectance
Wavelength (µm)

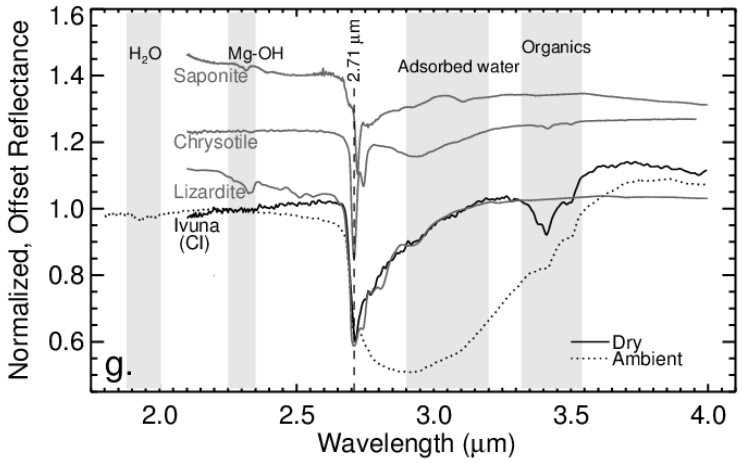
H2O
Mg-OH
Saponite
2.71 µm
Adsorbed water
Organics
Chrysotile
Lizardite
Ivuna
(CI)
g.
Dry
Ambient
Normalized, Offset Reflectance
Wavelength (µm)

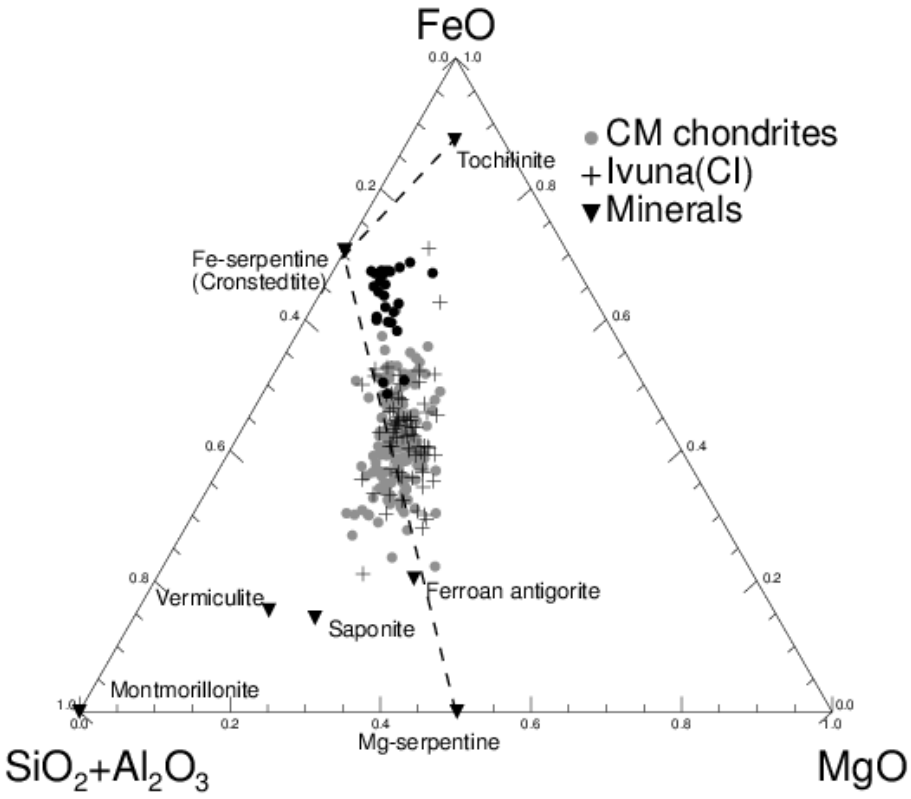

Figure B7. SiO_2+Al_2O_3-FeO-MgO diagram showing matrix compositions of CM chondrites and Ivuna, as well as some alteration minerals: serpentine - $Mg_3Si_2O_5(OH)_4$, montmorillonite - $(Na,Ca)_{0.3}(Al,Mg)_2Si_4O_{10}(OH)_2•n(H_2O)$, vermiculite - $(Mg,Fe2^+,Al)_3(Al,Si)_4O_{10}(OH)_2•4(H_2O)$, saponite-$(Ca/2,Na)_{0.3}(Mg,Fe^{2+})3(Si,Al)_4O_{10}(OH)_2•4(H_2O)$, ferroan antigorite - $(Mg, Fe^{2+})_3Si_2O_5(OH)_4$, and cronstdetite- $Fe^{2+}{}_2Fe^{3+}(SiFe^{3+})O_5(OH)_4$. Tochilinite data from Tomeoka and Buseck (1985). The matrix compositions lie along an approximately linear trend that extends from near the composition of cronstedtite (representing the least altered material) towards the SiO_2-MgO join near the composition of Mg-serpentine (representing the most altered material). The black filled circles represent QUE 97990 (the least altered sample in the present study). See Appendix B2 for more diagrams of matrix compositions of CM chondrites and Ivuna.

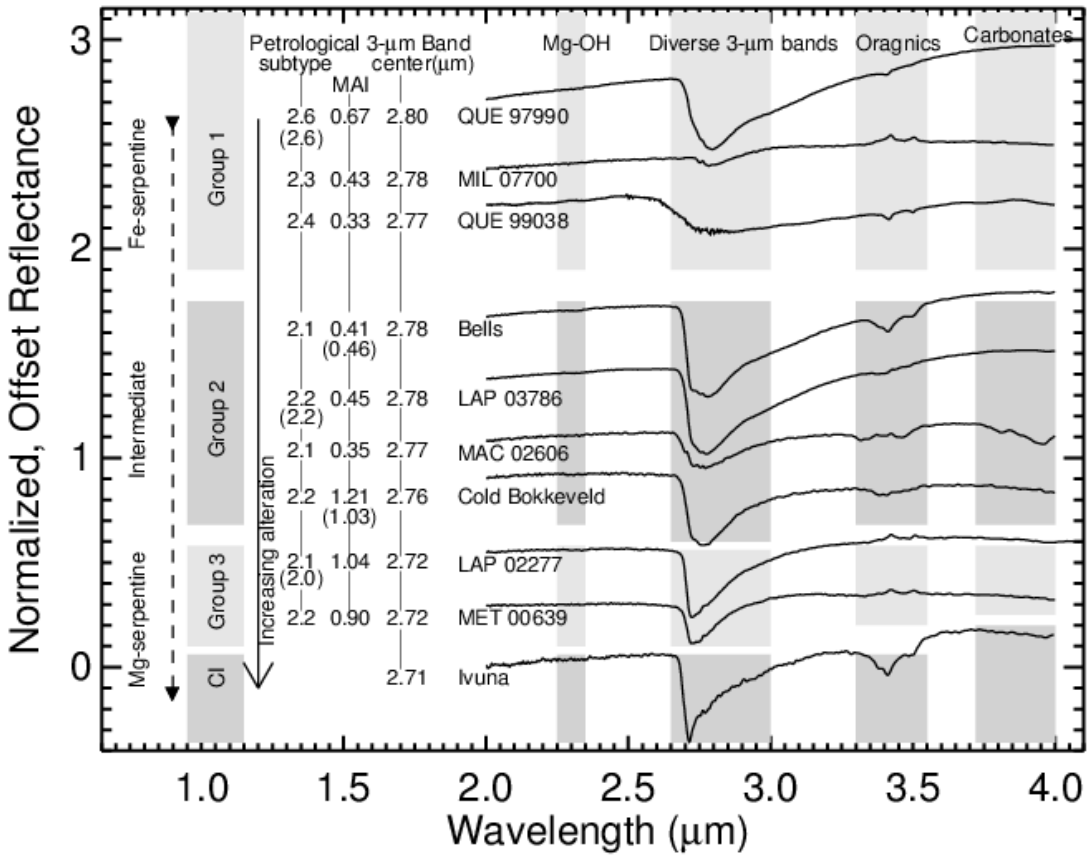

Figure B8. IR reflectance spectra of CM and CI carbonaceous chondrites measured under dry and vacuum conditions. The MAI and the petrologic subtype were determined applying the alteration scales of Browning et al. (1996) and Rubin et al. (2007), respectively. The MAI and petrological subtype values in parentheses are from Browning et al. (1996) and Rubin et al. (2007), respectively. Our spectral investigation revealed four distinct groups in CM and CI chondrites: Group 1(QUE 97990, QUE 99038, and MIL 07700), Group 2 (Bells, LAP 03786, MAC 02606, and Cold Bokkeveld), and Group 3 (LAP 02277 and MET 00639). Ivuna is the only CI chondrite analyzed in the present study. The 3-μm band center decreases with the increase of alteration.

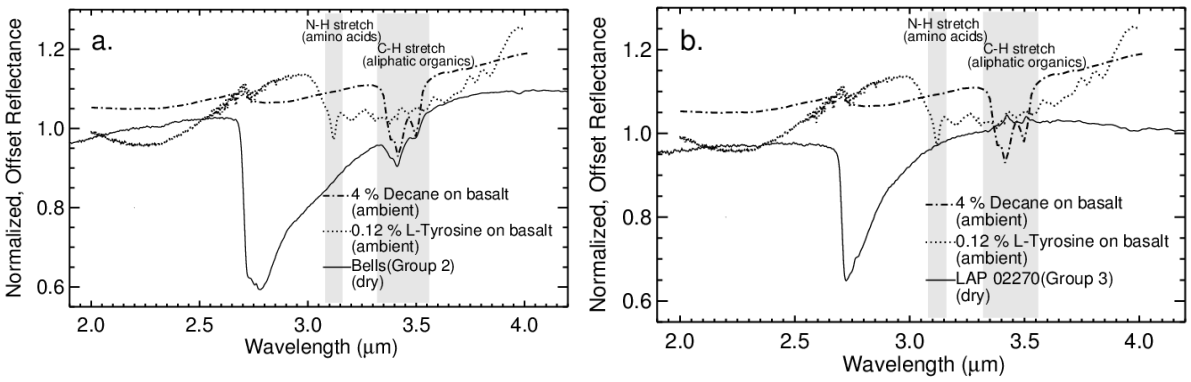

Figure B9a. Spectra of Bells (Group 2), and of decane alkane (4%) and L-Tyrosine amino acid (0.12%) mixed with basalt (BHVO-2F). The 3.1-μm feature in Tyrosine spectrum is the N-H fundamental stretch of amino acids. If Tyrosine were in the meteorite sample with similar grain sizes, our detectability would be around 0.01 wt % (100 ppm). The absorptions at 3.4-3.5 μm are the C-H stretch of aliphatic organics. **B9b.** LAP 02770 (Group 3) does not show the N-H stretch feature nor the C-H stretch feature.

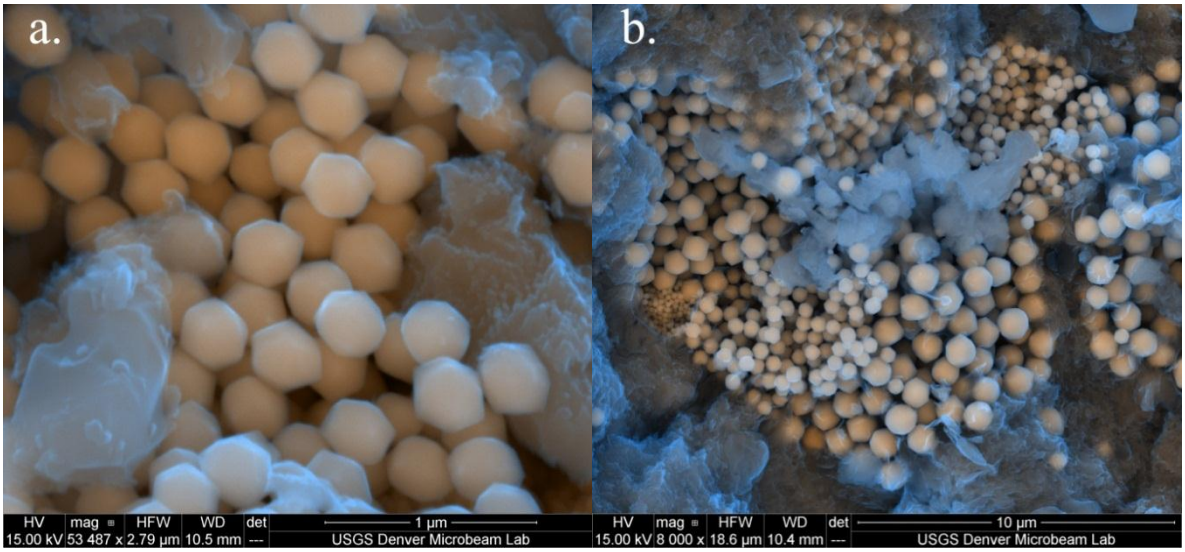

Figure B10a. Magnetite grains have been identified in Bells (Group 2) as framboidal aggregates with polygonal morphology. **B10b.** Similar framboidal aggregates of magnetite grains have also been found in Ivuna (CI).

Appendix B2. Spectra of CM and CI carbonaceous chondrites measured at different temperatures and pressures. Several spectra were averaged for each temperature step.

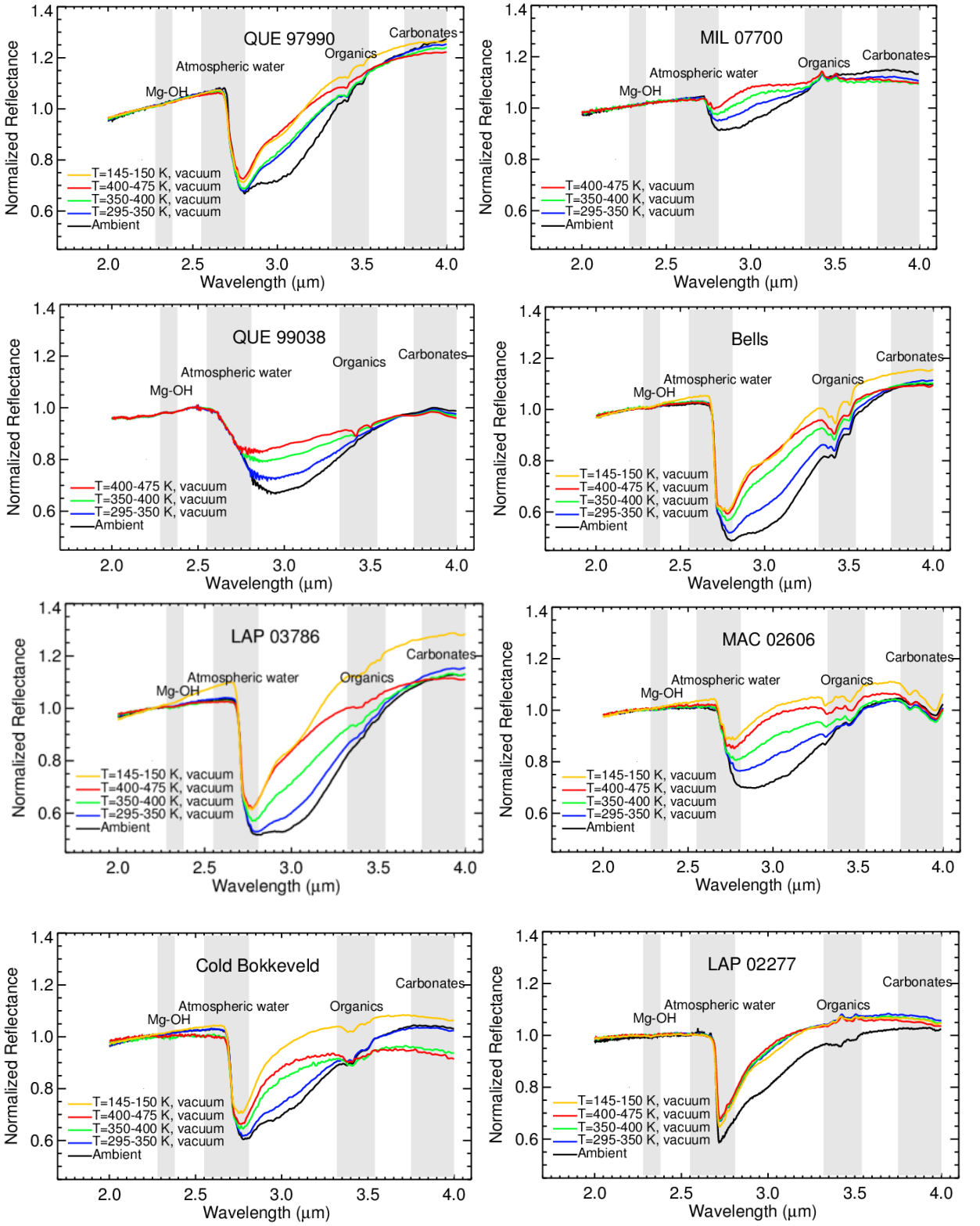

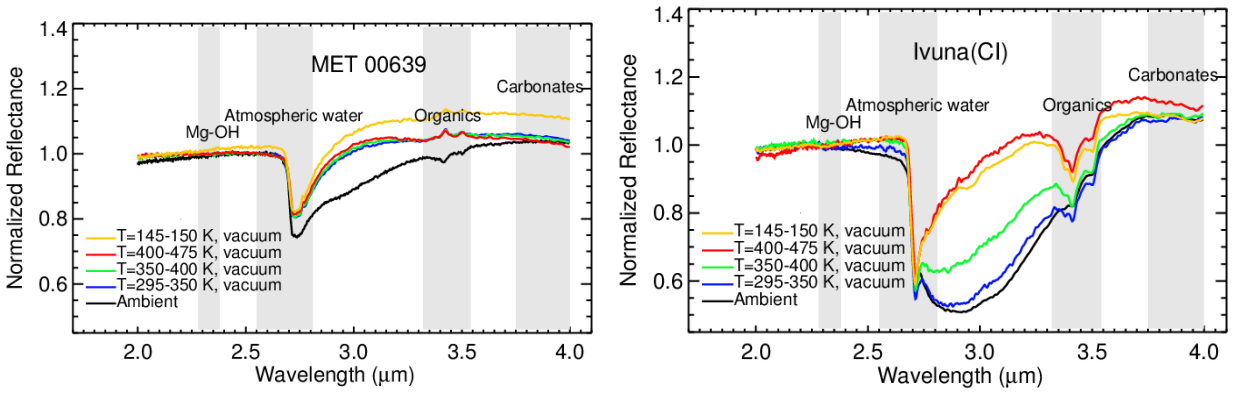
MET 00639
Ivuna(CI)
Normalized Reflectance
Wavelength (μm)
Mg-OH
Atmospheric water
Organics
Carbonates
T=145-150 K, vacuum
T=400-475 K, vacuum
T=350-400 K, vacuum
T=295-350 K, vacuum
Ambient

Appendix B3. Ternary diagrams of matrix compositions in nine CM and one CI carbonaceous chondrites.

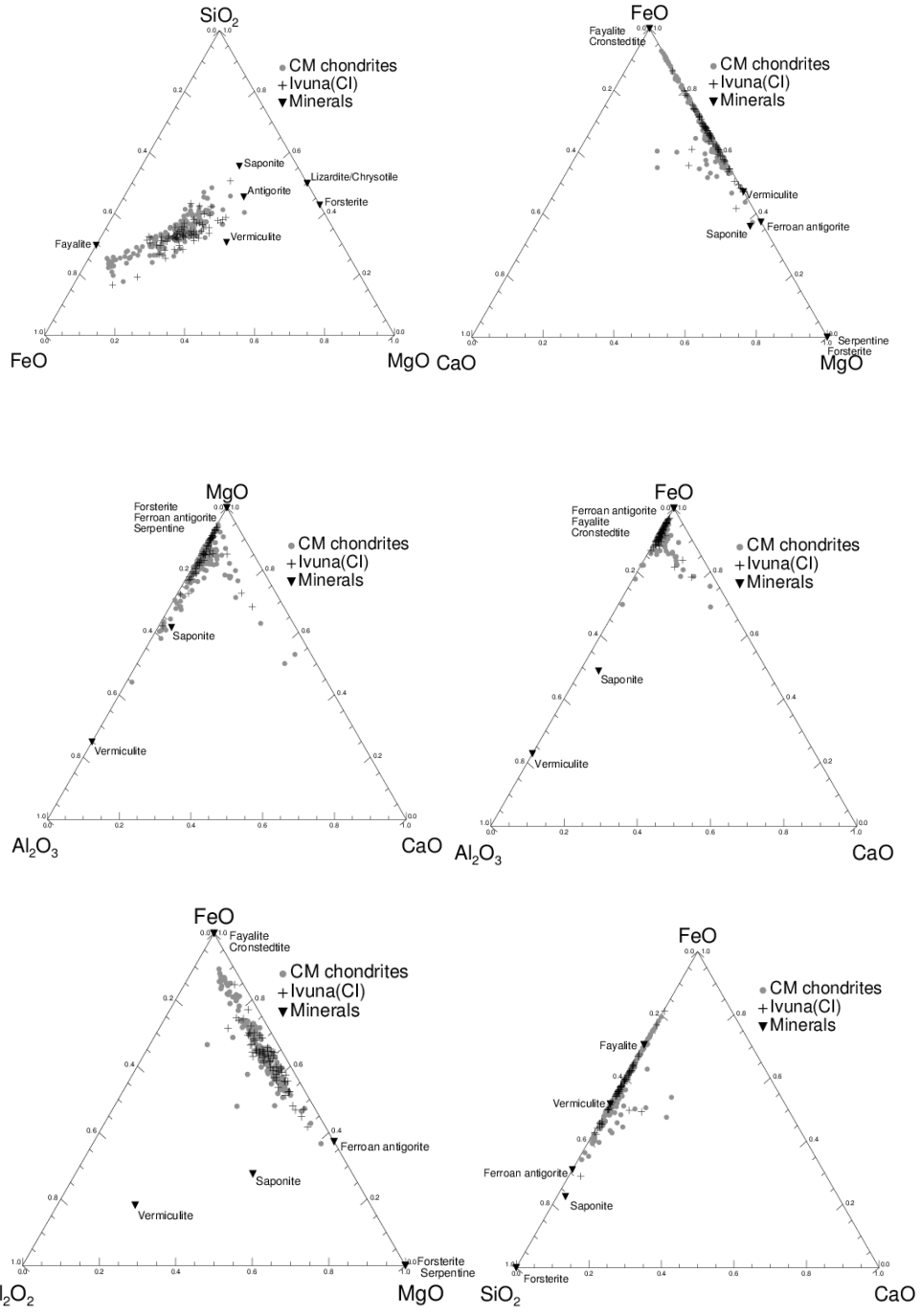

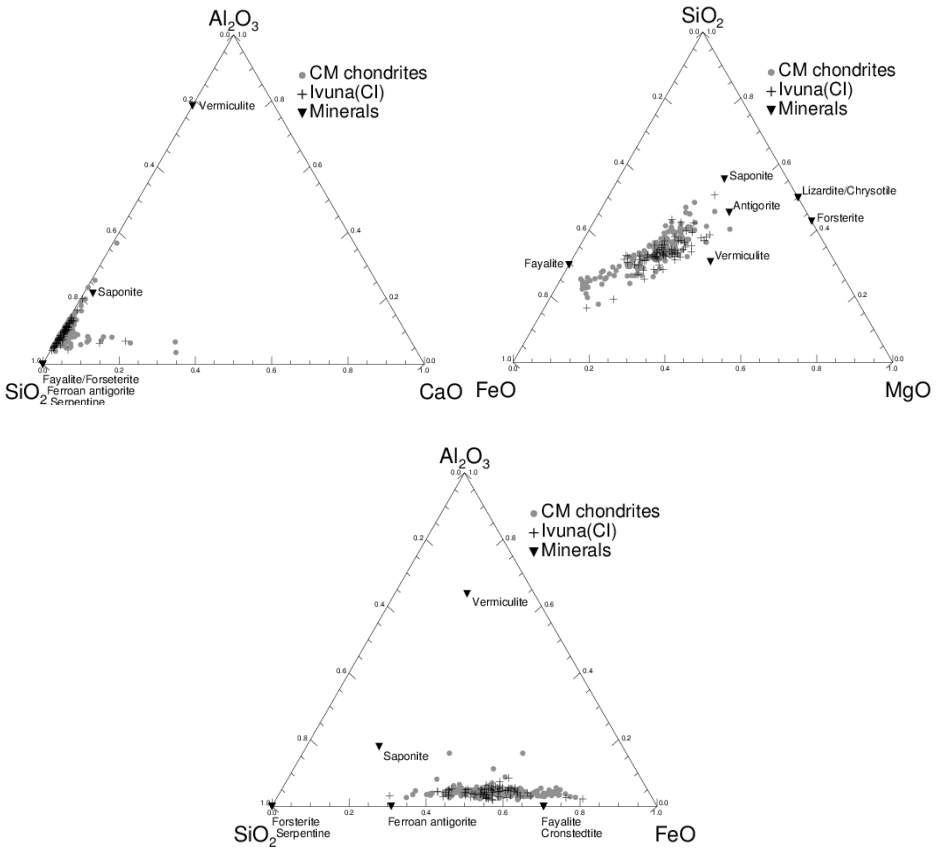
Al2O3
CM chondrites
+Ivuna(CI)
▼Minerals
Vermiculite
Saponite
SiO2
Fayalite/Forseterite
Ferroan antigorite
Serpentine
CaO
SiO2
CM chondrites
+Ivuna(CI)
▼Minerals
Saponite
Lizardite/Chrysotile
Antigorite
Forsterite
Fayalite
Vermiculite
FeO
MgO
Al2O3
CM chondrites
+Ivuna(CI)
▼Minerals
Vermiculite
Saponite
Forsterite
Serpentine
Ferroan antigorite
Fayalite
Cronstedtite
SiO2
FeO

Chapter 3

Implications of Aqueous Alteration in CM and CI Carbonaceous Chondrites for Outer Main Belt Asteroids

This chapter is a reformatted version of a paper, by the same name, to be submitted to Icarus in March 2014 by Driss Takir, Joshua P. Emery, and Harry Y. McSween.

Takir D., Emery J.P, and McSween Jr. H.Y. (to be submitted) Implications of Aqueous Alteration in CM and CI Carbonaceous Chondrites for Outer Main Belt Asteroids. *Icarus.*

Abstract

We investigate the linkage between CM and CI carbonaceous chondrites and outer Main Belt asteroids spanning the 2.5 < a < 4.0 AU region. The near-infrared spectra of chondrites were measured in the laboratory under asteroid-like conditions (Takir et al. forthcoming), and the spectra of asteroids were measured with the long wavelength cross-dispersed (LXD: 1.9-4.2-μm) mode of the SpeX spectrograph/imager at the NASA Infrared Telescope Facility (IRTF) (Takir and Emery 2012). The goal of the current investigation is to place constraints on the degree and location of aqueous alteration in the outer Main Belt region, and on the nature of phyllosilicate mineralogy on the surface of these asteroids. Using the 3-μm band shape indicator, we found that Group 2 CM chondrites is the possible meteorite analogs for asteroids with the sharp 3-μm features, located in the 2.5 < a < 3.3 AU region. Group 2 was previously found to be consistent with intermediate phases between endmembers Fe-serpentine and Mg-serpentine, with a petrological subtype, ranging from 2.2 to 2.1. No meteorite match was found for asteroids that are located farther from the Sun (3.0 < a < 4.0 AU) with rounded 3-μm feature, or for groups with distinctive spectra like 1 Ceres or 52 Europa. We do not expect to find any meteorite match for the rounded group because its 3-μm feature is attributed to H_2O ice. For the lack of matches within Ceres-like and Europe-like groups, we propose several possible scenarios and hypotheses that are testable with further laboratory work and spectral and orbital modeling.

1.0 INTRODUCTION

Outer Main Belt asteroids (e.g., C-, D-, G-, K-, F-, and B-types) that span the 2.5 < a < 4.0 AU are widely thought to be the main source of CM and CI carbonaceous chondrites (Bell et al. 1989; Gaffey et al. 1993). The chondrites exhibit evidence for past reactions with liquid water in the form of hydrated minerals, including water- and hydroxyl-bearing minerals (Lebofsky 1980; Vilas and Gaffey 1989; Rivkin et al. 2002; Brearley 2006). Several attempts have been made to link spectra of outer Main Belt asteroids with spectra of carbonaceous chondrites on the basis of the analyses of spectral slope and albedo and the 0.7 μm absorption feature (Gaffey et al. 1993; Pieters and McFadden 1994; Hiroi et al. 2001; Burbine 2001; Clark et al. 2010 and 2011).

In addition, analyses of the 3-μm absorption feature that include the band depth and the intensity have been used to characterize spectra of CM and CI carbonaceous chondrites (Miyamoto 1989, Miyamoto and Zolensky 1994, and Sato et al. 1997). Miyamoto (1989) showed that curvatures of absorption bands near 3-μm of CM chondrites are similar to that of serpentine. Additionally, Miyamoto and Zolensky (1994) showed that the integrated intensity of the 3-μm band (found by numerically integrating the area of the absorption feature in a continuum-removed reflectance spectrum) is closely correlated to the observed H content of carbonaceous chondrites. Later work by Sato et al. (1997) correlated the reflectance at 2.90 μm and 3.20 μm, divided by the reflectance at 2.53 μm, to the integrated intensity. These authors found that CM chondrites exhibit larger values of the integrated intensity of the 3-μm band than those of thermally metamorphosed carbonaceous chondrites, confirming that CM chondrites contain larger amount of hydrous minerals. Rivkin et al. (2003) used these meteorite analyses to determine the H/Si ratio for the asteroids that they observed, using the United Kingdom Infrared Telescope, in order to establish connections between CM chondrites and outer Main belt

asteroids. However, these meteorite spectra were measured under ambient laboratory conditions and are consequently contaminated by adsorbed water.

In the present study, we use high-quality near-infrared (NIR: 0.7-4.0 μm) spectra of 28 outer Main Belt asteroids ($2.5 < a < 4.0$ AU) that allowed the identification of four 3-μm spectral groups, each of which is, presumably, related to distinct surface mineralogy (Takir and Emery 2012). We also include additional spectra of asteroids that were recently observed. Takir and Emery (2012) identified the orbital distribution of four 3-μm spectral groups of asteroids. The sharp group exhibits a characteristically sharp 3-μm feature (reflectance decreases with decreasing wavelength into the 2.5-2.85-μm spectral region), attributed to OH-stretching in hydrated minerals (phyllosilicates). The majority of asteroids in this group are concentrated in the $2.5 < a < 3.3$ AU region. The rounded group, which is located in the $3.4 < a < 4.0$ AU region, is characterized by a rounded 3-μm band (reflectance increases with decreasing wavelength shortward of ~3.07 μm), attributed to H_2O ice (e.g., Rivkin and Emery 2012). The 1 Ceres-like group, which is located in the 2.5-3.3 AU region, has a narrow 3-μm band center at ~3.05 μm superposed on a much wider absorption from ~2.8 to 3.7 μm. The 52 Europa-like group has a 3-μm band centered at ~3.15 μm with longer wavelength band minimum and steeper rise on the long-wavelength edge of the absorption.

Additionally, Takir et al. (forthcoming) recognized three spectral groups of CM chondrites (in addition to the CI chondrite Ivuna) on the basis of the 3-μm band center and shape of spectra, showing that distinct parent body aqueous alteration environments experienced by different carbonaceous chondrites can be distinguished using reflectance spectroscopy. Group 1, which is the group exhibiting the lowest degree of aqueous alteration, is characterized by 3-μm band centers at longer wavelengths and is consistent with the occurrence of cronsdetite (Fe-

serpentine). Group 3, which is the most highly altered group, is characterized by 3-μm band centers at shorter wavelengths and is consistent with the occurrence of antigorite (Mg-serpentine). Group 2 is transitional between Groups 1 and 3 and presumably contains both serpentine minerals. Meteorite spectra were measured under dry conditions and vacuum to mimic the space conditions and removed the adsorbed water that affected the previous analyses of Miyamoto and Zolensky (1994), Sato et al. (1997), and Rivkin et al. (2003).

The goal of the present study is to apply the 3-μm spectral indicators (e.g., band center band shape, band depth) in CM and CI chondrites to outer Main Belt asteroids spanning the $2.5 < a < 4.0$ AU region in order to constrain the nature and location of aqueous alteration, and to provide more details on the alteration state and phyllosilicate mineralogy of these asteroids. Of particular interest is the question of the abundance and distribution of H_2O in the early Solar System and its significant role in the evolution of the mineralogy and cosmochemistry of outer Main Belt asteroids.

2.0 METHODOLOGY

Reflectance spectra of CM and CI carbonaceous chondrites used in the present study were measured by Takir et al. (forthcoming) under dry conditions (vacuum and elevated temperature) to remove adsorbed water, for subsequent comparison with reflectance spectra of asteroids. Takir et al. (forthcoming) also investigated degree of hydration in these chondrites, using previously defined alteration parameters, including the Mineralogical Alteration Index (MAI) and petrological subtype. The former parameter is based on the relative progress of coupled substitutions in the progressive alteration of Fe-serpentine (cronstedtite) to Mg-serpentine, which increases as alteration proceeds (Browning et al. 1996). The latter parameter is

based on an alteration sequence that varies downward from moderately altered petrologic type-2.6 chondrites to highly altered type-2.0 chondrites (Rubin et al. 1996). The petrological and geochemical parameters, which were determined using microprobe analyses and microscope observation, were found to be consistent with some of the spectral indicators of the 3-μm band, namely the band center and shape.

In addition to asteroid spectra that were presented in Takir and Emery (2012), the present study includes additional spectra, which were also observed using the long wavelength cross dispersed (LXD: 1.9-4.2-μm) mode of the SpeX spectrograph/imager at the NASA Infrared Telescope Facility (IRTF) (Table C1). The band depth, D_{λ}, at a given wavelength λ in both meteorite and asteroid spectra was calculated relative to the continuum that is defined as the regression line across the (k-band: 1.95-2.50-μm) region (Takir and Emery 2012):

$$D_{\lambda} = \frac{R_c - R_{\lambda}}{R_c}, \qquad (1)$$

where R_{λ} is the reflectance at a given wavelength λ, and R_c is the reflectance of the continuum at the same wavelength as R_{λ}. Further details on the observational and data reduction techniques as well as the analysis of the 3-μm band can be found in Takir and Emery (2012).

To characterize the shape of the 3-μm absorption feature in meteorites and asteroids, we chose representative wavelengths at 2.90 μm and 3.20 μm for nominal band depth calculation (Figure C1). We used a chi-squared test to quantitatively compare spectra of meteorites and asteroids and to determine the best matches. The calculated chi-squared is the sum of three chi-squared of the linear regression order polynomial fits across three representative regions: the 1.95-250 μm, 2.85-3.25 μm, and 3.50-4.00 μm (Figure C2):

$$\chi^2 = \chi^2_{1.95–2.50} + \chi^2_{2.85–3.25} + \chi^2_{3.50–4.00}. \quad (2)$$

The representative regions exlude the 2.50-2.85-μm region because asteroid spectra are affected by strong absorptions in Earth's atmosphere, and the 3.25-3.50-μm region because some meteorite spectra exhibit strong organics abosprtions.

In this chi-squared test, the predicted data are the meteorite data and the observed data are the asteroid data. The lowest chi-squared value represents the best match between spectra of an asteroid and a meteorite. For more analyses, we also determined the average χ^2 for each meteorite group (Group 1, Group 2, Group 3, and Ivuna).

3.0 RESULTS

3.1. Classification of Meteorite Spectra into the Sharp Group

In addition to the 15 asteroids that were previously classified in the sharp group, the present study includes five new asteroid spectra (Figure C3a-e), also found to possess a 3-μm band and classified in the sharp group (Table C2), following the techniques that were described in Takir and Emery (2012). Spectra were found to possess a 3-μm band if $D_{3.00} > 2\delta D_{3.00}$, where $D_{3.00}$ is the band depth at 3.00 μm and $\delta D_{3.00}$ is the uncertainly in $D_{3.00}$. Some objects in this group also exhibit a 0.7-μm feature with a generally convex NIR (0.85-2.5μm) spectrum. Tables 3a and 3b show the 3-μm band analyses of the meteorites and asteroids, respectively. The best fit across the 2.85-3.25-μm region in all meteorite spectra was found to be a linear regression, and the ratio of the reflectance at 2.90 μm ($R_{2.90}$) by the reflectance at 3.05 μm ($R_{3.05}$) was less than 1 ($R_{2.90}/R_{3.05} < 1$), the same criteria used by Takir and Emery (2012) for the sharp asteroid classification. Hence, the meteorite comparisons will be limited to asteroids that were classified into the sharp 3-μm group only.

3.2. Calculation of the Band Area in Asteroid Spectra

Figure C4 illustrates a good correlation between the 2.90-μm band depth and the 3.0-μm band area. We used this correlation to derive the following relation between the 2.90-μm band depth and the 3.0-μm band area in meteorite spectra that were measured under dry conditions and vacuum:

$$BA = 0.0045 * BD_{2.90} - 0.0016, \quad (3)$$

where *BA* is the band area and $BD_{2.90}$ is the band depth at 2.90 μm. Deriving such relation is useful to infer an accurate 3-μm band areas in outer Main Belt asteroids, affected by Earth's atmosphere absorptions that mask the 2.5-2.85-μm region. The corrected asteroid 3-μm band areas will address the question of whether the abundance of hydrated minerals among the outer Main Belt asteroids increases or decreases with the heliocentric distance ($2.5 < a < 4.0$ AU).

3.3. Spectra of Outer Main Belt Asteroids and CM and CI Chondrites

As described in section 2, we used chi-squared tests in order to quantitatively compare spectra of meteorites and asteroids and to determine what meteorite provides the best for each asteroid on the basis of computed chi-squared value, which can be affected by non-compositional effects such S/N of asteroid spectra (Table C4). Here, we show a few representative asteroids and their best meteorite matches where the χ^2 is less than half any other χ^2 (in bold in Table C4):

3.3.1. Group 1 Asteroids

Figure C5a shows spectra of 511 Davida (C-type, a =3.16 AU) and its best meteorite match QUE 99038 (petrological subtype = 2.4) with a chi-squared value of 0.291. Davida exhibits a very broad feature at ~1.0 μm and QUE 99038 also exhibits a feature at ~1 μm and another feature at ~2 μm.

Figure C5b shows spectra of 334 Chicago (C-type, a = 3.89) and its best meteorite match MIL 07700 (petrologic subtype = 2.3) with a chi-squared value of 0.812. Overall, both spectra have reddish slope, but MIL 07700 exhibits also a broad absorption feature in the 0.8-1.8-μm region.

3.3.2. Group 2 Asteroids

Figure C5c shows spectra of 511 Davida (C-type, a = 3.16 AU) and its best meteorite match MAC 02606 (petrological subtype = 2.1) with a chi-squared value of 0.303. MAC 02606 shows strong absorptions in the 3.4-3.5-μm and 3.8-4.0-μm regions. Both Davida and MAC 02606 exhibit a very broad feature at ~1.0 μm.

Figure C5d shows spectra of 54 Alexandra (C-type, a=2.71 AU) and its best meteorite match LAP 03786 (petrologic subtype = 2.2) with a chi-squared value of 0.338. In the 3-μm region, there is a very good match between the two spectra of LAP 03786 and Alexandra. There is also very good similarity between the slope (0.55-2.5 μm) in the meteorite and asteroid spectra. Only Alexandra's spectrum exhibits a 0.7-μm feature, with a shoulder at ~0.55 μm.

Figure C5e shows spectra of 36 Atalante (C-type, a = 2.75) and its best meteorite match Cold Bokkeveld (petrologic subtype = 2.2) with a chi-squared value of 0.356. In the 3-μm region, there is a good match between spectra of the asteroid and the meteorite. The VNIR slope (0.55-2.5 μm) in Atalante and Cold Bokkeveld do not match very well.

Figure C5f shows spectra of 121 Hermione (C-type, a = 3.44 AU) and its best meteorite match Bells (petrologic subtype = 2.1) with a chi-squared value of 0.468. In the 3-μm region, there is a very nice match between the spectra of Bells and Hermione. Also, both spectra exhibit a 0.7-μm feature, with a shoulder around 0.5 μm. The 0.7-μm feature in Hermione is stronger

than Bells. However, the visible and near-infrared (VNIR: 0.55-2.5 μm) slope do not match very well. The VNIR region is not included in the χ^2 calculation.

3.3.3. Group 3 and Ivuna-like asteroids

Figure C5g shows spectra of 511 Davida and its best meteorite match LAP 02277 (petrological subtype = 2.1) with a chi-squared value of 0.241. The two spectra also exhibit a broad feature in the 1-μm region.

Figure C5h shows spectra of 334 Chicago and its best meteorite match MET 00639 (petrologic subtype = 2.2) with a chi-squared value of 0.480. Overall, there is a nice match between Chicago and MET 00639.

Figure C5i shows spectra of 308 Polyxo and its best meteorite match Ivuna with a chi-squared value of 0.262. Both Polyxo and Ivuna have reddish slopes in the VNIR 0.55-2.5 μm region, with shoulders at ~0.75 μm. There is a good match between Polyxo and Ivuna in the 3-μm region.

4.0 DISCUSSION

4.1. Comparison Between CM and CI Chondrites and Outer Main Belt Asteroids

For a comprehensive comparison between altered carbonaceous chondrites and outer Main Belt asteroids, we used VNIR spectra of CM and CI chondrites and asteroids that cover the 0.5-2.5 μm region in addition to spectra that cover the 3-μm region. In comparing spectra of meteorites and asteroids in the 3-μm region, we have found some convincing matches, suggesting these meteorites and asteroids may have similar mineralogies, and possibly experienced analogous aqueous alteration processes. However, some meteorite and asteroid slopes do not match very well in the VNIR region. Many factors can cause a slope dissimilarity

in this region, including grain size, abundance of opaque phases, and viewing geometry (the phase angle for asteroids).

Several asteroids and meteorites exhibit a 0.7-μm feature, which is attributed to $Fe^{2+} \rightarrow Fe^{3+}$ charge transfer in phyllosilicates (Vilas and Gaffey 1989), with a shoulder at ~0.5 μm. Additionally, spectra of a few meteorites exhibit a broad feature in the 1-μm region, possibly due to Fe^{2+} in phyllosilicates and magnetite (Cloutis et al. 2011) or to Fe^{2+} in the M2 crystallographic site in olivine (Burns 1993). Yang and Jewitt (2010) attributed the presence of a similar 1-μm feature in a B-type asteroid, 335 Roberta, to magnetite.

QUE 99038 is a unique meteorite in that its exhibits a feature at ~1 μm and another feature at ~2 μm, attributed to Fe^{2+} in the M2 crystallographic site in olivine and pyroxene (Burns 1993). 704 Interamnia exhibits just the 1-μm feature, attributed to olivine (Burns 1993). MAC 02606 is also unique because it exhibits strong CO_3 absorptions in the 3.4-3.5-μm and 3.8-4.0-μm regions, attributed to carbonates (Clark et al. 2007). No asteroids among the sharp group show similar CO_3 absorptions in the 3.4-3.5-μm and 3.8-4.0-μm regions.

Although these spectral comparisons provide general insights on the degree of aqueous alteration of outer Main Belt asteroids, curve matching of spectra that include the VNIR region can be affected by processes that are not directly related to mineralogy (e.g., grain size, opaque phases, packing state). Hence, developing parameters that are more direct indicators of mineralogy is crucial to provide more details on the nature of phyllosilicate mineralogy on these asteroids.

4.2. Implications of the 3-μm Spectral Indicators for Outer Main Belt Asteroids

Takir et al. (forthcoming) developed two reliable 3-μm spectral indicators of mineralogy for CI and CM carbonaceous chondrites, the band center and the band shape, which can be used

to infer phyllosilicate mineralogy on the surface of outer Main Belt asteroids. Spectra of outer Main Belt asteroids were measured using ground-based observations, which were affected by strong absorptions of water vapor in Earth's atmosphere, especially in the 1.5-2.8-μm region. Therefore, it is not possible to directly measure the 3-μm band center in asteroid spectra, and infer the surface mineralogy. The band shape on the other hand, can be a useful indicator to provide more details on the alteration state and phyllosilicate mineralogy on these asteroids.

As described in section 2, we used two representative wavelengths at 2.90 μm and 3.20 μm to characterize the 3-μm band shape. Figure C6 shows a plot of the band depths at 2.90 μm and 3.20 μm for the chondrites and the sharp asteroids used in the present study. All chondrites and asteroids approximately follow a linear trend, except for the G-type asteroids 130 Elektra, 48 Doris, and 13 Egeria, which plot farther from the trend line. Sato et al. (1997) and Rivkin et al. (2003) also found a linear trend, but the chondrites they used were measured under ambient conditions, which consequently affect the interpretation of the 3-μm band. Our analyses show that the sharp asteroids are concentrated in an area that includes all Group 2 and Ivuna. This finding is supported by the calculated averaged chi-squared values for each meteorite group (Table C4). 10 sharp asteroids (55%) are best fit by Group2 meteorites (the χ^2 is less than half any other χ^2), and none are matched by Group 1. These results suggest that sharp asteroids and Group 2 meteorites, which experienced larger degree of aqueous alteration than Group 1 meteorites, may have similar phylosillicate mineralogy. Takir et al. (forthcoming) found that Group 2 is aqueously altered with a peterological subtype that ranges from 2.2 to 2.1, and is consistent with intermediate phases between endmembers Fe-serpentine and Mg-serpentine. The authors also revealed that Group 2 is characterized by adsorptive surfaces, with relatively higher abundance of magnetite than the other groups.

4.3.Grain size effects

The grain size of material can have some effects on the amount of the scattered, absorbed, and reflected light (Clark 1999). Photons interacting with larger grains have greater internal path according to Beers Law. On the other hand, smaller grains have more surface reflections than internal photon path lengths (Clark 1999). In the visible and near-infrared, the reflectance considerably changes as the grain size changes (e.g., Figure 8C). However, it appears that band centers at ~1 μm and ~2 μm are not affected by the change of the grain size.

The changes of the 3-μm band properties with the grain size in meteorites are not well documented. Milliken and Mustard (2007) found that grain size affects the 3-μm band depth in hydrated minerals (i.e., plagonite, nontronite). The authors did not investigate how the 3-μm band center changes with the grain size. Although the grain size may affect the 3-μm band shape and depth, we do not expect to see any changes in the 3-μm band center with the grain size, similarly to the 1-μm and 2-μm band centers in pyroxene. However, more laboratory work is necessary to determine how the grain size affects the 3-μm band properties in hydrated minerals and meteorites.

4.4. CM and CI Carbonaceous Chondrite parent bodies

All CM and CI chondrite spectra analyzed in the present study were found to be similar to sharp asteroid spectra. These results suggest that CM and CI chondrites are possibly the meteorite analogs for the sharp asteroids, located in the $2.5 < a < 3.3$ AU region. However, no meteorite match was found either for the rounded group, Ceres-like group (1 Ceres, 10 Hygiea, and 324 Bamberga), or Europa-like group (52 Europa, 31 Euphrosyne, and 451 Patientia). Because the 3-μm band in the rounded group is attributed to H_2O ice (Rivkin and Emery 2010; Campins et al. 2010; Licandro et al. 2011), we do not expect to find any meteorite match for this

group. However, several interpretations have been suggested for the 3-μm feature in Ceres-like group, including brucite (Miliken and Rivkin 2009). Although Takir and Emery (2012) suggested phyllosilicates with interlayer H_2O (along with OH) as a plausible explanation for the 3-μm feature in Europa-like group, more laboratory work and spectral modeling are needed to better characterize the hydration state of this group.

4.5. Heliocentric distance and degree of aqueous alteration in outer Main Bet asteroids

Jones et al. (1990) found a very weak correlation between the heliocentric distance and the fraction of hydrated asteroids, mostly C-class and subclasses, suggesting that planetesimals that were accreted closer to the Sun possibly experienced a higher degree of aqueous alteration than those accreted farther. This finding supports a scenario in which these asteroids were originally composed of mixtures of anhydrous minerals and ice that were later melted by heat released by decay of live ^{26}Al was available, forming hydrated minerals (Grimm and McSween 1989).

Asteroid spectra are affected by strong absorptions by water vapor in Earth's atmosphere, and hence band areas in the sharp asteroids are very difficult to compute. Here, we used the relation (equation 2) found between the 3-μm band area and the 2.90-μm depth in chondrite spectra, which were measured under dry condition and vacuum, to derive corrected band areas in asteroids (Table C3b, column 7). We found no correlation between the heliocentric distance and the corrected 3-μm band area for asteroids across the $2.5 < a < 3.3$ AU region (Figure C7). The lack of such correlation in this region can possibly be explained by the presence of opaque phases that suppress the 3-μm feature, and by the recent orbital evolution models that show that asteroids may not reside where they formed (e.g., Walsh et al. 2011).

5.0 CONCLUSIONS

We used CM and CI chondrite reflectance spectra, which were measured under dry conditions and vacuum for a direct comparison with outer Main Belt asteroids ($2.5 < a < 4.0$ AU). All analyzed meteorites were found to be similar to the sharp asteroids, which are located in the $2.5 < a < 3.3$ AU region. We used the 3-μm band shape as a spectral indicator to provide more details on the alteration state and phyllosilicate mineralogy on these asteroids. The band center, on the other hand, is very difficult to calculate in asteroid spectra because of the strong absorptions in Earth's atmosphere.

The 3-μm band shape was characterized on the basis of the band depths at 2.90 μm and 3.20 μm, as well as chi-squared tests in the 3.0-μm region. Using these analyses, we found that the sharp asteroids possibly have similar phylosillicate mineralogy as Group 2, suggesting that these asteroids and meteorites experienced similar aqueous alteration processes. These results suggest that CM and CI chondrites are possibly the meteorite analogs for these asteroids. Group 2 was previously found to have a petrological subtype that ranges from 2.2 to 2.1, and to be consistent with intermediate phases between endmembers Fe-serpentine and Mg-serpentine.

No meteorite match was found either for the rounded group, Ceres-like group (1 Ceres, 10 Hygiea, and 324 Bamberga), or Europa-like group (52 Europa, 31 Euphrosyne, and 451 Patientia). Because the 3-μm feature in the rounded group was attributed to H_2O ice, we do not expect to find any meteorite match for this group. For Ceres-like and Europa-like groups, we suggest several possible scenarios to explain the lack of meteorite matches in these groups: (1) The surfaces of these two groups contain mixture of H_2O ice-coated phyllosilicates. The dislodged fragments from Ceres-like and Europa-like groups then experienced H_2O ice sublimation before falling on Earth. (2) The dislodged fragments experienced re-accretion due to

the large escape velocity of these two groups, which have larger diameters than the sharp group (Figure A14). (3) Because asteroids in Ceres-like and Europa-like groups have larger diameters than the sharp group, it is possible that they did not experience impacts that exposed the deep interiors that might contain phyllosilicates detected in the sharp group (4) It is possible that Ceres-like and Europa-like groups are big enough to allow hydrothermal circulation inside the asteroid that causes water to be replenished on the surface (Grimm and McSween 1989), interacting with existing phyllosilicates to form the phases spectrally detected on the surfaces (e.g., brucite on Ceres). (5) The products of aqueous alteration on these two groups have not been spectrally recognized in the laboratory. Hence, laboratory work and spectral analyses of minerals under dry conditions and vacuum, as well as spectral models using new phylosillicate optical constants, are needed to test these hypotheses, and to characterize the spectral compositions of the two groups and possibly identify their meteorite analogs. Also, the Dawn spacecraft, which is on its way to asteroid Ceres, will provide more information about the surface composition of this asteroid.

ACKNOWLEDGEMETS

This work was partly supported by NASA Planetary Astronomy Program NNX08AV93G to JPE and NASA Cosmochemistry Program NNX10AH48G to HYM. We thank NASA IRTF staff for their assistance with asteroid observations. The IRTF is operated by the University of Hawaii under Cooperative Agreement No. NCC 5-538 with the National Aeronautics and Space Administration, Office of Space Science, Planetary Astronomy Program.

REFERENCES

Bell J.F., Davis D.R., Hartmann W.K., and Gaffey M.J. 1989. Asteroids: The big picture. In *Asteroid II,* edited by Binzel R.P., Gehrels T., and Matthews M.S. Tucson: University of Arizona Press, pp. 921-945.

Browning L.B., McSween H.Y., and Zolensky M.E. 1996. Correlated alteration effects in CM carbonaceous chondrites. *Geochimica et Cosmochimica Acta* 60:2621-2633.

Burbine T.H., Binzel R.P., Bus S.J., and Clark B.E. 2001. K asteroids and CO3/CV3 chondrites. *Meteoritics & Planetray Science* 36:245-253.

Brearley A.J. 2006. The action of water. In *Meteorites and the Early Solar System II*, edited by Lauretta D. and McSween H.Y. Tucson: University of Arizona Press, pp. 587-624.

Campins H. et al. 2010. Water ice and organics on the surface of the Asteroid 24 Themis. *Nature* 464:1320-1321.

Clark B.E.; Ziffer J., Nesvorny D., Campins H., Rivkin A.S., Hiroi T., Barucc M.A., Fulchignoni M., Binzel R.P., Fornasier S., DeMeo F., Ockert-Bell M.E., Licandro J., Mothé-Diniz T. 2010. Spectroscopy of B-type asteroids: Subgroups and meteorite analogs. *Journal of Geophysical Research* 115:E06005

Clark B.E., Binzel R.P., Howell E.S., Cloutis E.A., Ockert-Bell M., Christensen P., Barucci M.A., DeMeo F., Lauretta D.S., Connolly H., Soderberg A., Hergenrother C., Lim L., Emery J.P., Mueller M. 2011. Asteroid (101955) 1999 RQ36: Spectroscopy from 0.4 to 2.4 μm and meteorite analogs. *Icarus* 216:462-475.

Clark R.N, Swayze G.A., Wise R., Livo E., Hoefen T., Kokaly R., and Sutley S.J. 2007. USGS digital spectral library splib06a, Data Series, 231, U.S. Geol. Surv., Reston, Va. (http://speclab.cr.usgs.gov/spectral.lib06).

Cloutis E.A., Hudon P., Hiroi T., Gaffey M.J., Mann P. 2011. Spectral reflectance properties of carbonaceous chondrites: 2. CM chondrites. *Icarus*. 218:309-346.

Hiroi T., Zolensky M.E., and Pieters C.M. 2001. The Tagish Lake Meteorite: A possible sample of a D-type asteroid. *Science* 293:2234-2236.

Jones T. D., Lebofsky L. A., Lewis J. S., and Marley M. S. 1990. The composition and origin of the C, P, and D asteroids: Water as a tracer of thermal evolution in the outer belt. *Icarus* 88:172-192.

Gaffey M.J., Burbine T.H., and Binzel R.P. 1993. Asteroid spectroscopy: Progress and perspectives. *Meteoritics* 28:161-187.

Grimm R.E. and McSween H.Y. 1989. Water and the thermal evolution of carbonaceous chondrite parent bodies. Icarus 82:244-280.

Lebofsky L.A. 1980. Infrared reflectance spectra of asteroids: A search for water of hydration. *The Astronomical Journal* 85**:**573-585.

Licandro J. et al. 2011. 65 Cybele: Detection of small silicate grains, water-ice and organics. 2011. *Astronomy and Atrophysics* 525 A34.

Milliken R.E. and Mustard J.F. 2007. Estimating the water content of hydrated minerals using reflectance spectroscopy. II. Effects of particle size. *Icarus* 189:574-588.

Milliken R.E. and Rivkin A.S. 2009. Brucite and carbonate assemblages from altered olivine-rich materials on Ceres. *Nature Geosciences* 2:258–261.

Miyamoto M. 1989. Detection of hydrous minerals and carbonates in midinfrared diffuse reflectance spectra. Proceeding of Institute of Space and Astronautical Science Lunar and Planetary Symposium 22:99-105.

Miyamoto M. and Zolensky M.E. 1994. Infrared diffuse reflectance spectra of carbonaceous chondrites: Amount of hydrous minerals. *Meteoritics* 29:849-853.

Pieters C.M. and McFadden L.A. 1994. Meteorite and asteroid reflectance spectroscopy: Clues to early solar system processes. *Annual Review of Earth and Planetary Science* 22:457-497.

Rivkin A.S. and Emery, J.P. 2010. Detection of ice and organics on an asteroidal surface. *Nature* 64:1322-1323.

Rivkin A. S., Howell E. S.,Vilas F., and Lebofsky L. A. 2002. Hydrated minerals on asteroids: The astronomical record. In *Asteroids III*, edited by Bottke Jr. W.F., Cellino P., Paolicch P., and Binzel, R.P. Tucson: University of Arizona Press, pp. 235-253.

Rivkin A. S., Davies J.K., Johnson J.R., Ellison S.L., Trilling D.E., Brown R.H., and Lebofsky L.A. 2003. Hydrogen concentrations on C-class asteroids derived from remote sensing. *Meteoritics & Planetary Science* 38:1383-1398.

Rubin A.J., Trigo-Rodríguez J.M., Huber H., and Wasson J.T. 2007. Progressive aqueous alteration of CM carbonaceous chondrites. *Meteoritics & Planetary Science* 71:2361-2382.

Sato K., Miyamoto M., and Zolensky M.E.1997. Absorption bands near three micrometers in diffuse reflectance spectra of carbonaceous chondrites: Comparison with asteroids. *Meteoritic & Planetary Science* 32:503-507.

Takir D., and Emery J.P. 2012. Outer Main Belt asteroids: Identification and distribution of four 3-um spectral groups. *Icarus* 219:641-654.

Takir D., Emery J.P., McSween Jr. H., Hibbitts C.A., Clark R.N., Pearson N., and Wang A. Forthcoming. Nature and Degree of Aqueous Alteration in CM and CI Carbonaceous Chondrites. *Meteoritic & Planetary Science*, submitted.

Tedesco E.F., Williams J.G., Matson D.L., Veeder G.J. 1989. A three-parameter asteroid taxonomy. *Astronomical Journal* 97:580-606.

Tedesco E.F., Noah P.V., Noah M., Price S.D. 2002. The supplemental IRAS minor planet survey. *Astronomical Journal* 123:1056-1085.

Tholen D.J. 1984. Asteroid taxonomy from cluster analysis of photometry. Ph.D. Thesis, University of Arizona.

Vilas F. and Gaffey M.J. 1989. Phyllosilicate absorption features in main-belt and outer-belt asteroids from reflectance spectroscopy. *Science* 246:790-792.

Walsh K.J., Morbidelli A., Raymond S.N., O'Brien D.P., Mandell A.M. 2011. A low mass for Mars from Jupiter's early gas-driven migration. *Nature* 475:206-209.

Yang B. and Jewitt D. 2010. Identification of magnetite in B-type asteroids. *The Astronomical Journal* 140:s692-698.

Appendix C

Table C1. Observing parameters for asteroids observed with the LXD mode of SpeX at NASA IRTF.

Asteroid	Date (UT)	Time (UT)	Int (min)	Airmass	Standard star	Spectral type	B-V	V-K
41 Daphne	04/17/2012	5:07-8:04	140	1.0-1.8	SAO 97046	G0	0.62	1.41
211 Isolda	01/10/2013	10:21-12:42	120	1.0-1.3	HD 259551	G0	0.67	--
98 Ianthe	01/12/2013	10:18-13:04	140	1.1-1.2	HD 69027	G0	0.69	1.73
488 Kreusa	01/13/2013	10:13-11:33	80	1.0	HD 67149	G0	0.58	1.38
13 Egeria	01/12/2013	13:49-14:47	60	1.1-1.3	SAO 61716	G5	0.72	1.59

Table C2. Criteria used to classify the shape of the 3-µm feature.

Asteroid	Trendline[a]	3.00-µm Band depth (%)	$R_{2.90}/R_{3.05}$
41 Daphne	Linear	18.70±4.41	0.930±0.007
211 Isolda	Linear	15.35±3.16	0.945±0.003
98 Ianthe	Linear	17.41±3.09	0.951±0.003
411 Kreusa	Linear	14.53±3.32	0.950±0.003
13 Egeria	Linear	21.06±2.47	0.915±0.002

[a]The best fit across the 2.85-3.25-µm region.

Table C3a. Meteorite analyses.

Meteorite	2.90-µm Band Depth (%)	3.20-µm Band Depth (%)	Band Area[a] (μm^{-1})	$R_{2.90}/R_{3.05}$
QUE 97990	24.85	12.49	0.10±0.03	0.905
MIL 00770	1.71	-0.14	0.01±0.01	0.964
QUE 99038	19.16	16.12	0.11±0.01	0.966
Bells	31.23	17.00	0.15±0.03	0.893
LAP 03786	28.28	12.58	0.12±0.01	0.882
MAC 02606	11.98	6.50	0.04±0.01	0.941
Cold Bokkeveld	20.87	11.52	0.09±0.01	0.918
LAP 02277	13.23	1.49	0.05±0.01	0.911
MET 00639	3.01	-2.67	0.02±0.01	0.950
Ivuna	16.68	5.99	0.06±0.01	0.913

[a] Takir et al. (forthcoming).

Table C3b. Asteroid analyses.

Asteroid	Type[a]	a (AU)[b]	d(km)[c]	Albedo[c]	2.90-µm Band Depth (%)	3.20-µm Band Depth (%)	Band area (μm^{-1})
334 Chicago	C	3.89	158.5	0.062	15.55±6.4	8.81±8.01	0.07±0.03
121 Hermione	C	3.44	209.0	0.048	24.76±2.8	12.14±2.94	0.11±0.01
1015 Christa	C	3.21	96.9	0.046	18.37±18.18	12.22±21.49	0.08±0.08
488 Kreusa	C	3.17	150.13	0.059	16.86±3.12	6.77±2.80	0.07±0.01
511 Davida	C	3.16	326.1	0.054	16.51±5.28	9.97±3.79	0.07±0.02
104 Klymene	C	3.15	123.7	0.057	20.11±15.81	2.69±50.52	0.09±0.07
130 Elektra	G	3.12	182.2	0.076	22.52±27.33	3.60±21.5	0.10±0.12
120 Lachesis	C	3.11	174.1	0.046	19.93±17.87	10.97±5.52	0.09±0.07
48 Doris	CG	3.11	221.8	0.062	27.06±5.08	5.04±4.84	0.12±0.02
704 Interamnia	F	3.06	316.6	0.074	12.02±5.6	4.70±9.75	0.05±0.03
211 Isolda	C	3.04	143.19	0.060	18.74±2.68	3.97±2.65	0.08±0.01
41 Daphne	C	2.76	174.0	0.083	18.58±10.59	8.22±5.29	0.08±0.05
308 Polyxo	T	2.75	140.7	0.048	17.87±3.86	7.35±2.59	0.08±0.02
36 Atalante	C	2.75	105.6	0.065	17.51±6.55	14.14±7.12	0.08±0.03
187 Lamberta	C	2.73	130.4	0.057	17.83±11.08	6.94±3.68	0.08±0.05
54 Alexandra	C	2.71	165.7	0.055	25.73±5.20	9.54±4.10	0.04±0.04
34 Circe	C	2.69	113.5	0.054	10.16±8.67	4.94±8.30	0.10±0.03
98 Ianthe	CG	2.69	104.45	0.047	19.03±3.85	7.91±3.15	0.08±0.02
91 Aegina	CP	2.59	109.8	0.042	21.97±7.02	11.82±8.80	0.11±0.02
13 Egeria	G	2.58	207.6	0.083	27.66±2.91	-0.19±-6.22	0.12±0.01

[a]Tholen (1984).
[b]Source: http://ssd.jpl.nasa.gov/sbdb.cgi.
[c]Tedesco et al. (1989, 2002).

Table C4. Chi-squared (χ^2) test results for all meteorites and asteroids with the 3-µm sharp band.

	Group 1			Group 2				Group 3		CI			
Meteorite / Asteroid	QUE 97990	MIL 00770	QUE 99038	Bells	LAP 03786	MAC 02606	Cold Bokkeveld	LAP 02277	MET 00639	Ivuna	Group 1 Average	Group 2 Average	Group 3 Average
334 Chicago	2.486[a]	**0.812**[b]	2.284	6.024	4.098	0.902	4.556	1.002	**0.480**	1.027	1.861	3.895	0.741
121 Hermione	3.940	10.457	1.274	**0.468**	0.779	3.467	0.676	2.654	5.931	3.483	5.224	1.348	4.293
1015 Christa	2.916	3.577	4.163	6.443	4.678	2.836	6.518	2.927	3.217	2.297	3.552	5.119	3.072
488 Kreusa	3.128	6.260	0.474	1.402	1.050	1.401	0.427	0.953	2.826	1.865	3.287	1.070	1.890
511 Davida	2.117	3.139	**0.291**	2.241	1.374	**0.303**	1.187	**0.241**	1.083	0.866	1.849	1.276	0.662
104 Klymene	8.973	16.663	13.153	13.615	10.680	11.555	15.977	10.296	13.748	9.229	12.930	12.957	12.022
130 Elektra	5.509	14.493	5.043	1.944	2.356	6.891	3.774	5.557	9.784	5.449	8.348	3.741	7.671
120 Lachesis	1.088	3.063	1.795	3.303	1.892	1.041	3.516	0.908	1.903	0.637	1.982	2.438	1.406
48 Doris	5.636	11.997	2.037	1.189	1.782	4.583	1.052	3.782	7.089	4.948	6.557	2.152	5.436
704 Interamnia	1.483	0.892	2.902	5.788	3.707	0.960	5.467	1.177	0.978	0.678	1.759	3.981	1.078
211 Isolda	2.683	8.213	0.894	0.521	0.427	2.353	0.752	1.640	4.413	1.728	3.930	1.013	3.027
41 Daphne	2.195	7.210	1.012	0.868	0.486	2.017	1.089	1.316	3.857	1.151[c]	3.472	1.115	2.587
308 Polyxo	0.778	2.950	1.297	2.790	1.456	0.704	2.948	0.523	1.570	**0.262**	1.675	1.975	1.047
36 Atalante	5.954	10.509	1.089	1.637	2.159	3.610	**0.356**	3.169	5.729	4.495	5.851	1.941	4.449
187 Lamberta	2.598	5.151	0.664	1.919	1.269	1.118	1.074	0.789	2.350	1.542	2.804	1.345	1.570
54 Alexandra	1.690	5.574	0.882	0.845	**0.338**	1.445	1.255	0.905	2.944	1.301	2.715	0.971	1.925
34 Circe	2.835	4.351	0.605	2.416	1.671	0.816	1.157	0.660	1.783	1.450	2.597	1.515	1.222
98 Ianthe	1.520	4.646	0.455	1.424	0.660	0.797	1.183	0.440	2.128	0.811	2.207	1.016	1.284
91 Aegina	6.827	11.702	1.760	1.961	2.584	4.358	0.591	3.755	6.565	5.346	6.763	2.374	5.160
13 Egeria	5.818	13.517	2.374	0.830	1.516	5.222	0.902	4.065	8.038	5.313	7.236	2.118	6.052

[a]Chi-squared value computed using the sum of three sum of three chi-squared of the linear regression order polynomial fits across three representative regions: the 1.95-250 µm, 2.85-3.25 µm, and 3.50-4.00 µm. In this chi-squared test, the predicted data represent meteorite data and the observed data represent asteroid.

[b]The lowest chi-squared value (in bold) represents the best match between an asteroid and a meteorite.

[c]The χ^2 value highlighted in gray represents less than half of any other χ^2.

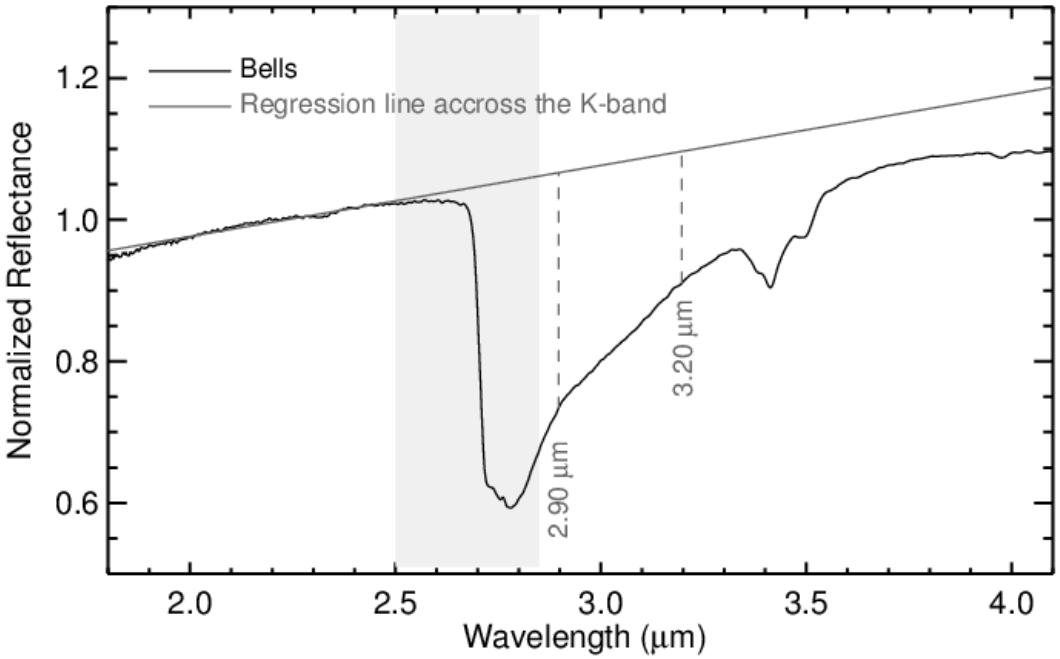

Figure C1. Near-infrared spectrum of the CM carbonaceous chondrite Bells, showing the 3-µm region. The solid gray line is the continuum that is defined as the regression line across the 1.95-2.50-µm region (k-band). The dashed lines show the band depths calculated at 2.90 µm and 3.20 µm, which were chosen as representative wavelengths to characterize the band shape of the 3-µm band.

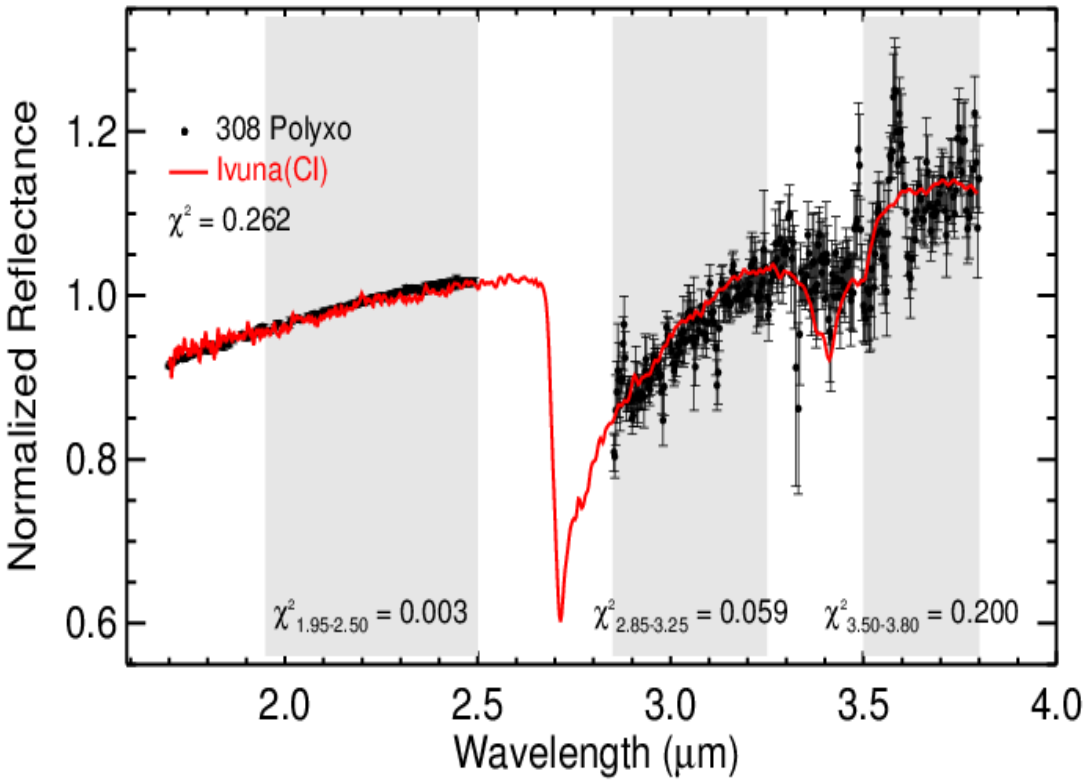

Figure C2. Comparison between the spectra of CI chondrite Ivuna and the asteroid 308 Polyxo, using the sum of three chi-squared of the linear regression order polynomial fits across three representative regions (gray): the 1.95-250 µm, 2.85-3.25 µm, and 3.50-4.00 µm. In this chi-squared test, the predicted data represent Ivuna and the observed data represent 308 Polyxo. The lowest chi-squared value of 0.262 shows that Ivuna is the match for Polyxo.

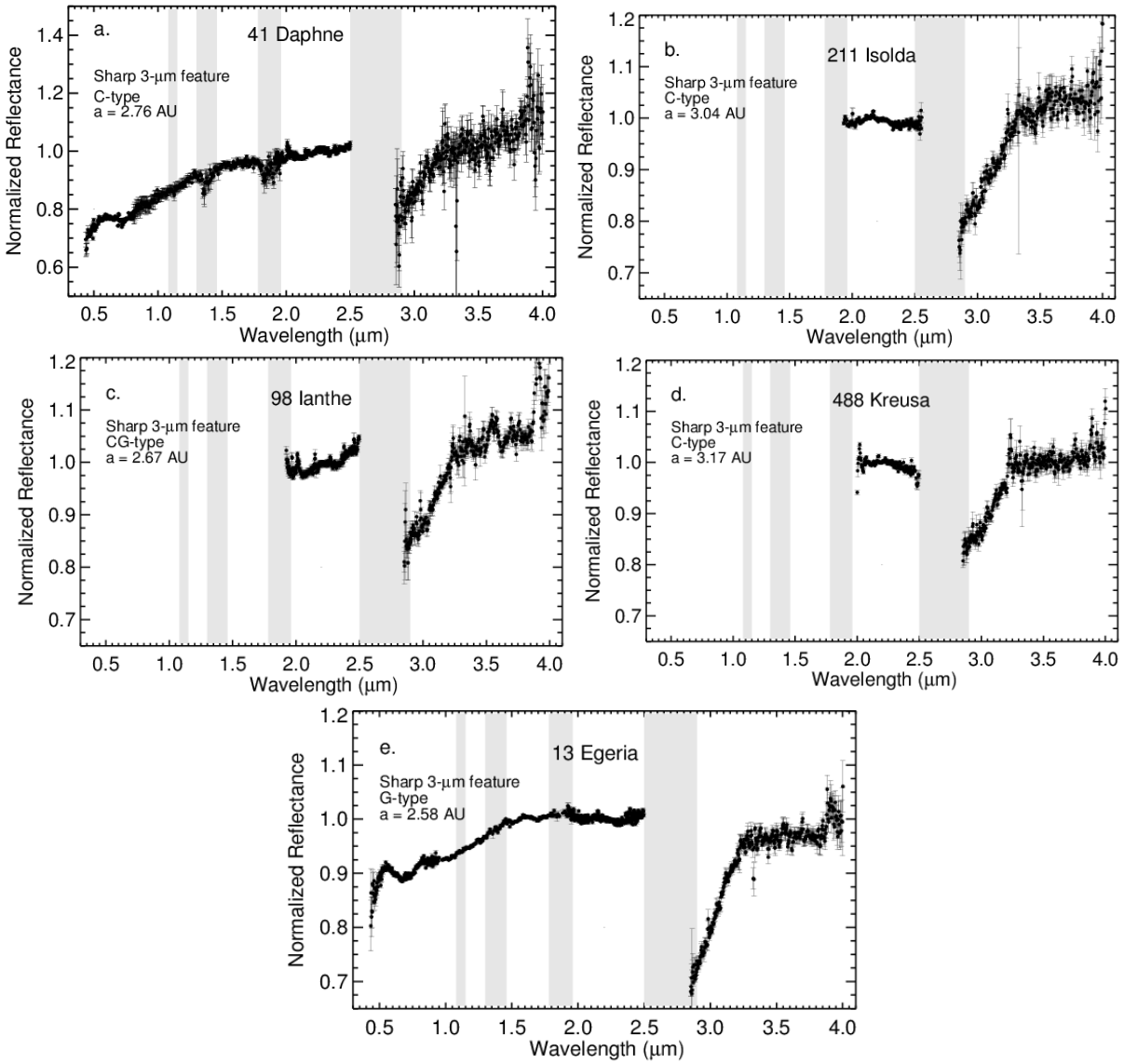

Figure C3. Spectra of asteroids that were classified in the sharp group. All spectra have been normalized to unity at 2.2 μm. The gray bars on each plot mark wavelengths of strong absorption by water vapor in Earth's atmosphere.

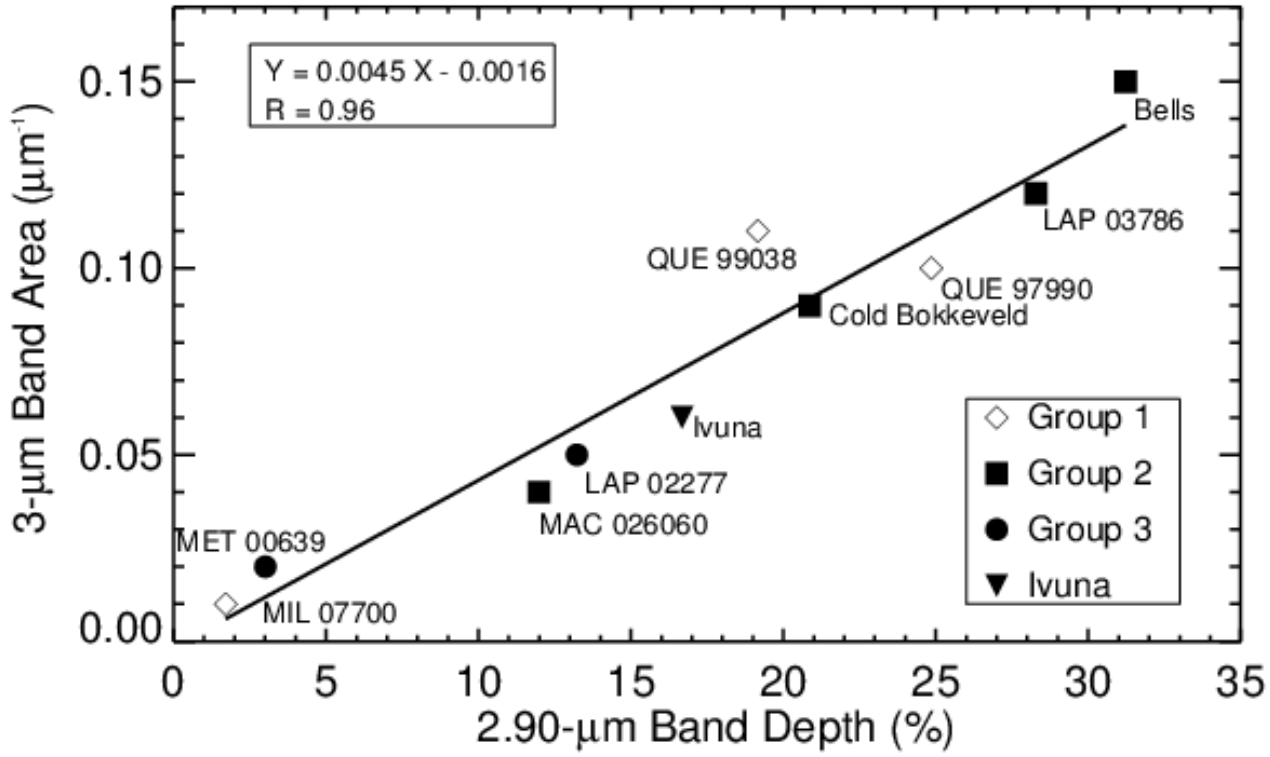

Figure C4. Correlation between the 2.90-µm band depth and the 3.0-µm band area in 10 carbonaceous chondrites. The classification of chondrites used here are from Takir et al. (forthcoming). The R (linear-correlation coefficient) value of 0.96 corresponds to a probability of ~1 (2σ) that the variables are correlated.

Figure C5. Comparison between CM and CI chondrites and outer Main Belts asteroids with the sharp OH 3-µm feature (2.5 < a < 3.3 AU). Chi-squared tests were used in the 1.95-250-µm region to quantitatively compare spectra of meteorites and asteroids and to determine the best matches, which were determined on the basis of the lowest computed chi-squared value.

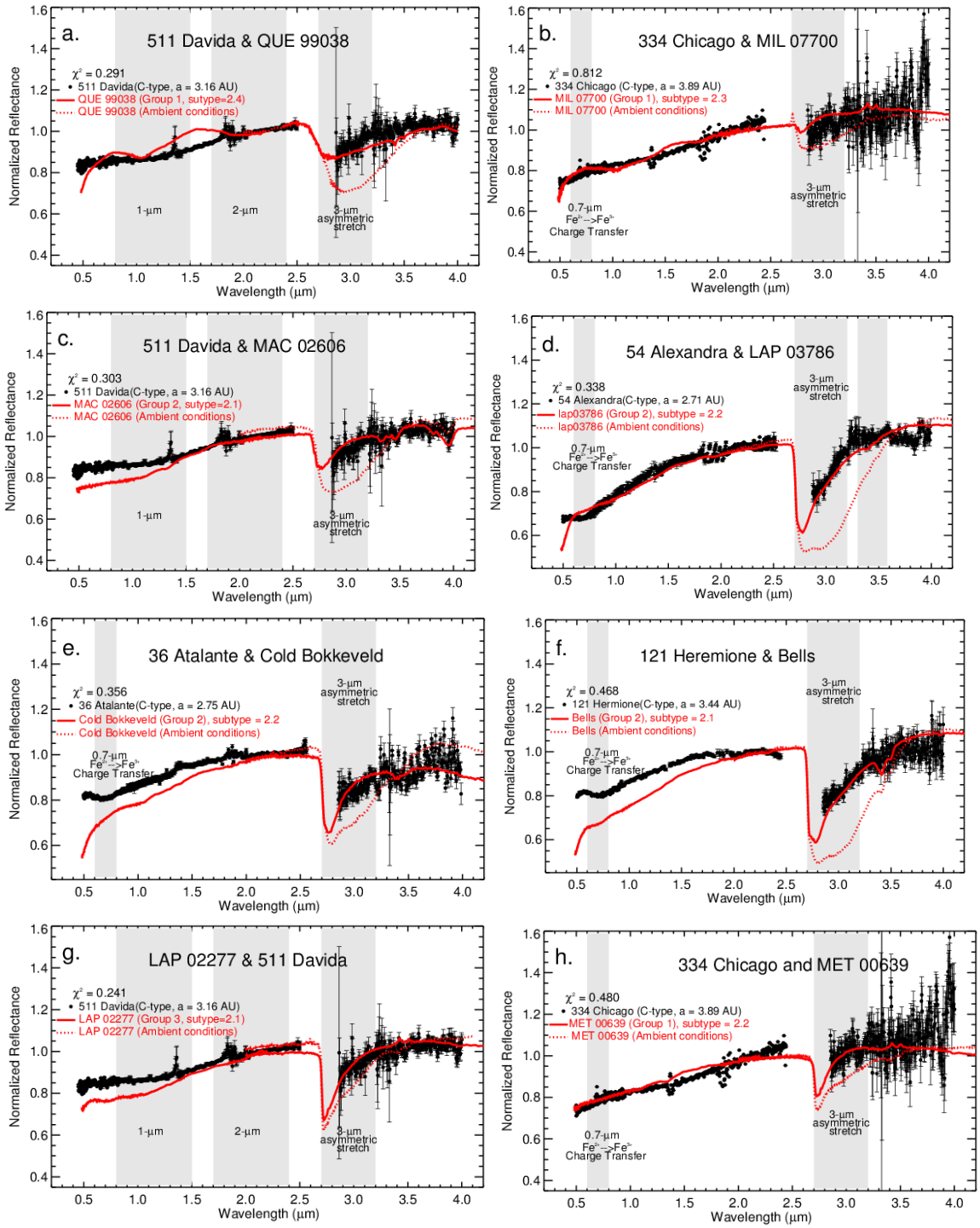

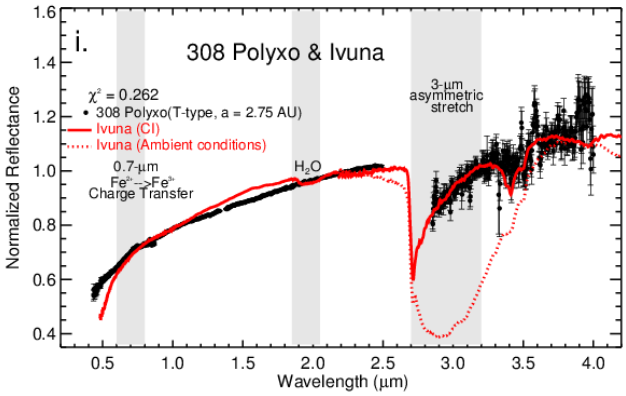
i.
308 Polyxo & Ivuna
χ² = 0.262
• 308 Polyxo(T-type, a = 2.75 AU)
Ivuna (CI)
Ivuna (Ambient conditions)
0.7-μm
Fe²⁺→Fe³⁺
Charge Transfer
H2O
3-μm
asymmetric
stretch
Normalized Reflectance
Wavelength (μm)
1.6
1.4
1.2
1.0
0.8
0.6
0.4
0.5
1.0
1.5
2.0
2.5
3.0
3.5
4.0

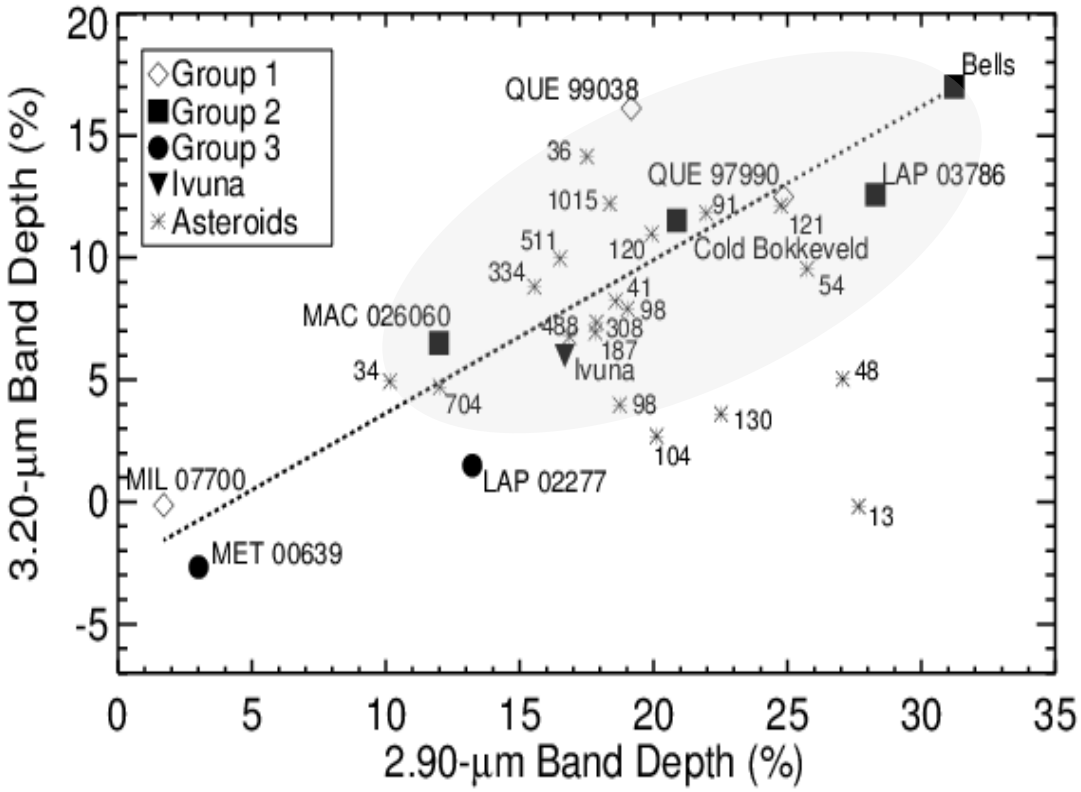

Figure C6. Plot of the 2.90 µm band depth vs. the 3.20 µm band depth that includes both the chondrites and the sharp asteroids used in the present study. The dashed line represents the regression line that includes the meteorites only with R (linear-correlation coefficient) value of 0.90, which corresponds to a probability of ~0.99 (2σ) that the variables are correlated. The classification of chondrites used here are from Takir et al. (forthcoming). 130 Eelktra, 48 Doris, and 13 Egeria, which are G-types, are farther from the regression line. Most sharp group asteroids are concentrated in Group 2 area, which also includes Ivuna (gray area).

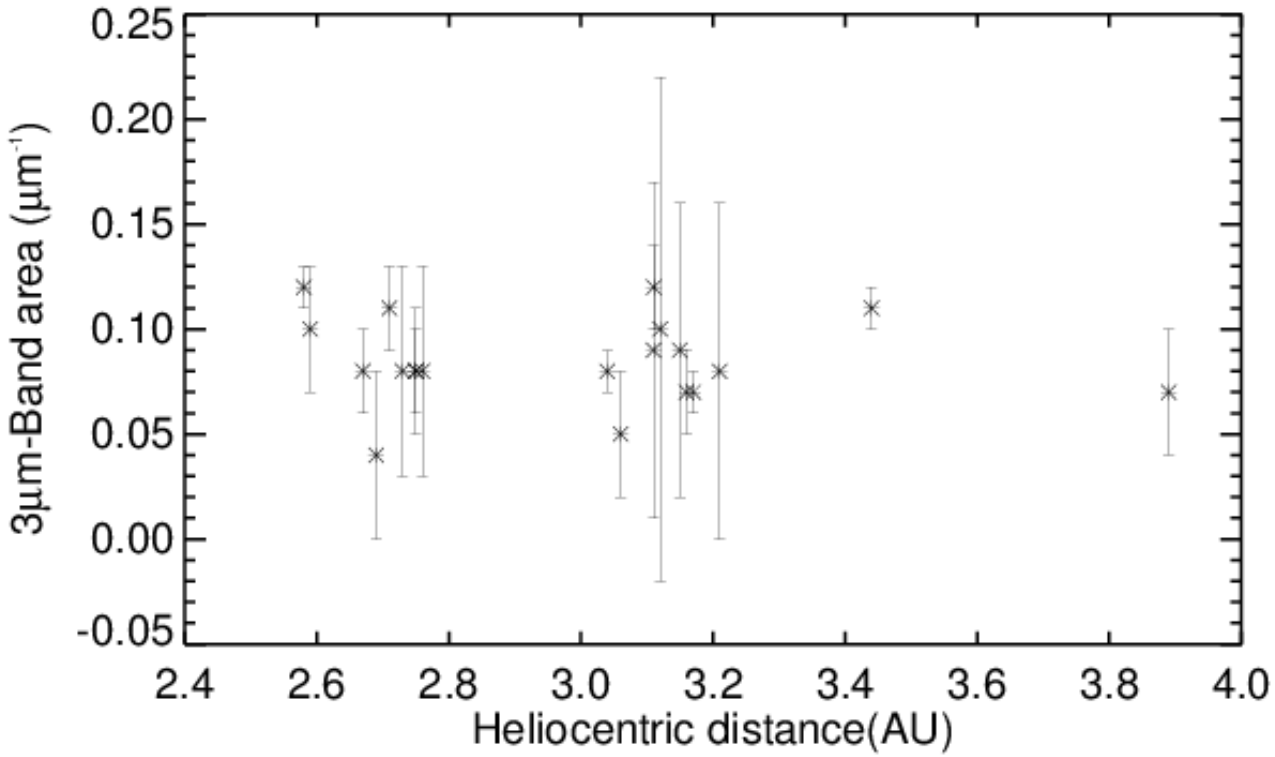

Figure C7. No correlation found between the helioncentric distance and the band area in asteroids that show the sharp OH 3-μm features.

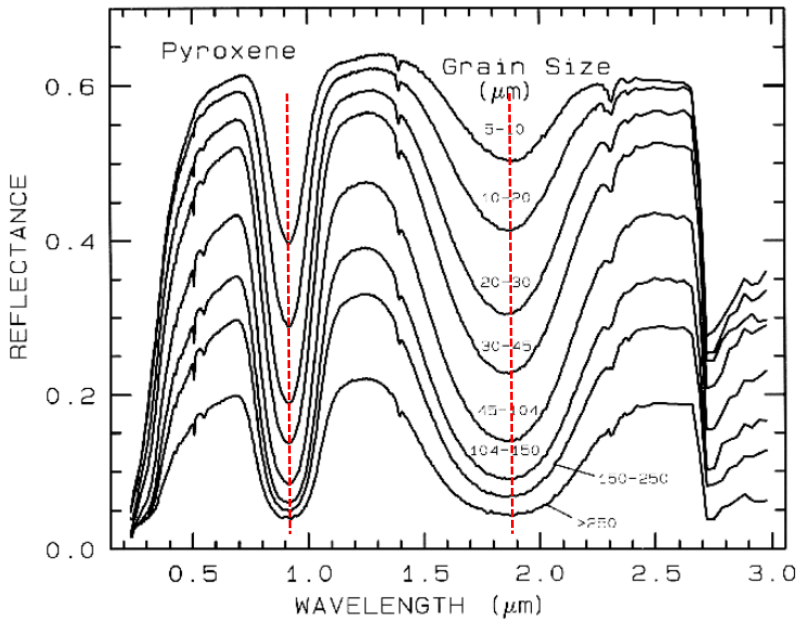

Figure C8. Reflectance spectra of Pyroxene. The grain size affects the reflectance but does not change the features' band centers. Adapted from Clark (1999).

Conclusion

In Chapter 1 we identified four spectral groups of asteroids based on the shape and position of the 3-μm absorption band: the sharp group, the Ceres-like group, the Europa-like group, and the rounded group. The sharp 3-μm band shape is inferred to be due to the presence of phyllosilicates on the surfaces. Asteroids with the sharp 3-μm feature are predominately located in the $2.5 < a < 3.3$ AU region. The rounded 3-μm band shape, on the other hand, is inferred to be due to the presence of H_2O frost on the surfaces rather than hydrated phases. Asteroids that exhibit this feature are predominately located in $3.3 < a < 4.0$ AU region. Our telescopic observations have revealed two asteroids with a 3-μm band shape and associated longer wavelength absorptions that are nearly identical in shape and position to that found in the spectrum of Ceres. The surface composition of Ceres is apparently not as unique as once thought. We have also identified a new 3-μm spectral group that is characterized by a broad absorption with maximum depth near 3.15 μm. This "Europa-like" group currently includes three asteroids (52 Europa, 31 Euphrosyne, and 451 Patientia).

In Chapter 2 we examined reflectance spectra of nine CM and one CI chondrites under dry and vacuum conditions to remove adsorbed water and mimic the space environments. These chondrites are classified into three groups, mainly on the basis of the 3-μm band center. Group 1, which is characterized by 3-μm band centers at 2.76-2.80 μm, is consistent with the endmember Fe-serpentine (cronstedite). Group 3, which is characterized by 3-μm band centers at ~2.72 μm, is consistent with the endmember Mg-serpentine (antigorite). Group 2 represents an intermediate mineralogy between the two endmembers. Ivuna, which is the only CI chondrite analyzed in the present study, has a unique 3-μm band centered ~2.71 μm, is consistent with lizardite and chrysotile. This diversity in the 3-μm band suggests distinct pre-terresterial aqueous alteration

conditions for these chondrites, which provide clues to parent body alteration. We also apply two previously published alteration scales nine CM carbonaceous chondrites. We found good agreements between the petrological and geochemical parameters, and spectral characteristics of these chondrites.

In Chapter 3 we applied the 3-μm spectral indicators developed in Chapter 2 to outer Main Belt asteroids observed in Chapter 1 to provide more details on the alteration state and phyllosilicate mineralogy on these asteroids. We found that CM Group 2 is possibly the meteorite analogs for the sharp asteroids. However, no meteorite match was found either for the rounded group, Ceres-like group, or Europa-like group. We suggested several scenarios that explain the lack of meteorite matches for these groups.

VITA

Driss Takir was born and raised in Morocco. He graduated from University of Hassan II in Casablanca with a Bachelor of Science degree in Physics, Portland State University in Oregon with a Bachelor of Science degree in Computer Science, and the University of North Dakota with a Master of Science in Space Studies. He expects to be awarded his Doctor of Philosophy degree from the University of Tennessee in Geology in May of 2013. Driss has begun a postdoctoral research associate position at Ithaca College, NY, working on asteroid science with NASA OSIRIS-REx mission.